Geothermal exploration involving structural geology and hydrochemistry in the Tarutung Basin, Northern Central Sumatra (Indonesia)

genehmigte Dissertationsschrift

an der Fakultät VI
Planen Bauen Umwelt
der Technischen Universität Berlin
zur Erlangung des akademischen Grades
Doktor der Naturwissenschaften (Dr. rer. nat.)

vorgelegt von
Mochamad Nukman MSc
aus Banyuwangi (Indonesien)

Promotionausschuss:
Vorsitzender : Prof. Dr. Uwe Tröger
Berichter : Prof. Dr. Wilhelm Dominik
Berichter : Prof. Dr. Inga Moeck

Tag der wissenschaftlichen Aussprache: 21. 03. 2014

Berlin 2014

D83

STATEMENT OF ORIGINAL AUTHORSHIP

I hereby declare that the work contained in this thesis has not previously been submitted for assessment, either in whole or in part, by either me or any other person at either the Fakultät VI – Planen, Bauen, Umwelt der Technischen Universität Berlin or at any other institution.

To the best of my knowledge and belief, the thesis contains no material which has been previously published or written by another person expect where due reference is made.

Mochamad Nukman

Zusammenfassung

In der Anfangsphase der Exploration (die sogenannte greenfield exploration) ist die Charakterisierung der Permäbilitaetsstruktur von besonderer Bedeutung und bedarf der integrativen Datenerhebung aus Strukturgeologie und Hydrochemie, verglichen mit der regionalen Geologie und dem rezenten Spannungsfeld. Eine Methodenkombination, bestehend aus Strukturgeologie und Hydrochemie, spielt eine wichtige Rolle in der Identifzierung geothermischer Systeme und der geologischen Kontrollfaktoren von Permeabilitätszonen, Temperaturverteilung, Fluidherkunft und dem allgemeinen Fluidfluss.

Eine Fallstudie im Tarutung Becken in Nord-Zentral Sumatra, 170 km südwestlich der Provinzhauptstadt Medan, widmet sich mit dieser vorliegenden Arbeit dem Forschungsthema der geothermischen Exploration von störungskontrollierten geothermischen Lagerstättentypen in tropischen Regionen.

Das Tarutung Becken liegt an einer rechtsseitigen Übersprungzone der bekannten rechtslateralen aktiven etwa 1650 km langen Sumatra Störung, die NW-SE orientiert ist. Durch die Auswertung von Satellitenbildern und Feldarbeit im Tarutung Becken wurde das Störungsmuster kartiert, das aus dominierenden NW-SE Störungen und untergeordneten N-S (Extensionsbrüche), NNE-SSW (synthetische Riedel-Scherbrüche) und NE-SW (antithetische Riedel-Scherbrüche) Störungen besteht. Rezent aktive N-S orientierte Extensionsbrüche und dilative Scherbrüche, die NE and NW-SE orientiert sind, dienen als bevorzugte Fluidflusswege. An diesen Brüchen befinden sich Heisswasserquellen, die kontinuierlich bikarbonat-dominierte Wässer von 38 – 65.6° C Temperatur schütten. Dieser Fakt deutet auf eine Kontrolle der Fliesswege durch das rezente Spannungsfeld mit einer horizontalen maximalen Kompressionsrichtung in N-S Richtung hin.

Schersinndaten von Störungen an Miozaenen Andesiten und Quartären Travertinen geben das heutige Spannungsfeld wieder, das ein Horizontalspannungsregime mit einer maximalen Horizontalspannung in N-S Richtung ist. Die Rotation von Sekundärstrukturen im Uhrzeigersinn deutet auf einfache Scherung als Deformationsmechanismus hin (im Tarutung Becken), das offenbar ein Zerrgraben (pull-apart basin) ist. Ein neu entwickeltes konzeptionelles Modell erklärt diese Blockrotation im Zusammenhang mit der Bildung von Dehnungsspalten zwischen den dominierenden NW-SE steichenden und den

untergeordneten NNE-SSE streichenden Störungen. Diese Dehnungsspalten sind assoziiert mit Heisswasserquellen, und das Auftreten von geothermischen Oberflächenmanifestationen an der Ostflanke des Tarutung Beckens kann mit diesem Konzept systematich erklärt werden. Die Rotation hat jedoch auch impermeable Zonen entlang ENE-WSE verlaufender Störungen hervorgerufen, die in einem steilen Winkel zur rezenten maximalen Hauptspannungsrichtung liegen. Diese Störungen fungieren offenbar als Barrieren für den Fluidfluss was durch die unterschiedliche Fluidchemie jenseits und diesseits dieser Störung hindeutet, sauere gegenüber neutral bikarbonatischen Wässerm am nördlichen Beckenrand.

Die Hydrochemiedaten zeigen, dass Kalzium-Bikarbonat Wässer mit signifikantem Chloridinhalt die Quellen am östlichen Rand des Tarutung Beckens dominiert. Die Wassertemperaturen dieser Quellen liegen bei etwa 65.5°C. Ein Ungleichgewichts-Stadium zwischen Fluid und Gestein kann in einem Vier-Kationen-Diagramm (Na-K-Mg-Ca) gezeigt werden und deutet für das Tarutung Beckem auf Lösungsprozesse im unteren Temperaturbereich hin. Es gibt keine Hinweise in der Hydrochemie auf Hochtemperatur Fluid-Gesteins Wechselwirkung. Aus diesem Grund ist ein Silizium-basiertes Geothermometer gewählt worden und nicht ein Kation-basiertes Geothermometer. Somit kann eine maximale Temperatur des Quellwassers von 115°C bestimmt werden mit einer wahrscheinlichen Herkunft aus dem östlichen Flankengebiet des Tarutung Beckens. Basierend auf Isotopen (Oxygen und Deuterium) kann ein Einfluss von magmatischem Wasser bestimmt werden, der bei etwa 10% liegt. Damit sind die im Tarutung Becken zirkulierenden Wässer zu 90% meteorischen Ursprungs und mit etwa 10% magmatischen Fluiden gemischt. Die strukturell bedingten Hochpermeabilitätszonen am Ostrand des Tarutung Beckens werden hierbei als die Infiltrationsareale gedeutet, während die Mischungszone mit den magmatischen Fluiden in größerer Tiefe liegen muss.

Zusammenfassend lässt sich festellen, dass das Tarutung Becken nicht assoziiert ist mit aktivem Magmatismus, dass aber sehr wohl eine tiefere magmatische Intrusion als Wärmequelle und Ursprungsort der magmatischen Wässer dienen kann. Die Fließwege des hauptsächlich meteorischen Wassers sind kontrolliert durch dilative und scherende Brüche, die N-S, NW-SE und NE-SW verlaufen, während Fluidbarrieren in ENE-WSW Richtung vorliegen.

ABSTRACT

Characterizing the permeability structure in geothermal greenfield exploration requires collection and integration of hydrochemical and structural geological data related to background geology and present-day stress field. A methodological combination of field based structural geology with hydrochemistry plays an important role in identifying the geothermal system and geologic controls on permeable zones, temperature distribution, fluid origin and the overall flow pattern.

A case study in the Tarutung Basin in North Central Sumatra 170 km SW from the provincial capital city Medan, is addressed to this research topic in geothermal greenfield exploration of fault controlled geothermal plays in tropical environments. The Tarutung Basin is located at a right sided step over region of the prominent right lateral active 1650 km long Sumatra Fault Zone oriented in NW-SE. Satellite imagery and field mapping of the Tarutung Basin evidenced dominating NW-SE faults with secondary fractures striking N-S (extensional fractures), NNE-SSW (synthetic Riedel shears), and NE-SW (antithetic Riedel shears). Recently active extensional fractures and extensional shear fractures striking N-S & NW-SE serve as preferential fluid path ways. From these fractures, hot springs continuously discharge predominately bicarbonate water of 38 – 65.6° C and suggest that the permeability structure is controlled by the regional current stress regime in N-S direction.

Fault slip data in on Miocene andesite and Quaternary travertine reflect the present-day stress field with the maximum principal stress as horizontal in N-S and a strike-slip stress regime. Clockwise rotation of secondary fractures indicates simple shear deformation in the Tarutung Basin, which is obviously a pull-apart basin. A conceptual model is developed to accommodate this rotation with the formation of dilational jogs between NNE-SSW striking secondary faults and the NW-SE striking major fault. These dilational jogs are associated with hot springs and a systematic pattern of geothermal surface manifestations can be explained that occurs at the eastern margin of the Tarutung Basin. This rotation also generated impermeable zones along ENE-WSW oriented faults that are at a high angle to the maximum principal stress direction. These faults act as barriers and might control the separation of two spring complexes of different chemical composition (acidic versus pH neutral bicarbonate water) at the northern basin margin.

Hydrochemistry data show that calcium-bicarbonate water with significant chloride content dominates the composition of spring water at the eastern margin of Tarutung Basin. The surface temperature of these springs is up to 65.5°C. A non-equilibrium state of fluid-rock as shown with a four-cations-diagram (Na-K-Mg-Ca) suggests that a dissolution process in a low temperature condition is dominant in the Tarutung geothermal system. There are no evidences in spring water hydrochemistry for fluid-rock interaction processes at high temperatures. For this reason a silica geothermometer is selected rather than a cation based geothermometer and results in a maximum temperature of 115°C which could occur underneath the eastern spring area of Tarutung Basin. Only up to 10% of thermal water in the Tarutung Basin is of magmatic origin revealed from oxygen and deuterium isotopes. This isotope data imply that meteoric water is more dominant in this field. A permeable zone at the eastern side of the Tarutung Basin, as interpreted from structural geological data, provides a favorable pathway for meteoric water to infiltrate the area and to mix with the deeper fluids.

Summarizing the Tarutung Basin is not associated with active magmatism. Instead a deep intrusion might generate the heat source for the hot spring waters that are recharged by predominately meteoric water. Fluid pathways are controlled by dilational and shear fractures striking N-S, NW-SE and NE-SW while ENE-WSW faults act as barriers.

ACKNOWLEDGEMENTS

I would like to thank Prof. Inga Moeck and Prof. Wilhelm Dominik for the support encouragement. DAAD (German Academic Exchange Service) is greatly thanked in providing the PhD scholarship for the period 1 October 2010 - 31 March 2014. The field and laboratory work was supported by Helmholtz Centre Potsdam GFZ (German Research Centre for Geosciences), which is funded by BMBF (Grant 03G0753A 'Sustainability concepts for exploration of geothermal reservoir in Indonesia'). I express my thanks to Badan Geologi Bandung (Indonesia) and Dinas ESDM Kabupaten Tapanuli Utara (Sumatra Utara, Indonesia) for the discussions and field campaign support, with special thanks to Mekto Purba. I also appreciate and express thanks to the Geophysics Study Program of UGM (Gadjah Mada University, Yogyakarta, Indonesia) for allowing and supporting my study leave.

Prof. Manfred Hochstein is acknowledged for the fruitful discussions on geothermal exploration sciences. PD. Dr. Traugott Scheytt and Ms. Iris Pieper of Geochemistry Laboratory, Department of Applied Geosciences at TU Berlin are thanked for supporting the spring water chemical analysis. I also thank Dr. Fiorenza Deon for the petrology discussions. Dr. Thomas Wiersberg is acknowledged for the noble gases discussions. My interpretation on the subsurface of Tarutung Basin could not have been accomplished without any discussions with Muksin Umar, Sintia Windhi, and Klaus Bauer through their geophysical knowledge and images. Dr. Kemal Erbas, Dr. Makky S Jaya, Prof. David Bruhn, Prof. Ernst Huenges are thanked for general discussions on the project. All colleagues in Section 4.1 (Reservoir Technologies) of Helmholtz Centre Potsdam GFZ are thanked for the wonderful years during my work in Germany.

And finally, I would like to express my deep and unlimited appreciation to my beloved wife Sasmeita Barliani, my daughter Amelia, my son Rheinka who spent their valuable time with me on this long journey.

for my family;

Sasmeita Barliani, Amelia Ima Madani, Rheinka Nukman
Abdussamad Abbas, Hamidah, (Alm.) Hindun,
(Alm.) Cholis Syafii, Mastna Masfufah,

in Banyuwangi - Ost Java, Indonesien

Contents

List of Figures

List of Tabels

Chapter 1

Introduction

1. Introduction

The identification of the exploration play type and the geologic controls therein on heat source, temperature distribution, permeability structure and fluid type belong to the major goals of geothermal exploration. Indonesia hosts a variety of different geothermal systems, and most of the developed systems are located in volcanic fields with active or recent volcanism. Amagmatic structurally controlled systems are hitherto less or not developed. One reason for this might be the lack of clearly defined and efficient exploration strategies for structurally controlled geothermal systems. This thesis addresses whether the methodological combination from structural geology and hydrochemistry is suitable for a green field exploration.

Geothermal activities at the surface are known to be an indicator for the sub-surface conditions based on their fluid chemical composition. At the same time, information about the control on permeability, derived from structural geology studies, are also required to understand the thermal fluid flow pattern in a geothermal system. Classification of hydrochemical composition and the equilibrium state of discharging fluid-rock interaction as derived from spring water analysis are used to constrain the interpretation of the geothermal system and its relationship with the overall structural setting of the area. The research area of this green field study is located at a right-hand step over region of the Sumatra Fault System (SFS) in North Central Sumatra, approximately 40 km southwest of the prominent giant caldera of Lake Toba.

1.1 Aims of Research

The aims of this research are;

1. Identification of the structural setting of the Sipoholon Geothermal Field (SGF) at a local scale and its context at a regional scale, and characterizing structural controls on the surface from thermal activities of the SGF.
2. Identification of the fluid type and flow pattern. Estimation of subsurface temperature to be conducted as well as assessment of possible heat source by considering the state of fluid rock interaction.
3. Construction of a conceptual model of the geothermal system along the SGF, characterizing fluid composition within its structural setting, and defining the dynamics of the fluid mixing system and its relationship with permeability structures. Interpretations of deeper structures are supported by geophysical studies gained from the research program (e.g. Indonesian Geothermal Project of BMBF 03G0753A – GFZ, 2010-2013).

1.2 State of current knowledge

1.2.1 Previous study on the Tarutung Geothermal Area

There are only a few research studies available which cover geothermal exploration of the Tarutung area. One of the first published reports is by van Padang (1951) who re-registered the number of hot springs (43 sites) and sulphur springs (7 sites), including the spring from Tarutung from earlier data sources (e.g. Volcanological Survey of Indonesia). In van Padang's report, the spring complex is called Helatoba-Tarutung, which is now referred from north to south area as the Butar (in Tarutung) and Namora-I-Langit (in Sarulla). Spring mapping is missing in this report. Aldiss et al., (1983) describe in more detail the hot springs related to regional geology. Springs discharging along the basin and off the basin are well mapped. The compiled work of mapped hot springs and reference to background geology by Aldiss et al. (1983) is useful, although the list of recorded springs may not be complete.

The published work by Hochstein & Sudarman (1993) about Sumatra's geothermal potential is probably the first published geochemical assessment of the Tarutung springs. The discussion of Hochstein & Sudarman (1993) is focusing only on the two largest spring sites (namely Ria-Ria , also known as Sipoholon, and Panabungan), their indication of areas with high discharge of dry CO_2, and the extensive travertine deposits indicating the dominant bicarbonate water. More recent work on geochemistry is done by Ardiwinata et al. (2005). Eight springs sites in Tarutung Basin are listed. Their subsurface temperature was estimated using silica and cations geothermometer (critically discussed in Chapter 7). The authors also executed the first oxygen isotope and deuterium survey from this field without publishing the complete data set of isotope value and fluid chemical concentration.

Hot springs located in the southeast (e.g. Sarulla Basin) and northwest (e.g. Pusukbukit Field) of Tarutung have higher temperatures than discharging springs from the Tarutung Basin. Temperature springs in Sarulla Basin are in the range of 68-101°C, and the geothermal system has been proven by exploratory wells (Gunderson, 2000; Indo-Press, 2012); whereas the highest temperature in Tarutung is only 66°C as identified from Ria-

Ria site by Hochstein & Sudarman (1993). Additionally, fumaroles with near boiling temperatures located in northwestern of Tarutung (~ 50 km), namely Pusukbukit field, might be controlled by remained magma of the last giant Toba eruption (i.e. 74,000 years ago) (Hochstein & Sudarman, 1993 & 2008). These evidences of the viable geothermal resource in Sarulla and the (possibly) remaining large magma chambers lying underneath Toba evokes interest in the area of Tarutung, which is located in between these areas.

1.2.2 Previous work on structural geology as general method in a geothermal exploration

For more than three decades, structural controls on hydrothermal activity were investigated (Grindley, 1970; Currewitz & Karson, 1997, Rowland & Sibson, 2004, Hickman et al., 2004; Khodayar et al., 2010; Faulds et al., 2012; and many others). Grindley (1970) describes how active fault systems control the production steam wells in at Broadlands geothermal field (New Zealand). In more current research, with particular attention on structural geology roles on the occurrences of hydrothermal activities, a hot springs catalogue from various tectonic settings by Curewitz & Karson (1997) shows that the interaction area of fault system plays an important role in the localization of hot springs. A case study from South Iceland geothermal fields also shows that the highest discharge and temperature of springs are found at the intersection fracture system within rift settings (Khodayar et al., 2010).

In a more detailed description, step overs structure and the intersection of normal fault and strike slip fault are found to have the most control on the localities geothermal activities in the Great Basin of the Basin and Range Province (USA) (Faulds et al., 2010). Additionally, a close relationship between a volcanic center with a major fault system (e.g. strike slip fault) is shown to be a major control on the localities and the permeability structures of four geothermal systems in North Central Sumatra (namely Sarulla Field) (Hickman et al.(2004), which is 30-40 km southeast from the current research area discussed in this dissertation.

From those previous works above, it is shown that the structural interaction zone, extensional or transtensional fault regime type, and the existence of volcanic center, play an important role in the permeability structure of a geothermal system.

However, two questions arise, i.e.

1) *"Do the interaction zones of faults always act as a permeable zone through time? How could we explain those fault systems dynamically affecting the permeability structure?"*
2) *"To what extent could the probable extension of geothermal reservoirs be outlined with high permeable and high temperature characteristics by combining structural geology and hydrochemistry data?"*

The methodology applied in this research is a structural geological analysis which is mainly field work based. The structural data were measured from outcrops and also inferred from the distribution of hot springs and travertine deposits which were used for fault and fracture analyses related to the current stress field. Quaternary travertine deposits were investigated to delineate the interaction of tectonic stresses and fluid flow. Water sampling from springs were also collected during the structural field campaign. A comprehensive interpretation of various data consisting of fractures, fluid composition and its origin, lithological types, and equilibrium state of fluid-rock interaction were ultimately used to outline a geothermal system in the Tarutung Basin. The detail of methodology of this research is described in Chapter 3.

1.4 Geographic site of research area

The research area is located in the North Sumatra Province of the Republic of Indonesia (Fig.1). The Tarutung area is located at a longitude of 98 - 100° E, latitude of 1- 3° N, and lies about 40 km to the south of the prominent super-volcano Toba Lake which last erupted 74,000 years ago. The average elevation is 900 m above sea level. The area is accessible by land transport from Medan City (capital of North Sumatra) and by air transport from Medan to Silangit Airport at Siborong-borong Town. The Tarutung area

belongs to Tapanuli Utara (North Tapanuli) District, under North Sumatra Province. The area of this district is approximately 3,800 km^2 with population of 278,897 (based on civil census in 2010; Board of Statistics Indonesia, BPS, 2013). Most of the people are working as farmers. The land use in Tapanuli Utara District is in form of housing, farming areas (i.e. paddy, corn, peanut and various horticultures), estate crops (i.e, incense and arabica coffee), fishery (at the south vicinity of Toba), and production and conservation forest (data from Board of Statistics Indonesia, BPS, 2013). Road conditions are only good in the center of the town, and not good in remote areas where the steep topography with unconsolidated soil is mostly located. Landslides mostly occur during the rainy season in such areas, due to a high rainfall rate (420 mm/year) and a lack of strong road construction.

The mining industries are in the form of stone mining (for house and road materials, and raw materials for cements), whereas manufacture industries are mostly conducted on the family scale for food and clothing. Areas hosting warm springs (i.e. public bath) attract domestic tourists, who visit for religious (Protestant-Christian) based reasons. The supply of electrical power comes from outside the Tapanuli Utara District. On the regional scale, the electricity supply in North Sumatra is limited in their reserve which leads to occasional blackouts for some time (i.e. if one of the power plants, which are mostly powered by fossil energy sources, are shutting off due to unexpected reasons) (data from Energy & Mining Board of North Sumatra or called as Dinas Energi & Pertambangan Sumatra Utara, 2012).

There are two geothermal fields in North Sumatra proven to have deep wells, namely Sibayak (~ 135 km NNW from Tarutung) and Sarulla (~ 40 km SE of Tarutung). The only geothermal power is supplied from Sibayak Geothermal Power Plant, for 11 MW, which is only 0.6 % of the total available electricity sources (1881 MW) as powered by fossil fuel (data from Dinas Energi Sumut, 2012).

1.5 Topographic

Lower elevation in Tarutung occurs in the basin center and the eastern side. The depression area within the Tarutung Basin is 2.5 x 15 km in size, and elongated in shape striking NW-SE. A lower elevation eastern area is forming a half circular shape indicating presumably a fossil caldera (Nukman & Moeck, 2013) (see also Section 6.4). A radial drainage pattern is the consequence of this shape. Higher elevation at the western side of Tarutung Basin occurs in mountainous terrain aligned in NE-SW direction, composed of Paleozoic phyllitic slate and Miocene andesite. A straight (12 km long) and abrupt bended drainage pattern can be found at the lithology contact of the Permian granite with the Miocene andesite (Fig. 13). This topographic difference induces a hydraulic gradient. The flow of surface water and (possibly also) shallow ground water are trending from east to west and from northwest to southeast towards and off the Tarutung basin.

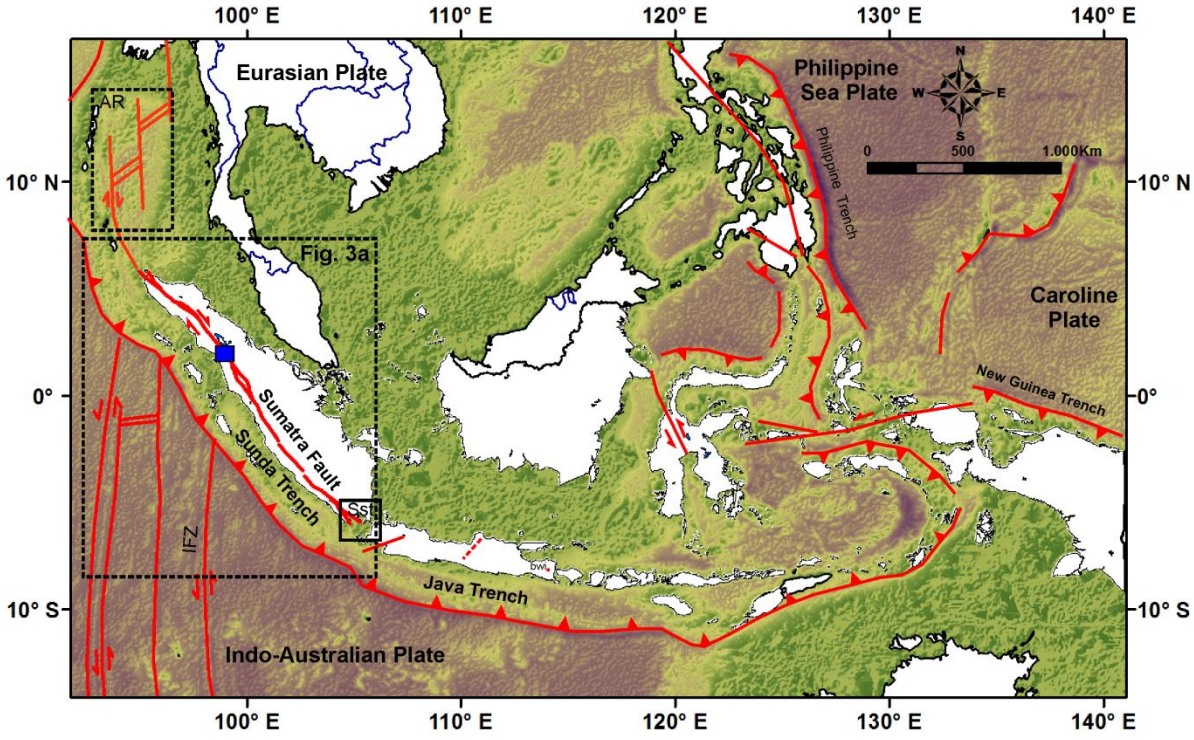

Figure 1. Locality of Sumatra along the South Eastern Asian plate.The Indo-Australian plate is obliquely subducting the Eurasian plate. The formed trenches due to the subduction are extended NW-SE (known as the Sunda trench) and then E-W (known as the Java trench). The area within a solid blue square is shown in Figure 3. Abbreviation : AR = Andaman Rifting; IFZ = Investigator Fault Zone; Sst = Sunda Strait.

Chapter 2

Regional Geology

In this section, the summary of Sumatra's history (Paleozoic-Mesozoic time) is described, summarized from several published works by previous researchers.

2.1 Tectonic Settings

Present-day Sumatra is a part of the southwestern segment of the Eurasian continental plate which is now against the Indo-Australian oceanic plate within a convergent tectonic relationship (i.e. an oblique subduction system (Katili, 1971; Hamilton, 1979; McCaffrey, 2009). Prior to the present-day position, the island of Sumatra developed separately (Fontaine & Gafoer, 1989; Hutchison, 1993). During the mid-Paleozoic era, Sumatra consisted of two different blocks, namely East and West Sumatra (Fontaine & Gafoer, 1989; Hutchison, 1993; Barber, 2005) (Fig. 2). The East Sumatra Block belonged to the Southeast Asia plate; whereas the West Sumatra Block belonged to Gondwana of North West Australia which was situated at the far eastern direction from the West Sumatra

Block. These two Sumatra blocks were separated by Paleo-Tethys during the late Carboniferous to early Permian (Fig.3) (Barber, 2005).

In later development during the early Triassic era, the opening of Meso-Tethys occurring in the southwestern part of SE Asia plate generated transcurrent strike slip faulting (Barber et al., 2005). A right lateral movement segment from this transcurrent strike slip fault (which is also known as Medial Sumatra Line of Hutchison, 1993) is interpreted to control the displacement of the East Sumatra Block to the western direction, and is now attached with the East Sumatra Block (Barber et al., 2005; Fig.3b). In the present-day, the northern parts of the Medial Sumatra Line are overprinted by the modern Sumatra Fault System (SFS). The research area of this work is situated in the junction of these two major structures (Fig. 3a). The implications of overprinted structures to the permeability structures of the area are explained in Chapter 6.

The subduction of the Indo-Australian plate under the Eurasian plate started in the Cretaceous (~100 Ma; McCarffrey, 2009). The spreading centre in the Andaman Sea to the north tip of Sumatra Island and graben development in the Sunda Strait to the south end of Sumatra required an accommodation zone which is now known as the Sumatra Fault System (later called by SFS). The oblique subduction of the Indo-Australian and the Eurasian plate caused dextral strike slip on the accommodation zone and the generation of a volcanic arc along Sumatra Island. The plate converge vector is North-South with a velocity of 10-22 mm/year (Bellier & Sebrier,1995) on the dextral strike slip faulting along SFS serves as melts from the upper part of the subducting mantle to shallower depth in the crustal layer.

The formation of the modern SFS started in the early Miocene when rifting begun in the Andaman Sea at the off northwest of Sumatra (Fig.1 and Table 1). Andesitic magmatism as known by its product as Toru Formation occurred afterward (i.e. middle Miocene of Aldiss et al., 1983). A proto-type of Tarutung Basin was probably formed in this period or shortly afterward as evidenced by the displacing of this middle Miocene andesite outcrops by approximately 20 km. The dynamic faulting system in this formation is analyzed in this dissertation.

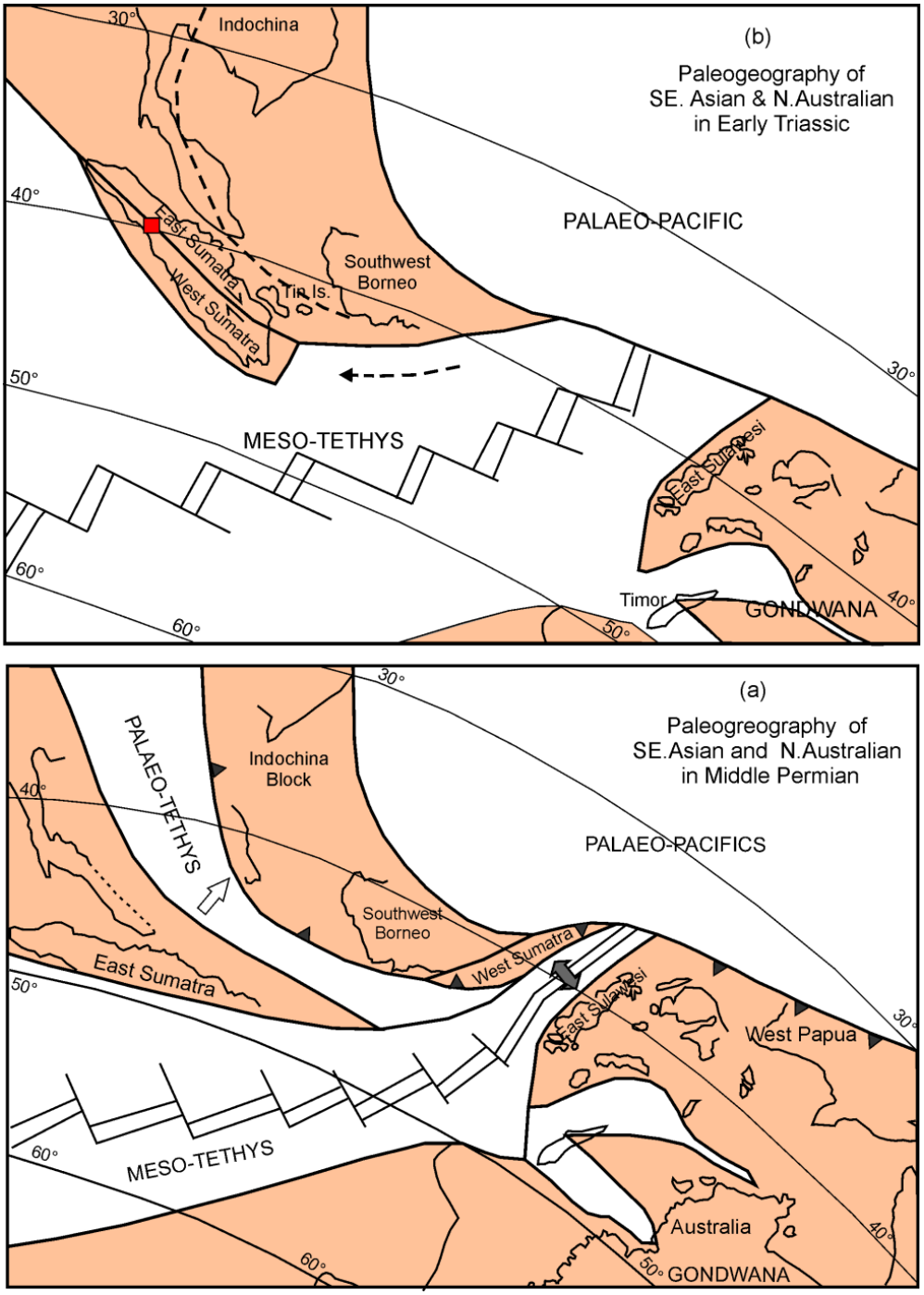

Figure 2. Palaeogeography of South East Asian and North Australian plates in Middle-Permian (a) and Early-Triassic (b) (after Barber et al., 2005). The red solid in square in figure 'a' is the approximate location of present-day Tarutung Basin

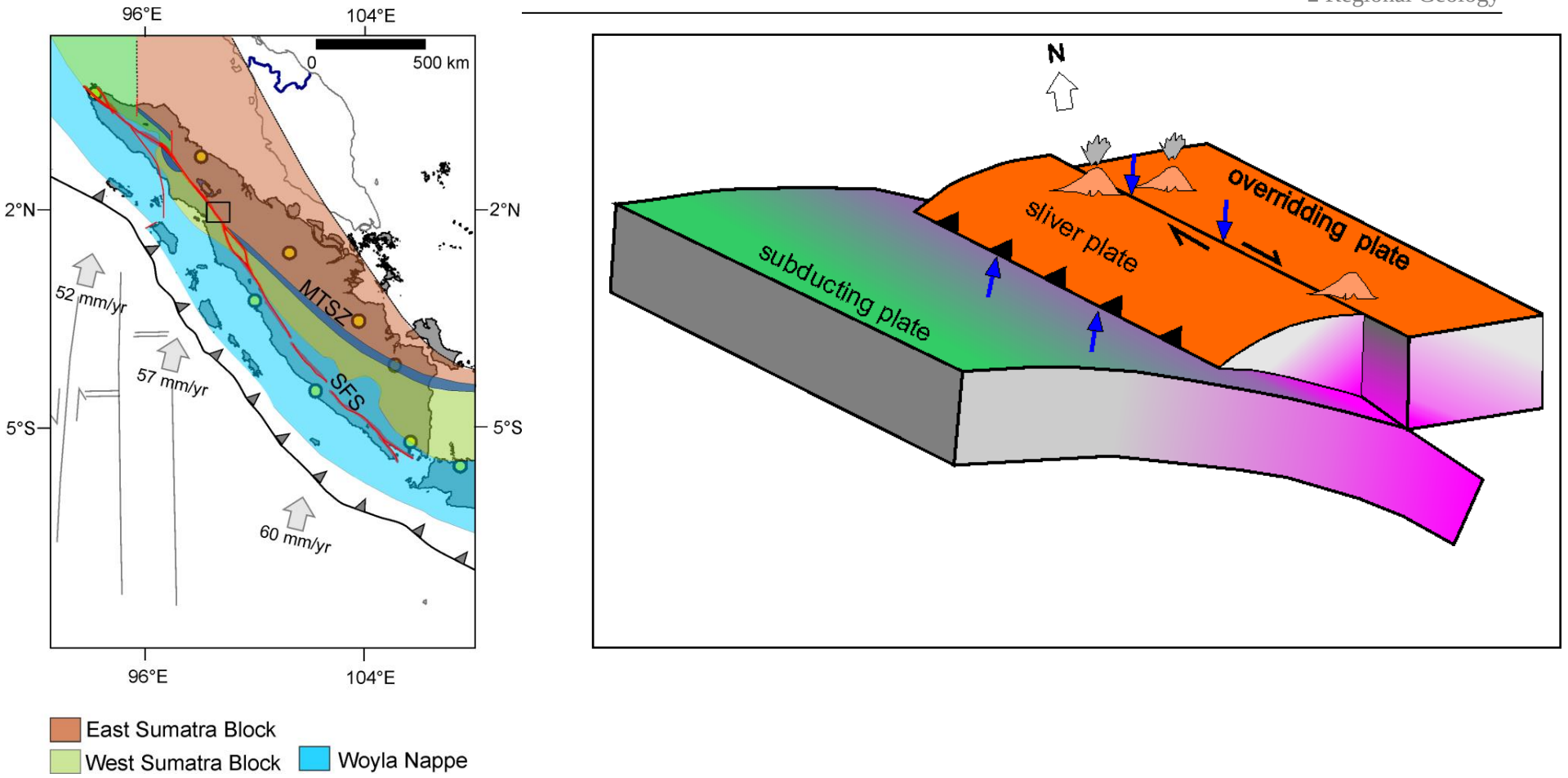

Figure 3. a) Major tectonic map of Sumatra Island (after Barber et al., 2005).The rectangle is location of Tarutung Basin. b) A sketch shows slip partitioning components occurring in Sumatra (modified from McCaffrey, 2009). The compressions from subducted plate are accommodated by the dextral strike slip of Sumatra Fault System which occur at the overriding pate (Eurasian plate).

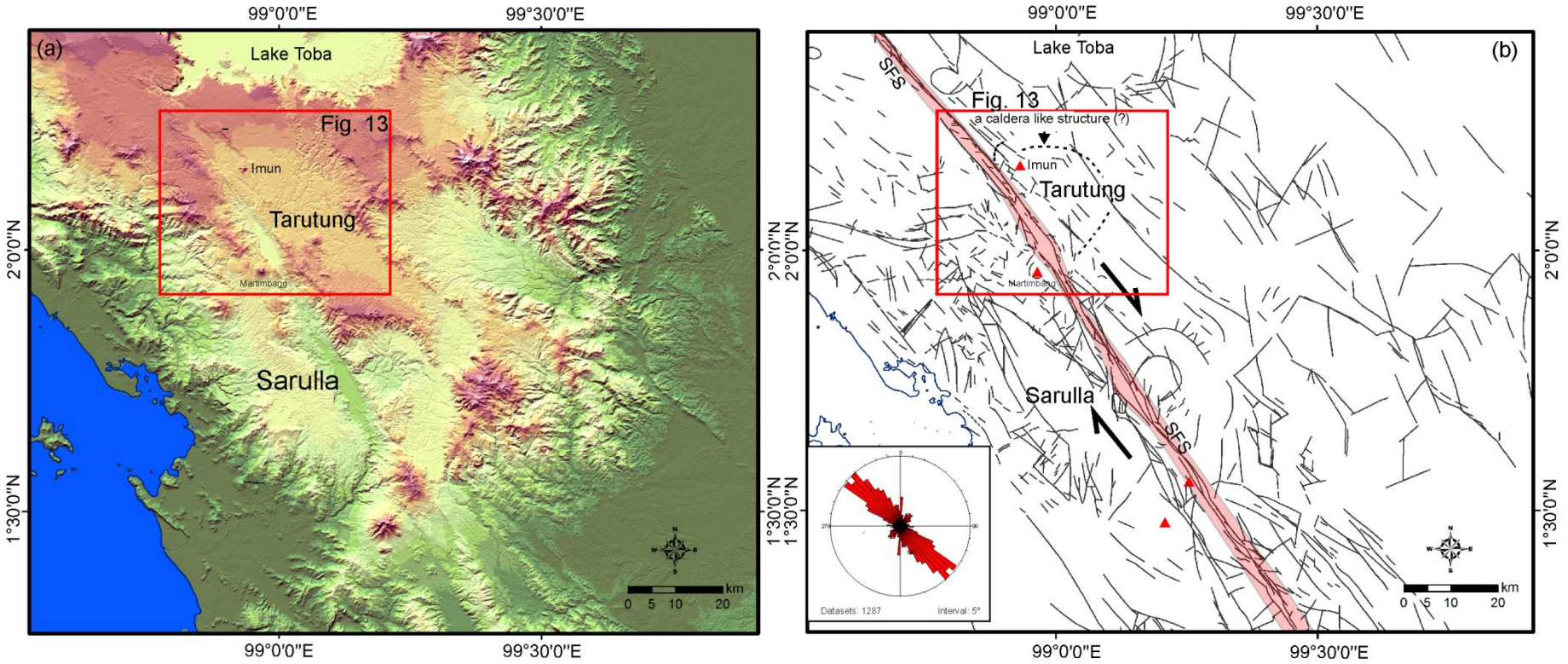

Figure 4. a) DEM with resolution 90 m of Northern Sumatra.. b) Delineation of fractures based on DEM (a). The light orange colour represents Sumatra Fault System (SFS). The caldera- like structure is observed on the eastern area of Tarutung Basin. Average strikes of all fractures are plotted on the rose diagram(c) showing major fracture trend in NW-SE and some minor fractures in N-S to NE-SW (modified from Nukman & Moeck, 2013). Geothermalmanisfestations are extensively discharging within and on the margins of the Tarutung (in the north) and Sarulla Basin (in the south). (see also Fig. 27)

2.2 Tarutung pull-apart and Sarulla graben basin

The en-echelon segmentation along SFS generates step-over region. Right hand-sided step overs along a dextral strike slip fault represent dilatational zone (Sieh and Natawidjaja, 2000) or pull-apart basins (Muraoka et al., 2010). Only a few left hand-sided along SFS step overs generate restraining bends (Sieh & Natawidjaja, 2000). The Tarutung Basin is located at a right hand sided step over region and therefore supposed to be a dilational zone. The eye-shaped of Tarutung basin is derived from a DEM map (Fig. 4). A typical rhombohedral shape indicating a pull-apart basin is not clearly observed although a morphological depression indicating dilation. Instead, the shape might be controlled by complex secondary fracture pattern caused by simple shear along the SFS. The basin is 15 km long and 2.5 km wide and extends in NNW-SSE direction along the prominent NW-SE striking SFS.

A possibly comparable structure is the Sarulla graben located 30 km south of the Tarutung Basin (Fig. 4b). The Sarulla graben is also formed in a mature right hand sided step over region of SFS and host geothermal resources. A releasing step over does not exist at the Sarulla Graben (Hickman et al., 2004) but a basin composed of at least indicating half-graben. Hot springs occur in both Tarutung Basin, but only in the Sarulla graben geothermal system is evidenced. However, spring temperatures and hydrogeochemistry characteristics are different in both basins. The differences of these two geothermal fields are discussed in Chapter 7, Section 7.10.2.

2.3 Regional Stratigraphy

The oldest rocks in Northern Sumatra consist of limestone of the Carboniferous (Visean) (MetCalfe, 1983). This rock is known as Alas Formation which is distributed from the Alas graben in the Southern part of Aceh province to the south west direction along the SFS. The southernmost known occurrence of the Alas Formation is located in Batuharang area (Aldiss et al., 1983; Fig.13). The Alas Formation is exposed within and closed by the SFS, possibly indicating a wide distribution to North Sumatra (Aldiss et al., 1983). The distribution of the Alas Formation at the proximity of Tarutung Basin is still speculative.

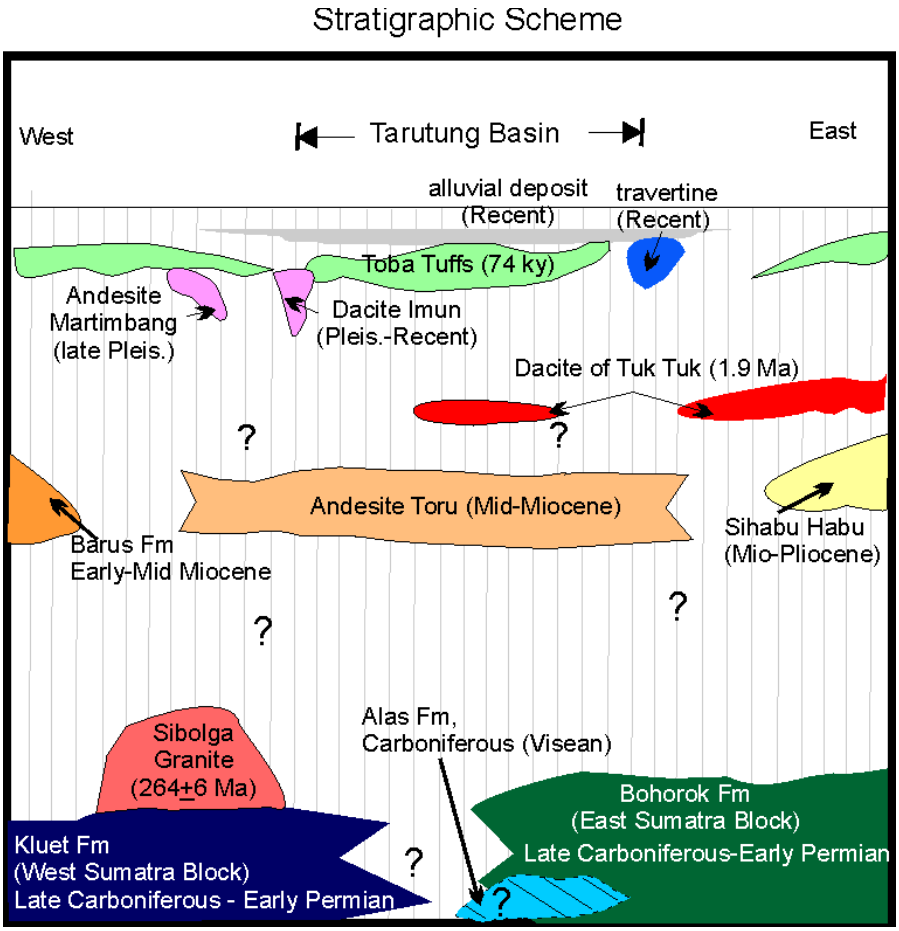

Figure 5. Stratigraphic scheme of vicinity Tarutung Basin, northern central Sumatra (compiled from Aldiss et al, 1983; Apsden et al, 1982; Clarke et al, 1982; Nukman & Moeck, 2013).

The next oldest rock (late-Carboniferous) in the southern part of North Central Sumatra is a phyllitic slate complex of the Kluet Formation of Late Carboniferous age. The Kluet formation is exposed at the western of the Tarutung Basin. Quartz arenites of Bohorok Formation exposed at the eastern edges of the Tarutung Basin is also dated late-Carboniferous (Aldiss et al., 1983). The Kluet Formation is considered as a distal zone of the Bohorok Formation and both have been metamorphosed (Rock et al., 1982; Aldiss et al., 1983, Barber, 2000). A granitic intrusion, part of the Sibolga batholith, intruded these late Carboniferous rocks in early Permian (i.e. 264 $\pm$ 6 M.a of Aldiss et al., 1983 and Apsden et al., 1982). The exposure of this granite is elongated in NW-SE direction and exposed only on the western side of the Tarutung Basin.

A large hiatus between lower Permian and Miocene occurred due to uplifting (Barber, 2000). Volcanism mostly andesitic in composition started in mid-Miocene (known as Toru Formation) (Aldiss et al., 1993). Toru Formation overlies the Permian Granite at both the western and eastern side of the Tarutung Basin. The exposures of Toru Formation on the eastern basin side are localized in the south-east region. On the western basin side, the Toru Formation is located at the northwestern region and offset ~20 km from the exposures in the eastern basin side along the SFS, indicating a dextral simple shear along SFS after deposition of Toru Fm (Nukman & Moeck, 2013).

Quarternary deposit consists of the Toba Volcanic Complex (TVC) consisting of two members. The older member of the TVC is a recent dacite which might refer to Tuk Tuk Dacite at Toba Lake of Yokoyama's (1989) (Nukman & Moeck, 2013) dated at ~ 1.9 Ma (Yokoyama, 1989). The Tuk Tuk dacite consist of pyroclastics interbedded in dense welded tuff which are widely distributed over the Tarutung Basin. Exposures are located at the northern area (Silangkitang) and in the eastern area of the basin (Panabungan).

The younger member of the TVC is the Toba Tuff which is aged 180 – 74 kya consisting of pumice tuff in a welded structure. Biotite crystal (1-3 mm length) observed by the author within the welded pumice tuff, might have formed in magma chamber prior to the eruption as previously described by Chesner (1998). The youngest units in Tarutung area are travertine and alluvial deposits. Travertine deposits consist of travertines which are exposed only at the eastern and southeastern margin of Tarutung Basin. Exposures from north to south are *Ria-Ria* (RIA), *Hutabarat* (HT), *Sitompul* (STP), and *Pansur Napitu* (PN). The basin center and river valleys are covered by alluvial deposits.

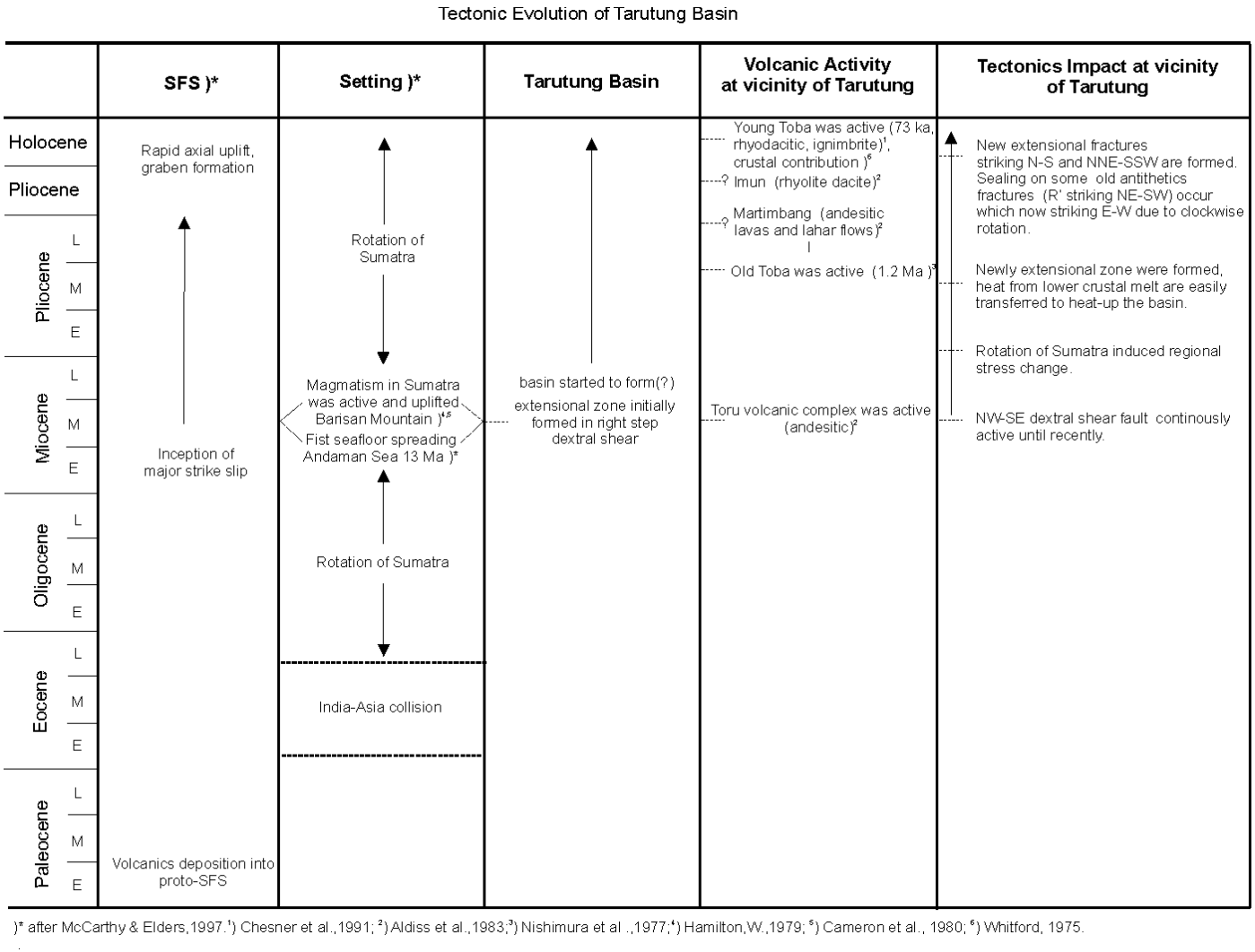

Table 1. Regional tectonic evolution of Sumatra Fault System (SFS) in the Tertiary Period. Tarutung Basin evolution is included into context of the regional SFS evolution which probably started in mid-Miocene. Regional tectontic ages are referred to McCarthy & Elders, 1997, Chesner et al., 1991; Aldiss et al., 1983: Nishimura et al., 1977, Hamilton, 1979; Cameron et al.,1980; Whitford, 1975)

2.4 Geothermal Potentials in Sumatra

Most areas of geothermal prospects in Indonesia are associated with Quartenary volcanic fields (arc volcanism), and also underneath the slope of active or dormant stratovolcanoes (Hochstein & Sudarman, 2008). Those fields are characterized by active geothermal surface manifestations, steaming ground with acid fluids, fumaroles, hot pools, minor geysers, and travertines. The first four manifestation types are typical for high temperature systems. The presence of boiling water and high chloride content are common indicators of high temperature (Hochstein & Browne, 2000). The drilled wells mostly reached volcanic rock reservoir, e.g. andesite, and minor dioritic and basaltic rocks (Hochstein & Sudarman, 2008).

The assessment of the geothermal potential of Sumatra started in the early 1970's by PERTAMINA (State Oil Enterprise of Indonesia). Exploration surveys were mostly conducted at the high entalphy reservoirs in Java (Radja 1985). Currently, there are more than 200 geothermal prospects hosted in Indonesia arc, and 70 fields among those were founded as potential high-temperature systems with almost half of them located in Sumatra (Hochstein & Sudarman, 2008). By 2008, the installed capacity had reached ~1000 MWe from 7 fields in 2008 (Hochstein & Moore, 2008).

Productive wells in Sumatra along the Sumatra Fault System and are located in *Sarulla* geothermal filed at the North Sumatra and *Ulubelu* geothermal field at South Sumatra (Gunderson et al, 2000; Kamah, 2001). A few attempts have been undertaken to determine the mechanism of the fault evolution and its effects of subsurface fluid flow and geothermal activity at *Sarulla* geothermal field (Gunderson et al. (2000) and Hickman et al. (2004) p; without, however, defining specific exploration methods or targeting favorable drill sites.

Chapter 3

Methodology

Methodologies of this research are published in Journal of Asian Earth Sciences 74, 2013, 86-96, by authors : Mochamad Nukman & Inga Moeck, and submitted paper in Geofluids (2013).

The methodology applied in this work consists of two major parts, i.e. structural geological and hydrochemistry analysis. Details of the methods are described in the following sections:

3.1 Structural geological analysis

Structural geological analysis was conducted on various scales, and encompasses the larger scale mapping of lineaments, basin boundaries, and drainage pattern from topographic maps and satellite images (i.e. Digital Elevation Model, DEM 90 m in resolution). The field works were conducted 5 times during a period of 3 years, e.g November- December 2010, July-August 2011, February-March 2012, July-August 2012, and October-November 2012, with the total duration approximately 5 months.

The field based structural geological measurements encompassed standard mapping techniques including fault plane analysis after Petit (1987) (Fig.10) and fracture network

analysis after Hancock (1985) (Fig.20). In order to perform fault analysis, structural data were required (Fig.6), i.e. strike and dip of fault plane, dip and plunge direction of striations, sense of slip, strike and dip of joint, strike and dip of subsidiary fractures (Riedel shears). Mapping of hot springs and hydrothermal deposits were also conducted, which provide trend of morphological ridges and discharges points of thermal water. In this research, 95 measured slip planes and 349 of the joints were measured, including the trends of travertine deposits. The results of field measurement are listed in Appendix 1. The fault and fracture data sets are statistically analyzed using TectonicFP software (Ortner et al., 2002). Fault slip data are plotted into the lower hemisphere projection while morphological ridge trends are plotted into directional rose diagrams.

Major orientations of the fault are compiled into strain ellipses (Fig. 15) which consist of an ideal trend of formed faults or fractures with respect to a known direction of a maximum principal stress. The ideal trends of formed faults or fractures are based on the Andersonian concept (see Section 4.4.2). In the case of Tarutung Basin, the direction of maximum principal stress refers to the regional stress in Sumatra which is in N-S direction. The relative position (e.g. optimal and non-optimal angle) of measured fault trends with respect to the Andersonian state are analyzed by considering the major tectonic settings (Chapter 5, Section 5.1).

ArcMap software (Version 9.3 of ESRI) is used for map compilation and georeferenciation. The ERDAS software is used for improving visualization and analysis of satellite images. A sharper visualization of topography in a particular angle of lightening was derived from a relief - shaded method.

To understand structures at a deeper level, physical anomalies as revealed from geophysical survey results are used to confirm the interpreted structures from geological analysis, e.g. seismic tomography by (Muksin et al., 2013a, b) and magnetotelluric by Sintia et al., 2012).

3.2 Hydrogeochemistry Analysis

Field work covers fluid sampling from 18 cold, warm and hot springs. The sampling procedure included 30 ml plastic bottles of fluid samples for later analysis of cations, anions, and isotopes. All the fluids are filtered with 0.45 μm of membrane filter. The samples for

cation were treated with two drops of strong acid (HNO_3) to prevent rapid mineral precipitation during the transit time from the field to the laboratory which covered no more than 2 weeks. The sample bottles for cation and anion analysis are polyethane bottles with a sealing cap preventing gas exhalation. Sample bottles for isotope analysis are glasses bottles, also with a sealing cap. The on-site measurements taken directly at the discharge location of the spring included pH, temperature, total dissolved solid (TDS), and carbonate content. Flow rates (liter per second) of the springs were manually estimated using a bucket with a known volume (i.e. 1 liter). Fluid samplings were conducted from 10 – 17 March 2012. The ambient temperature is in the range of 22-26°C (daytime).

The chemical analyses were conducted at the Geochemistry Laboratory, Department of Applied Geosciences, Technische Universität Berlin. The anions (Cl^-, B^-, SO_4^{-2}) were measured by ion-chromatography (Dionex DX120). The cations (Li^+, Rb^+, Ca^{2+}, and Mg^{2+}) were measured by Inductively Coupled Plasma (iCap 6300). Na^+ and K^+ were measured using an Atomic Absorption Spectrophotometer (AAS). Silica was measured by a visible range spectrophotometer. Five percent of the ionic balance of the anions and cations ratio is considered an indicator of an acceptable analysis. The analysis results are plotted with the plotting program developed by Powell & Cumming (2010). Bulk oxide composition of rock samples were measured using X-ray fluorescence conducted at the Department of Geology in University of Salzburg, Austria.

Oxygen ($\delta^{18}O$) and hydrogen isotope (δD) analysis were determined using a Finningan MAT Delta-S mass spectrometer at the Alfred Wegener Institute (AWI) for polar and Marine Research – Research Unit Potsdam. The results of noble gases survey in particular helium isotopes by Halldorrson et al. (2013) and are also used to support the interpretation of hydrochemical and oxygen isotope analysis. These helium isotopes enrich the understanding of a heat transfer and its origin on the geothermal system in a more deeper level.

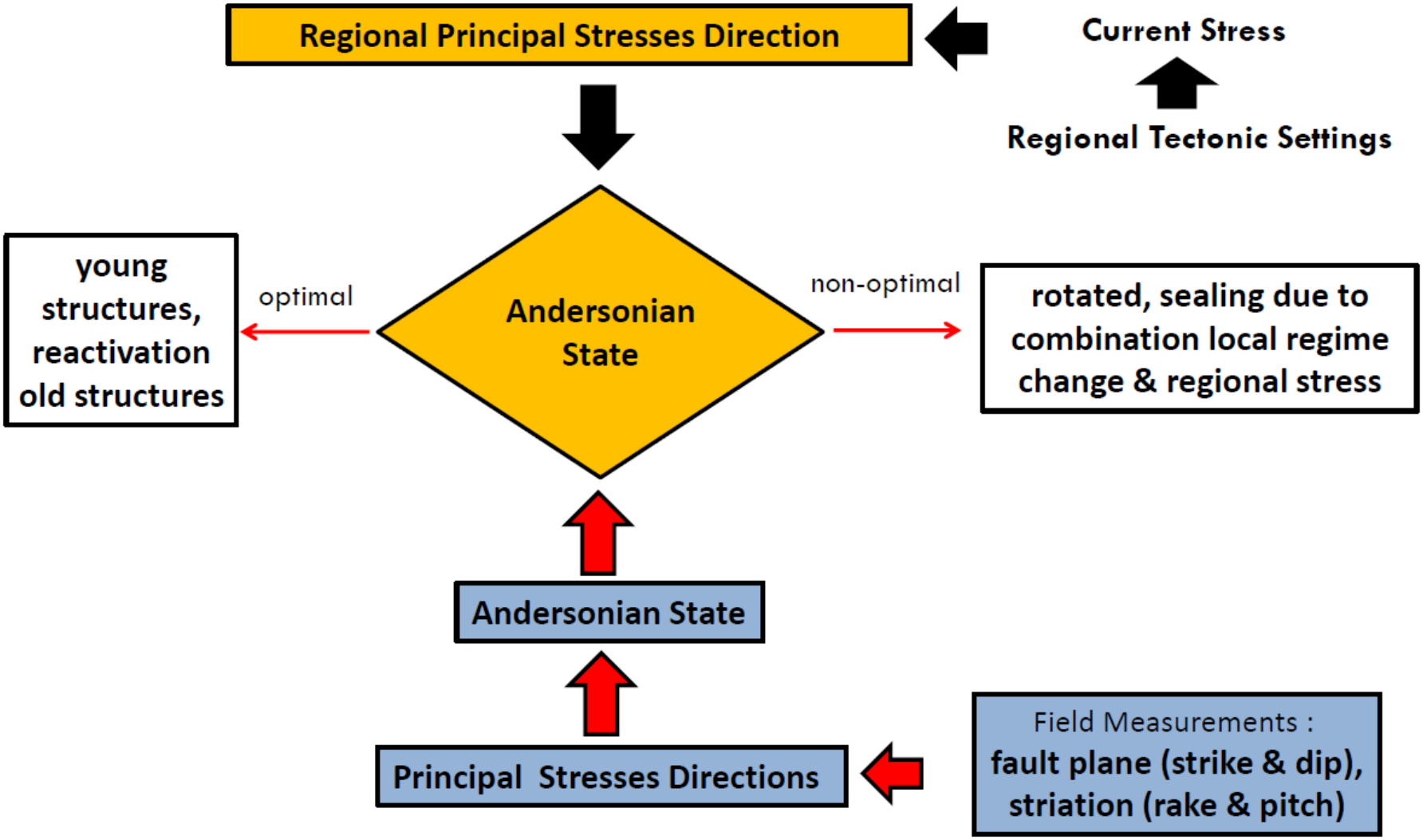

Figure 6. Flow chart of structural geological analysis in Tarutung Basin

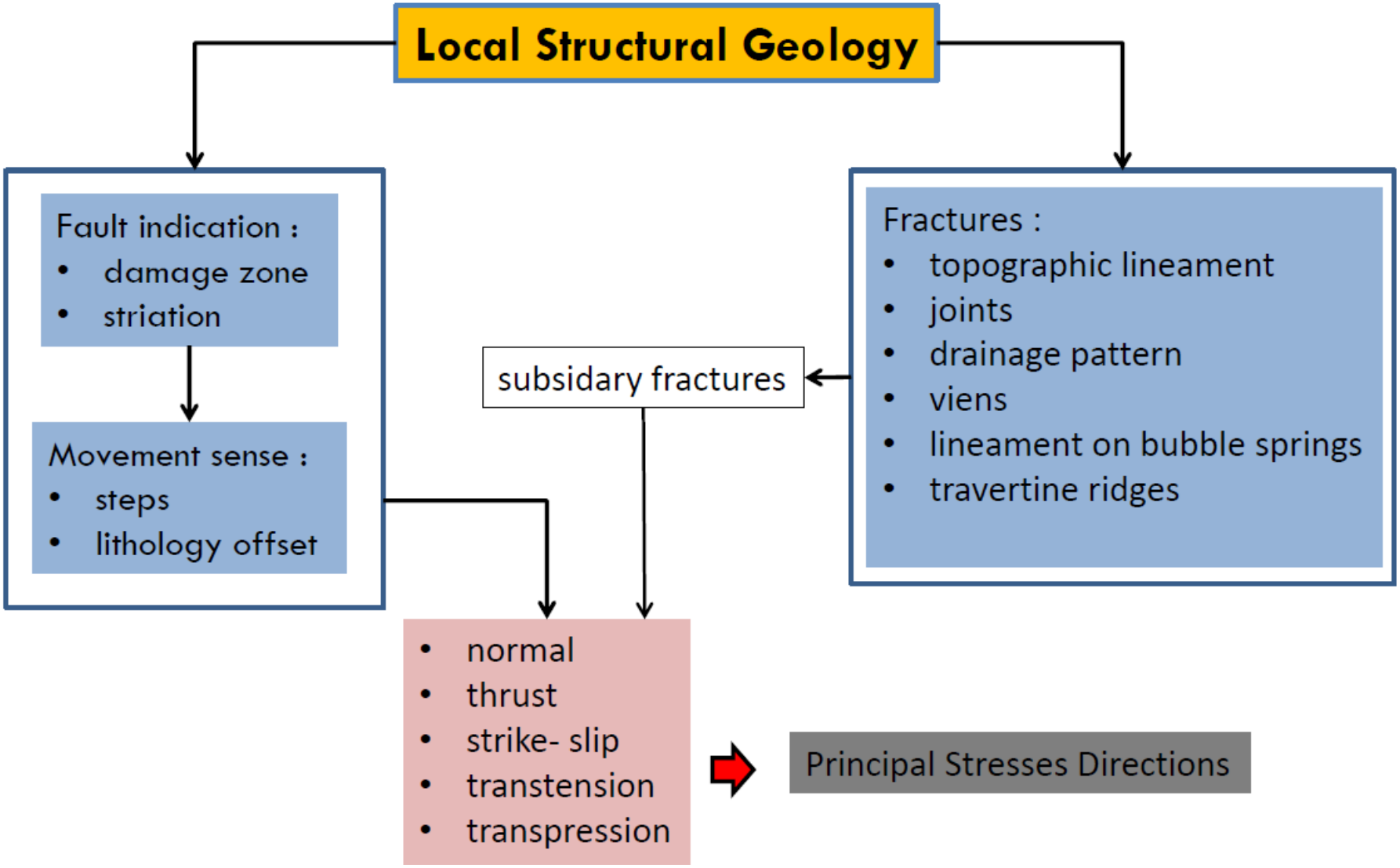

Figure 7. Flow chart of structural geological measurements to define principal stresses directions

Chapter 4

Exploration of fault controlled for geothermal systems

4.1 Geothermal systems

Hydrothermal energy is defined as potential energy stored on hotwater or steam which are concentrated at a particular geological setting on the upper crust levels (Ellis & Mahon, 1977; Rybach, 1981). Hydrothermal systems are commonly convection dominated and require permeability to allow circulation, porosity for storage, and an elevated thermal gradient zone (Rybach, 1981). Most developed geothermal systems are located close to active plate boundaries, i.e. divergent, convergent, and transform margins (Moeck, 2013). Localization of a geothermal system relative to adjacent terrain is characterized by the occurrences of geothermal anomalies (Raybach, 1981) (see Section 3.2) which are the target zone of exploration activities.

4.2 Explorations for geothermal resources

Generally, exploration of geothermal prospects starts at locations where geothermal manifestations at surface indicate geothermal activity from the subsurface. Exploration gets challenging when geothermal systems are hidden or blind, or if dense vegetation and thick soil hides geothermal manifestations. In such cases an integrated approach combining field structural geology, geothermal mapping, and geophysical methods is required. The aim of such an exploration campaign is to identify which faults from a complex fault pattern dominates fluid flow, which faults act as barriers, and what the origin of fluids and heat source is.

In terms of geochemistry anomalies, the geothermal system would show a distinct chemical composition on its discharge points, in comparison with the chemical composition of the surface or ground water. The chemical compositions include the composition of solutes, gasses, or isotopes of the gasses and the solutes.

Geophysical anomalies in a high temperature and shallow geothermal system would be indicated by a lower resistivity anomaly, for an example, as controlled by the existence of hot liquid or clay as an alteration product (Bibby et al., 2009), or lower magnetic anomalies than the surrounding area as controlled by the existence of a demagnetized body due to hydrothermal alteration (Soengkono & Hochstein, 1992; Hochstein & Soengkono, 1997), or a lower P-wave velocity controlled by the existence of a dry steam in the reservoir (Zucca et al., 1994).

Those are a few examples from several geophysical methods which have been widely applied in hydrothermal exploration of convective systems (Moeck, 2013, submitted). However, the interpretation of those geophysical anomalies should be constrained by geological and geochemistry data to interpret the existence of the geothermal system as addressed in this research.

4.3 Exploration geothermal potential using structural geology concept and its combination with geochemistry

In a viable hydrothermal system, hot water and steam is transported through permeable structures or formations to reservoir with elevated porosity. A shallow permeable zone, where hot water or steam from the deeper reservoir are ascended and accumulated at shallow depth, has more economic value than a deeper one, because drilling of shallow wells is efficient. Thus, mapping of permeable zones become the major goal in exploration.

A vertical permeable zone or also known as conduit zone is mostly controlled by secondary permeability, i,e. in a fault system, rather than primary permeability control (Sibson, 1996) while lateral permeable zones are controlled by stratigraphy. In defining the fault system, it is important to understand regional tectonics and the context of local structural geology with respect to regional tectonics. Defining the local tectonic regime requires numerous field data.

Ideally, the structural geological work should be conducted parallel with geochemistry work to obtain information of the thermal fluid type and its origin, and an estimated subsurface temperature. Thus, by applying structural geology and geochemistry methods in the early exploration stage, two important parameters can be obtained, i.e. the location of favorable permeable zones, and estimated subsurface temperature. These two parameters will be used as important consideration for the next exploration and assessment.

In the following sections, an overview is given on structural geology and hydrochemistry.

4.4 Overview of structural geology

Transtensional and purely extensional fractures play a role as conduit for fluid flow (Sibson, 1986). An accurate fault interpretation will therefore help to better understand and quantify the relationship between fracture type, fracture orientation and permeability structure. Observing, recording and analyzing the structural inventory in the field will provide a basis for geological interpretation and structural controls on fluid flow.

The formation of fluid pathways through faults and fractures is governed by brittle tectonics, which is the dominating failure process in the upper 7-12 km crust. This crustal level also hosts geothermal reservoirs, and therefore geothermal reservoirs are dominated by brittle failure. The following section describes the field based applications structural geological analysis of brittle deformation, i.e. identification of deformation path, fault plane analysis, stress regime controlling the fault relationships between fault and spring location.

4.4.1 Brittle Deformations

The definition of deformation in a brittle structure type has been described by many workers. A deformation or a fault zone consists of a fault core, damage zone, and intact rock (Caine et al., 1996; Fossen, 2010). The fault core is an accommodated zone of the fault displacement which consists of anastomosing slip surfaces, unconsolidated clay-rich gouges, cataclasite, fault breccia and geochemically altered zone (Sibson, 1977; Chester and Logan, 1986). Damage zone comprises subsidiary fractures set, small faults and veins, and cleavage (Sibson, 1977; Bruhn et al., 1994; Caine et al., 1996). Formed fractures set related with the kinematic fault can be observed in the damage zone (Sibson, 1977; Scholz and Anders, 1994). The intact or protolith rock is a non-deformed zone.

4.4.2 Fault & Stress

Fractures in the upper crust of brittle are due rock stress exceeding rock tensile or shear strength. The orientation and type fractures are controlled by the direction of principal stresses. The relationship between faulting regime and stress regime was first described by Anderson (1942). His description is based on his field analysis on fault and dyke systems, and their analogy to rock mechanical experiments by Daubree (1879) (in Pollard & Aydin, 1988 and Angelier , 1994).

According to Anderson (1951), the relationships between faulting and stress regime are:

1) normal faulting stress regime; $\sigma_1 = \sigma_v$, $\sigma_H = \sigma_2$ parallel to faults strike, $\sigma_h = \sigma_3$ perpendicular to fault strike.
2) strike slip faults with $\sigma_1 = \sigma_H$ at about 30 – 45° to fault strike, $\sigma_h = \sigma_3$, and $\sigma_H = \sigma_2$.
3) reverse faulting with $\sigma_1 = \sigma_H$ perpendicular to fault strike, $\sigma_h = \sigma_2$ parallel to fault strike $\sigma_v = \sigma_3$.

Depending on stress field changes and orientation of faults in a new stress field, oblique faulting may result from non-optimally oriented faults or in a transtensional regime (Angelier, 1994; Fossen, 2010). Oblique slip or hybrid faults exhibit oblique slickensides; whereas dip slip fault exhibit slickenslides along maximum dip (Ramsay & Lisle, 2000; Fossen, 2010).

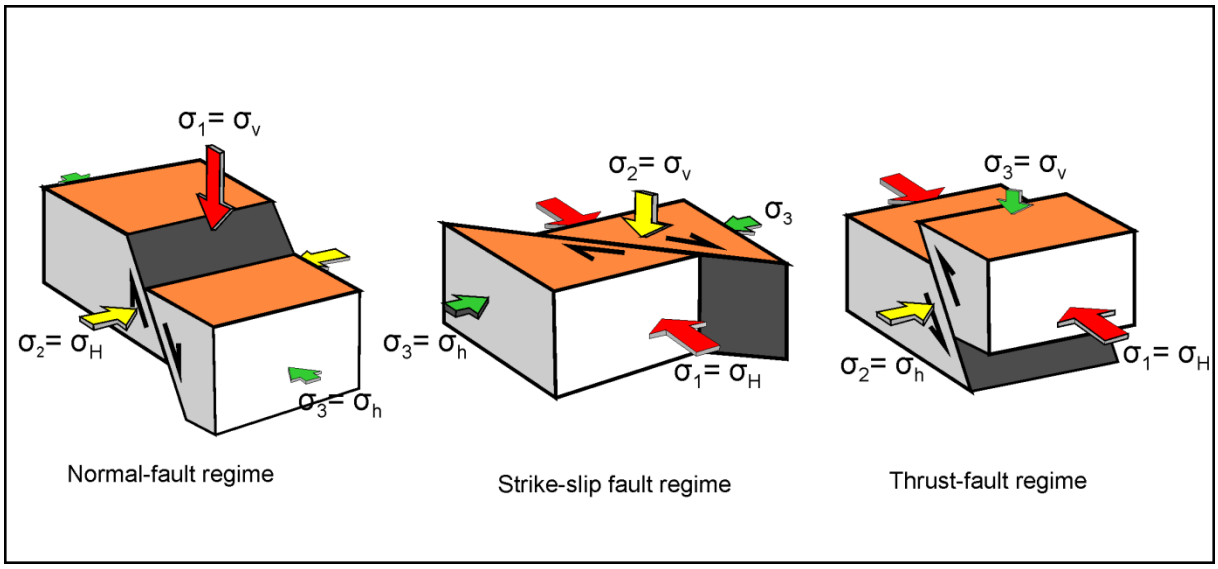

Figure 8. The relationships of principal stresses directions with the tectonic regime (after Anderson, 1951).

The orientation of shear fractures is controlled by the shears angle which is 30 – 45° for most brittle rocks with respect to the orientation of maximum principal stress (Fig. 9a). Extensional fracture stands in the plane of σ_1 and σ_2, and perpendicular to σ_3. Based on this relationship, stress orientation can be reconstructed or derived from fault outcrops (Ramsay & Lisle, 2000).

4.4.3 Fault and Structural Permeability

Extensional and extensional-shear fractures provide an open space which is also known as a permeable zone (Sibson, 1996). In other words, the directional permeable zone could be inferred from the orientation of extensional or extensional-shear fractures. Extensional fractures occur in a normal fault system, which strikes parallel with an intermediate principal stress or a maximum horizontal stress or ($\sigma_H = \sigma_2$). The direction of open space is perpendicular with a least principal stress or minimum horizontal stress ($\sigma_h = \sigma_3$). Meanwhile, a strike slip fault might have both extensional and extensional-shear fractures (Sibson, 1996). The extensional fractures in a strike slip fault strike parallel to a maximum principal stress or a maximum horizontal stress ($\sigma_H = \sigma_1$). In the case of a step over zone, which is a discontinuity zone within a strike slip fault, the extensional regime would generate a dilational jog. In a large scale the dilation jog is known as a pull-apart basin (Aydin & Nur, 1980; Segall & Polard, 1980).

Extensional-shear fractures generally occur in an oblique-strike slip fault. The extensional-shear fracture is associated with subsidiary fractures around the main fault which is also known as Riedel shears fractures after Riedel's (1929) clay experiment (Tchalenko, 1970; Woodcock & Shubert, 1994). The Riedel shears stand at a particular angle to main fault (M-plane). The Riedel which forms a low angle to the main fault plane is called a synthetic Riedel (R) shear; whereas a Riedel shear forming a high angle to the main fault plane is called an antithetic Riedel (R') shear. The sense movement of a synthetic Riedel is parallel to the main fault movement; in contrast, the movement of an antithetic Riedel shear is in an opposite direction to the main fault movement. In a step over setting, the extensional-shear

fractures might be interlinked with each other, or even with an extensional fracture forming a more complex permeable zone (Fig. 9c) (Sibson, 1996).

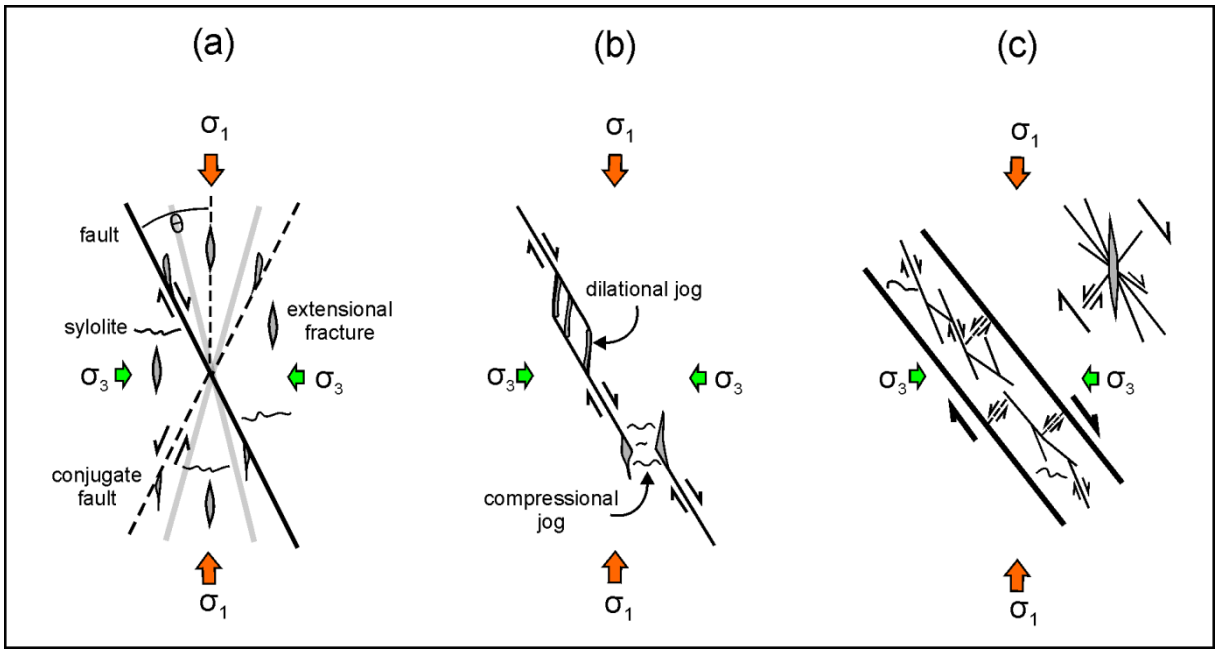

Figure 9. Various types of permeability structures (after Sibson, 1996). a) a relationships of stress with formed fractures; b) the permeability structures of compressional and dilational jogs within step over setting (after Segall & Polard 1980); c) the pattern of Riedel shears (after Tchalenko, 1970)

A permeable zone would have impermeable properties due to the presence of clay gouges within the fault core, or mineral precipitation from geothermal fluids filling the open fractures (Chester and Logan, 1996). The sediment filled by later process after the forming fault or during the faulting (i.e. shearing mechanism) might also cause a reduction of porosity and permeability of the fault zone. In such condition, only few amount of fluid does not nor lesser amount of it flow through the ultimate impermeable zone.

4.4.4 Kinematic Indicators

The kinematics of faults can be evidenced in several ways. The most obvious kinematic indicator is a displacement of a marker horizon. However, a marker horizon is not always

available. Therefore, people used other indicators to define a rock displacement, i.e. striations (Petit, 1987; Angelier 1994), mineral growth (crystallization) and ploughing (Fig. 10f; Petit, 1987) as observed on the fault plane (Fig.10). These striations represent the last movement of the faulted block (Ramsay & Lisle, 2000).

The kinematics of faults can also be identified by subsidiary fractures that are formed during slip along the main fault (m-plane in Fig.10). Petit (1987) defines these subsidiary fracture as tensile fractures, Riedel shears, and Pressure ridges (T-, R-, P-shears in Fig. 10b-d). Tensile fractures can be either tension gashes (Fig. 10b) or extensional fractures. The latter is caused by the movement along the major fault plane while tension gashes are oriented parallel to σ_1. Major plane is very often curved and indicate a small amount of shear from the center point of the convex shape. The convex shape indicates the movement of fault slips of the fault block on which the fractures are observed.

Riedel shear fractures are characterized by shear fractures dipping at an acute angle (<25°) with respect to a major fault plane. The acute angle and the orientation of the Riedel plane represent the sense movement (Fig.10b.i). Riedel fractures always dip against direction of the slip of the observed fault block. The intersection line of extensional fractures with a major plane can be a straight line (Fig. 10b.ii) or curved.

P-fractures are pressure ridges or compressional shear fractures dipping at a low angle in a slip direction of the observed fault block. P-ridges can also occur as an undulated surface (Fig. 10d, ii). Striation can only be clearly observed on a surface that is oriented towards slip movement acting as small scale ramps (Fig. 10d, i).Undulations on major slip planes are small scale pressure ridges, but do not show any striation.

Harder fragments, pebbles or any stronger mineral grains than a fault plane could form a lee and a ridge on its fault plane. This feature is known as ploughing (Fig. 10e). The sense movement of the observed block fault is shown on the opposite site of the ridges. The ploughing sometimes shows lineations.

The crystallization of mineral could occur on the small dilation jogs. The mineralization is extended along the ‘buried step’ as seen from the observed block (Fossen, 2010). The

sense of movement can be determined from the cross section of the observed block which is perpendicular to the extension of mineralization (Fig. 10f).

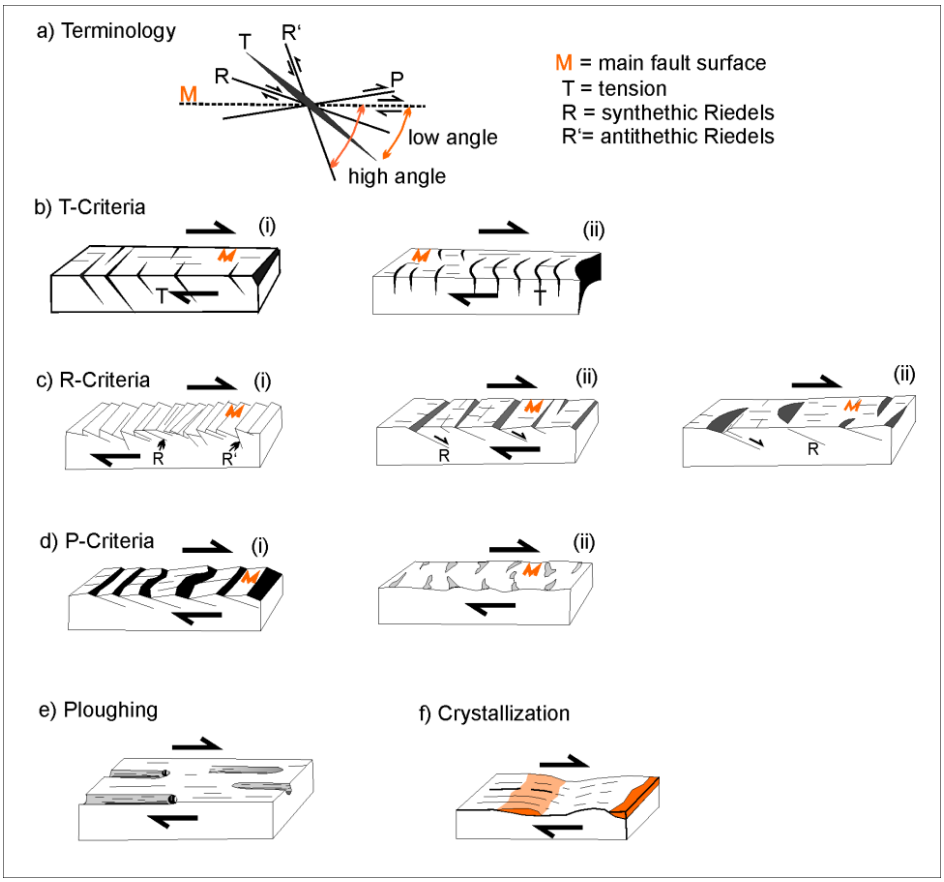

Figure 10. The indicators of fault kinematics (after Petit, 1987). The movement setting is in a dextral sense.

4.5 Overview of hydrogeochemistry, oxygen, deuterium, and helium isotopes

Fluid (e.g water and gas) geochemistry survey has been widely used in an early stage of geothermal exploration activities. The aims of fluid geochemistry analysis are to define the origin of the fluid, to outline the geothermal system (i.e. delineating an upflow and an outflow zone), and to estimate subsurface temperatures (Ellis & Mahon, 1977; Browne, 1978; Henley et al., 1984; Giggenbach, 1997; Arnorsson & Stefannson, 2007). The upflow

zone refers to the center area of a geothermal system, where the thermal fluid is flowing vertically; whereas the outflow zone refers to a peripheral area of the geothermal system where a lateral fluid flow is more dominant.

The concept behind a geochemistry method is that the composition of geothermal fluids results from the reaction between fluids and rocks (Ellis & Mahon, 1977; Giggenbach, 1988). The fluid-rock interaction itself is dependent on the temperature, pressure, pH, duration of interactions, mineral composition of the host rock, sources of recharge waters and contribution of volatiles from magmatic or metamorphic sources (Ellis & Mahon, 1977; Browne, 1998; Browne & Rodgers, 2006).

Fluid mixing and boiling process which occur during ascending fluid from depth to the surface would also influence chemical concentrations of the remaining fluid as well as its ultimate temperature (i.e. cooling state) (Fournier, 1979; Arnorsson et al, 2007). The flow rate of the fluid, however, plays a role in the residence time of geothermal fluids within a system to interact with the host rock. The flow rate of the fluid itself is controlled by either the initial amount of the fluid or the permeability structure of the host rock (Fournier 1979). Hence, by understanding the chemical processes as discussed above with some constraints from geological settings (i.e. permeability structure and also hydrological factor), a geochemical analysis would provide a better meaning for interpreting the subsurface conditions.

The major focus of geochemistry analysis in this research is on water geochemistry (later called hydrochemistry) analysis, in which I collected the fluid sample from the field; whereas a gas geochemistry interpretation is performed based on a survey result from other researchers (i.e. Halldorrson et al., 2013). The fluid sampling procedures are described in Chapter 3, Section 3.2.

4.5.1. Major composition of hydrothermal solution

Major compositions of a hydrothermal solution based on anions concentrations comprise of chloride (Cl^-), sulfate (SO_4^{-2}) and bicarbonate (HCO_3^-). Because of its unreactive properties, chloride water is used as an indicator of a deep fluid source. The sulfate water

originates from the oxidation process of hydrogen sulphide (H_2S) from a steam condensation by cooler waters at shallower depth. The bicarbonate water in a geothermal system is due to absorptions of carbon dioxide (CO_2) and a steam condensation into cooler groundwaters (Hedenquist, 1990), which commonly occurs at the peripheral area of a geothermal system (i.e. ouflow zone), particularly at a volcanic setting (Hochstein & Browne, 2000). In this thesis, the presence of bicarbonate waters on a geothermal system is compiled with other information (i.e. oxygen and helium isotope, geothermometry result, and equilibrium state) for characterizing the heat source of the geothermal system in Tarutung Basin (Chapter 7). The result of the analysis also proposes an idea for interpreting a heat system at other low geothermal systems (Chapter 8). The data presentation of these three major anions (Cl^-, SO_4^{-2}, and HCO_3^-), with their setting on a geothermal system, could be shown on a ternary diagram as introduced by Giggenbach (1988).

The major cations of a hydothermal solution comprises of Na, K, Mg, Ca (Henley 1984; Giggenbach, 1997; Marini, 2000). The concentration of these cations within a solution is controlled by equilibration and dissolutions processes of the fluid and rock, as well as by the compositions of the host rock. The condition of equilibration, which is called an equilibrium state, represents the reaction condition in which no further ion exchange occurs. In such an equilibrium state, the amount of a product and the reactant are shown in an equal amount (Fournier, 1989).

In the context of a geothermal system, an equilibration process occurs in a high temperature system (Giggenbach, 1997); whereas a dissolution process occurs in a low temperature system. Several techniques of data presentations are available for cations analysis, i.e. ternary diagram and binary diagram. Both diagrams (i.e. in Na-K-Mg Ternary Diagram and Na-K-Mg-Ca Diagram of Giggenbach, 1988) are also complemented with equilibrium lines indicating a temperature in which the system reaches an equilibrium state. Data deviations from the equilibrium line indicate a dissolution process which dominate the system instead of an equilibration process (Reyes, 2010; Hochstein 2010 & 2013).

Geothermal waters also contain significant traces elements such as boron (B^{+3}) and lithium (Li^{+}) in comparison with non-geothermal water. B^{+3} has a volatile and soluble character in a high temperature condition (Ellis & Mahon, 1977; Glover, 1988). Due to its soluble character, B^{+3} remains in the solution after they are expelled from the rocks and would not be ready to interact with secondary minerals (Mahon, 1970); hence, their concentration in the solution is relatively un-changed (Schmidt et al., 2011). The latter properties of B^{+3} provide that B^{+3} could be used as an indicator for host rock composition (Schmidt et al., 2011). In case field studies in Los Humeros geothermal field (Mexico), a single linear trend of B^{+3} and Cl^{-} indicate a particular reservoir; whereas a variation trend on their correlation line shows a different reservoir (Bernard et al., 2011).

4.5.2 Geothermometry

Geothermometry is a temperature estimation method which considers the concentration of silica or cations (i.e. alkalies) on the fluid as collected from surface springs or geothermal wells. The assumptions of a geothermometry method are (Fournier, 1977); 1) the equilibrium state of fluid and rock is achieved (see Section 4.5.1 for a definition); 2) there are neither re-equilibration states nor fluid mixing occurring during the fluid flow; 3) a temperature-dependent reaction involving rock and fluid occur within the system. In a non-equilibrium state, the cations geothermometer would not represent the actual temperature since the reaction is in imbalance (see: the geothermometry assumptions). Alternatively, the silica geothermometer is selected and used. However, a selection of silica geothermometer type (i.e consisting a quartz, chalcedony, and amorphous silica) should be performed by considering their solubilities (described below). This case occurs in the geothermal system of Tarutung Basin as discussed in Chapter 7, Section 7.7.

Silica geothermometer is used based on their solubility on the solution, which is temperature dependent. The assumptions of silica geothermometer are (Fournier, 1989); 1) equilibrium of fluid and quartz occurs; 2) fluid mixing does not occur during ascending fluid to shallower depth. Among the three silica polymorphs, chalcedony has very fine

crystal grains in providing a larger surface energy than quartz; hence, their solubility is higher than quartz, particularly within a medium temperature system (< 120°C) (Fournier, 1989). The quartz itself is more soluble in a high temperature system.

The type of dissolved silica in a solution could be determined from the relationships of silica concentration (i.e. log concentration of SiO_2) with respect to the concentration of potassium and magnesium (i.e. log concentration of K^2/Mg) (Giggenbach & Glover, 1992). The temperature in which the silica and the other two cations (i.e. K & Mg) attained an equilibrium state is estimated by using K/Mg geothermometer of Giggenbach (1988). The equilibrium line is included within the diagram of log SiO_2 versus log (K^2/Mg) (Chapter 7, Fig. 24) (Giggenbach & Glover, 1992).

4.5.3 Oxygen Isotopes

Rock is mostly consisting of oxygen and its isotope can be exchanged with the circulating fluid (Craig, 1963; Truesdell & Hulston, 1980; Blattner 1985). The composition of oxygen stable isotopes is dependent on the isotope fractionation which occurs due to isotope exchange reactions, mass differences from chemical reactions, and physical processes. These physical processes are evaporation, boiling condition, and fluid mixing. The isotope fractionation can be different depending on the fluid origin, i.e. rain water, sea water, and magmatic water (Faure, 1991). Hence, oxygen stable isotope analysis can be used to identify the physical processes of the water circulation and transport pathways, and also the environment of the water origin.

Craig (1963) describes for the first time the environmental origin of the water from geothermal springs based on oxygen and hydrogen stable isotopes. Most of the geothermal water has depleted oxygen and lies at the proximity of the meteoric water line (Craig, 1963). These results suggest that geothermal water originates mainly from meteoric water (Ellis & Mahon, 1977; Truesdell & Hulston, 1980).

The elevation where waters are located also affects the concentration of the oxygen stable isotope. The water from a higher elevation would have a lower oxygen isotope because lower precipitation commonly occurs in higher elevations where the temperature is lower (Clark & Fritz, 1997).

4.5.4 Helium Isotopes

Noble gases can be used as an indicator to identify and characterize fluids of different origin (e.g, deep mantle, asthenosphere mantle, lithospheric mantle, and crust) (Ballentine et al., 2002). The inert and volatile characters of noble gases (i,e. not reactive with the surrounding host rock during their ascent and its mobile attitude) make them useful traces in a geochemical analysis.

One of the noble gases used in a geothermal exploration is Helium (He) isotopes, which comprises ^{3}He and ^{4}He. ^{3}He is derived from the mantle (Mamyrin & Tolstikhin, 1984) and is also referred to as primordial helium (Craig & Lupton, 1976; Mamyrin & Tolstikhin, 1984). In contrast, most of ^{4}He is formed by radioactive decays of parent nuclides (e.g. Uranium and Thorium) (Ballentine at al., 2002).

By definition, helium isotope ratios are given in the R**a** notation (**a** stands for **atmospheric**) in which 1R**a** = $(^{3}He/^{4}He)$**a** = $1.388 * 10^{-6}$. As an end member, the helium isotope from mid-ocean ridges, which are generally 8 R**a,** can be used. In contrast, the R**a** from the crust is generally less than 0.1 (Craig & Lupton, 1976; Mamyrin & Tolstikhin, 1984).

In the case of an investigation area situated at a distance from the mid-ocean ridge, mantle derived helium is probably transported through a crustal extension or by an orogeny process (Ballentine & Burnard, 2002). Additionally, helium from magma generation and degassing can contribute to the total helium budget (Oxburgh et al., 1987; Ballentine & Burnard, 2002). In brief, tectonic setting and the presence of a magma chamber could control the helium isotope as sampled from hotsprings or wells (Polyak & Tolstikhin, 1985; Oxburg & O'Nions, 1987).

Chapter 5

Structural controls on Sipoholon geothermal field, Tarutung Basin.

Most of materials in this chapter is published in Journal of Asian Earth Sciences, 74, 2013, 86-96., by authors : Mochamad Nukman & Inga Moeck

5.1 Introduction

Fault in the vicinity of Tarutung basin are indicated by the striations fault planes, and also orientation of extension gashes and Riedel shear fractures (Fig.11). The striations (Fig.11a,b,f) are mostly observed in magmatic rocks as Miocene andesite and Pleistocene dacite. Striations are hardly observed in the travertine, therefore fault slip analysis in the travertine is conducted by measuring and recording the orientation of Riedel shears (Fig. 11d).

5.2 Structural geology and geothermal manifestations

5.2.1 Northern and Eastern basin edge

The northern basin shoulder is dominated by N-S to NE-SW oriented fracture sets and E-W to NW-SE striking fault planes as shown in stereographic great circle plots (Fig.13). Striations indicate left-lateral slip along ENE-WSW faults, oblique reverse faulting along

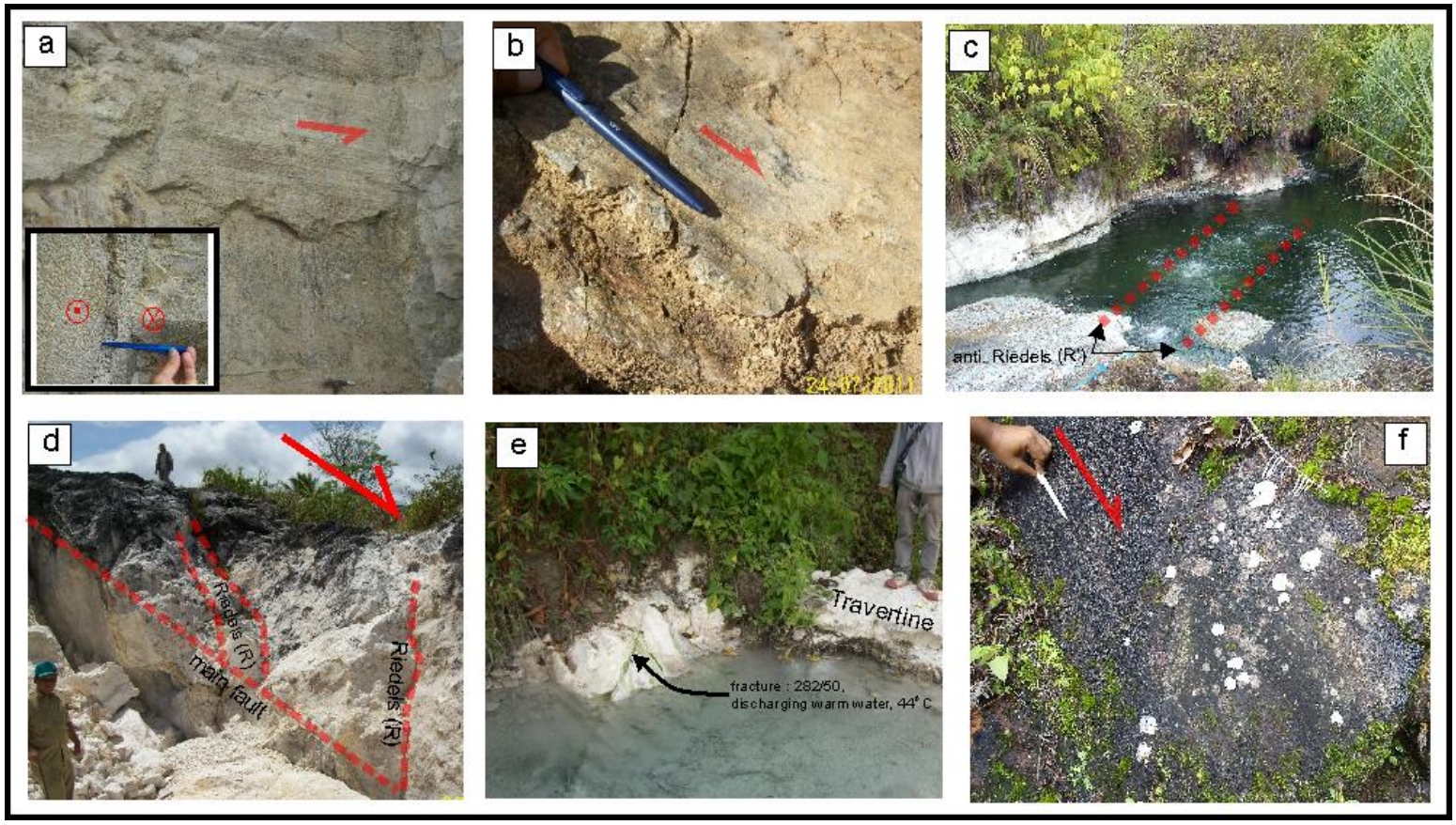

Figure 11. Exposure of striations, steps, Riedel shears fracture, and bubble springs lineaments as observed at various lithologies; a) Striations on dacitic rock unit shows left lateral movement. Fault gouges are also observed. Loc: Silangkitang (SLK); b) Steps on andesitic Miocene showing normal movement. Loc: Rumah Kapal (RK); c) Bubble springs lineaments on a spring pond; Loc: Hutabarat (HTB); d) Riedel shear fractures on travertine exposures show a right-lateral movement. Loc: Ria-Ria; e) A minor normal fault as observed on travertine in Akbid-Sitompul; e) Striations indicating a normal oblique fault on andesite Miocene. Loc: Ugan (UG).

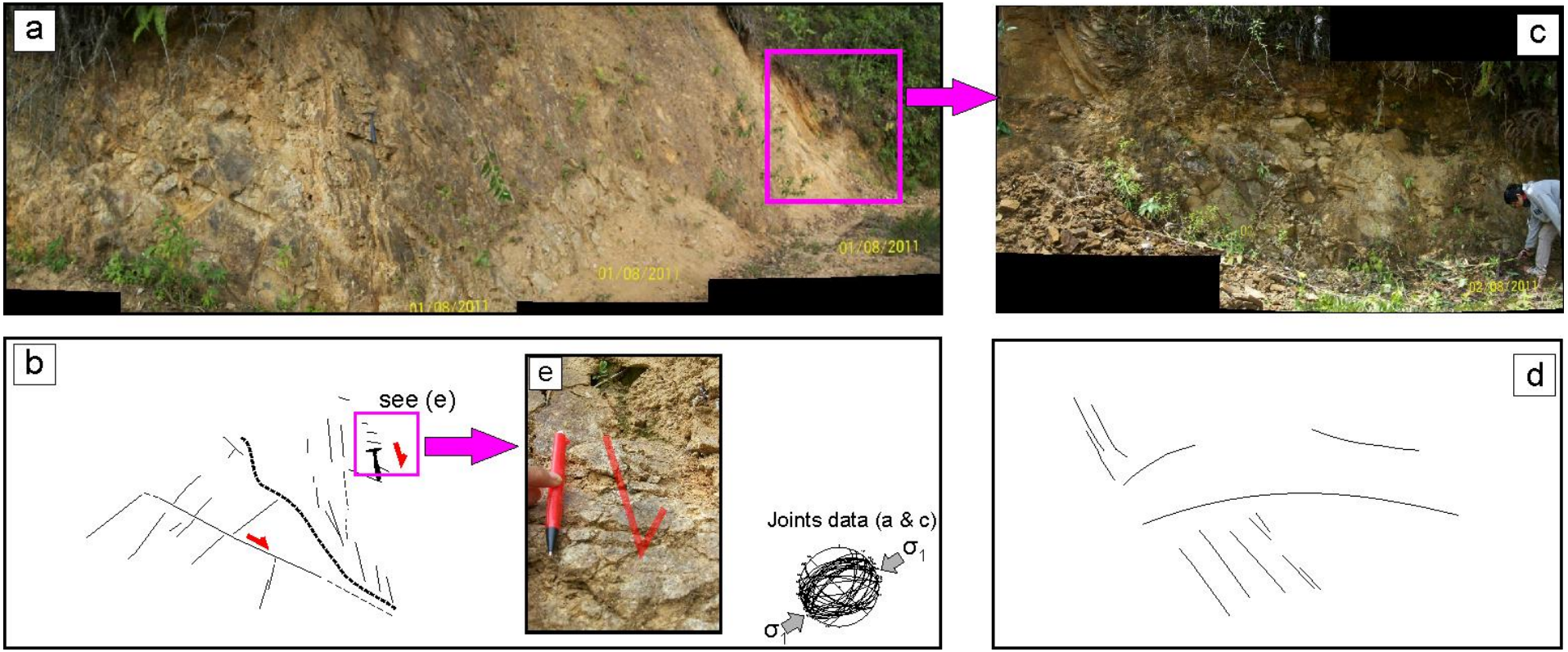

Figure 12. Joint system andesite Miocene at Rumah Kapal exposure shows NE-SW trend (**a-b**). Striations in this ourcrops indicate a normal fault striking WNW-ESE (e).

Table 2. Fault slip data from the Tarutung Basin (see also Appendix 1)

	Dip Direction*(°)	Dip *(°)	Trend *(°)	Plunge* (°)	Lithology	Features **	Kinematics
Silangkitang	352	74	88	37	dacite	striations with fault gauge	sinistral
Hutabarat	5	62	345	60	andesite	steps	thrust
Akbid	221	46	174	35	andesite	steps	normal
Rumah Kapal	187	66	179	68	andesite	steps	normal
Ugan	44	71	335	42	andesite	striations	normal oblique
PNB 1	236	61	224	60	dacite	steps	normal
PNB 2	52	65	36	65	dacite	steps	normal
PNB 3	49	66	41	66	dacite	steps	normal
Sitaka	55	69	64	61	andesite	steps	thrust
Tunjul	219	60	_	_	andesite	quartz veins	normal***

* dip direction, dip, trend, plunge are in average value
** movement indicators based on Petit's (1987) classification
*** vertical fractures as Riedel shears indicating normal faulting

WNW-ESE faults and normal faulting along WNW-NW oriented faults at the southern basin shoulder. Normal faulting also occurs along N-S trending faults in the southern basin region. As identified by the DEM map, the river network follows the NW-SE trend as well as the N-S trend possibly tracing fracture zones whereas NE-SW trending rivers follow the general topographical gradient towards the basin centre. The average of fault slip and raw data are compiled in Table 2 and in the Appendix 1 subsequently.

Cold springs are discharging at a location where several sets of Riedel shear fractures consisting of NW-SE and NE-SW striking fractures are exposed (Fig. 14a, joint stations 1-3). The springs are aligned along a lineament striking NNE-SSW. Bubbles gas, probably CO_2, is also discharging from these springs.

An ENE-WSW striking sinistral fault is exposed north of Ria-Ria in the dacitic TukTuk unit (fault SLK in Fig.13). The fault plane is steeply dipping towards NNW and filled with fault gauge consisting of unconsolidated fine grained fluvial sand with a thickness of 2-3 cm (Appendix 1a). This fault has obviously an impact on the river valley morphology. Approximately 400 m southward of the outcropping fault, the river turns sharply from a N-S to E-W direction forming a nearly orthogonal bend (Fig. 13). Several warm springs discharge in the river valley directly at a cross point where the ENE-WSW striking left-lateral fault transects a NNW-SSE striking fracture zone. The pH value of these springs is low (i.e. 1.26 - 2.3).

Further south a WNW-ESE striking fault indicates reverse faulting in the Miocene andesitic of Toru Formation (location HT in Fig.13). Striations and steps indicate dip slip reverse faulting. At the southern edge of the Tarutung Basin two sets of normal faults strike E-W and NW-SE, (locations RK for Rumah Kapal; and AK for Akbid in Fig. 13). The E-W striking normal fault is a dip slip fault associated with nearly vertical sheeting joints whereas the NW-SE striking normal fault is associated with N-S oriented travertine dykes.

5.2.2 Western basin edge

The western edge of the Tarutung Basin is dominated by WNW-NW striking faults and a complex fracture pattern. In Miocene andesite of the Toru Formation a gentle dipping (40-50°) N-S oriented fault is exposed where the sense of slip could not be determined through slickensides (location TJ stands for Tunjul in Fig. 13). The fault is accompanied with a set of N-S trending vertical fractures which could have served as Riedel shears indicating normal faulting.

Further south a WNW-ESE oriented reverse fault is exposed in the Toru Formation (location STK in Fig. 13). The hanging wall of this reverse fault is characterized by sheeting joints possibly formed through horizontal compression. The footwall consists of unconsolidated laharic breccia probably representing a younger rock unit. A narrow steep canyon occurs at the damage zone of the fault hanging wall. Oblique striations on a 70-80° NE dipping fault plane indicate oblique normal faulting (location Ugan in Fig. 13 & Appendix 1f). The fault can be traced to a cliff towards northwest direction where warm springs discharge (location AN in Fig. 13).

The complex fault pattern of normal and reverse faults indicates local compression and extension which can be observed at major strike slip faults. Possibly rotation of fault blocks might have induced this deformation pattern with implications on fluid flow along local extensional zones.

5.3 Interpretation

Fault plane analysis helped to identify fault kinematics in different parts of the Tarutung Basin edge; however the data set from nine outcropping faults with sufficient numbers of slickensides is too small to employ stress inversion from fault slip data to determine the stress field. Geothermal exploration in fault controlled systems requires, however, a systematic concept to delineate fractures from a complex fault and fracture pattern acting as conduits and barriers. One possibility to determine which faults are preferential fluid pathways is to look at their structural position and their strain type within the present-day stress field.

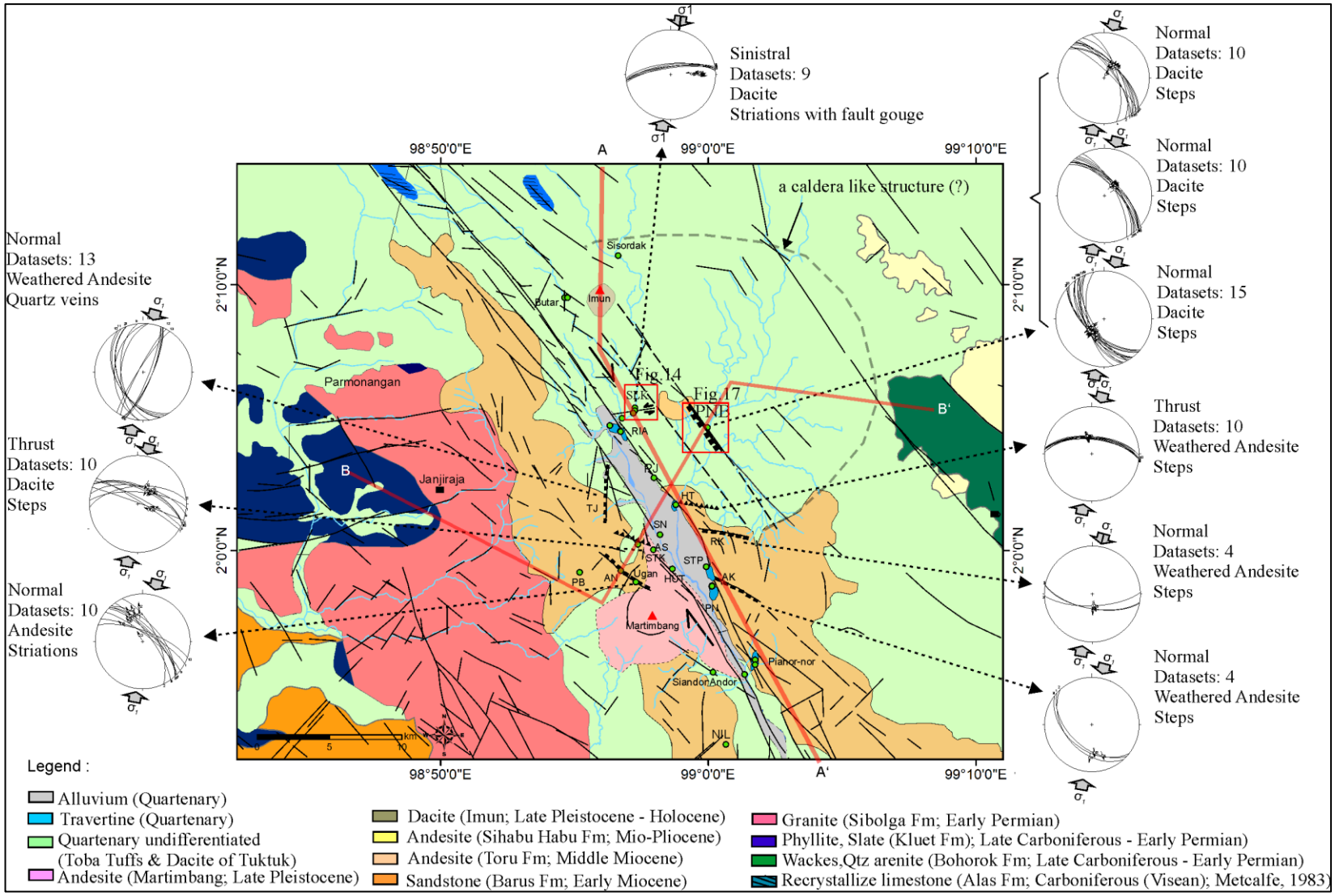

Figure 13. The result of structural measurements are shown in lower hemisphere projections. The interpreted faults, current findings of springs and geothermal sinters sites are overlaid on the existed geological map of Tarutung Basin by Aldiss et al. (1983), Clarke et al. (1982, and Apsden et al. (1983) (see also Fig. 28). Abbreviations*: SLK* = Silangkitang*; RIA* = Ria-Ria; *PNB* = Panabungan; *HT* = Hutabarat; *STP* = Sitompul; *PN* = Pansur Napitu; *PB* = Pancur Batu; *AS* = Air Soda; SN = Sait Nahuta; *AN* = Aek Nasia; *TJ* = Tunjul; *AK* = Akbid; *RK* = Rumah Kapal; *NIL* = Namora- I-Langit; *STK* = Sitaka.

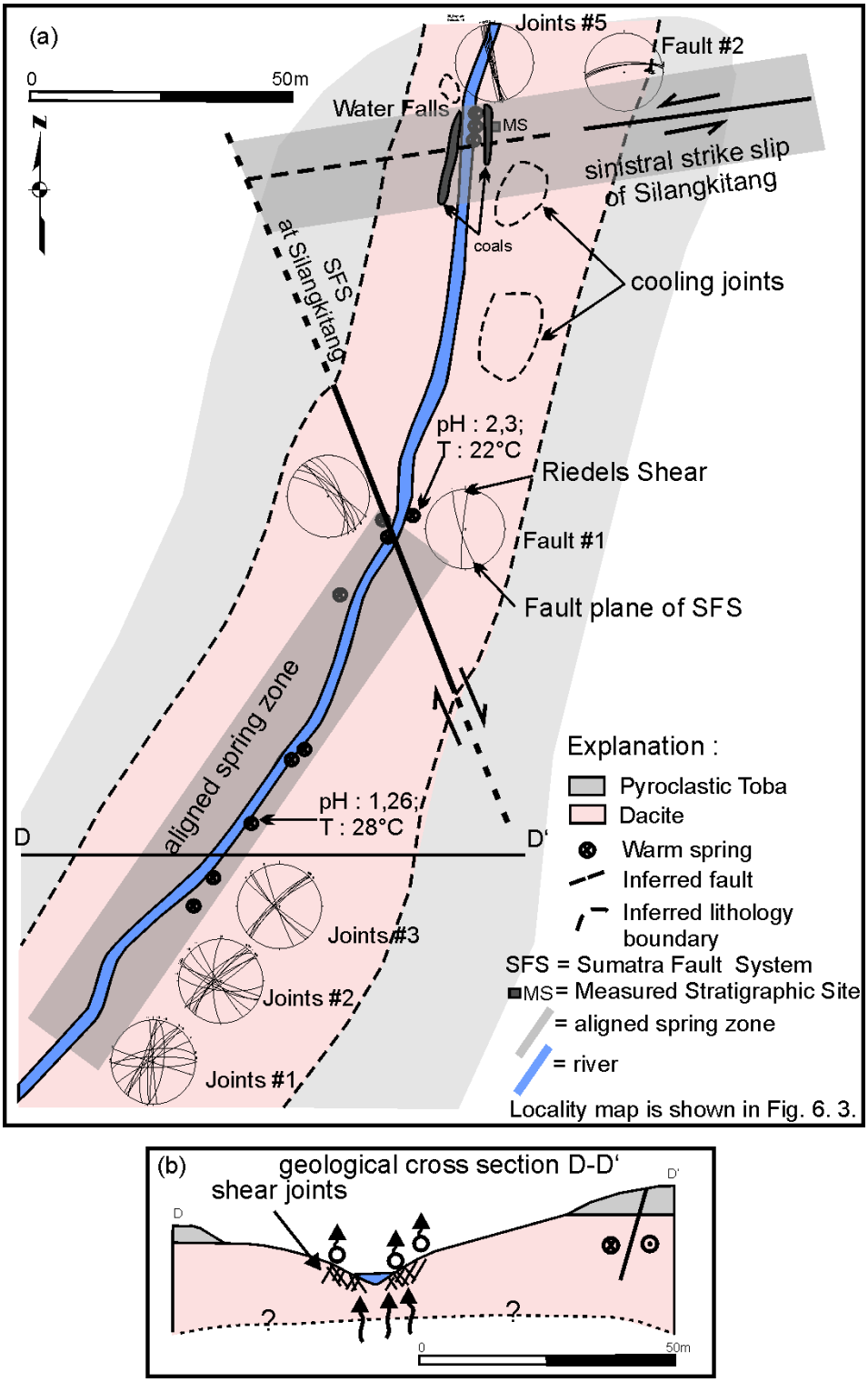

Figure 14. a) Detailed structural geological map of the area SLK = Silangkitang as indicated by left red box in Fig. 13. The sinistral strike-slip striking nearly E-W forms a high angle to SFS while the aligned spring zone (ASZ) forms a low angle to SFS. Joints at station 1, 2, and 3 shows a shear joint type and discharging cold springs. (b) An E-W geological cross section of the Silangkitang area shows the occurrences of springs associated with shear fractures along the riverside.

The pattern of faults types, fractures, joints and travertine dykes can be used to determine if the fault and fracture pattern is consistent with the stress regime provided all fractures were generated in the same stress field. This approach is based on the assumption that in brittle tectonics, faults and fractures have a specific orientation to the stress regime that caused faulting assuming the Andersonian faulting concept (Anderson, 1951) (see Section 4.4.2). Optimally oriented faults form in angle of 30-45° to the maximum principal stress resulting in conjugate left- and right-lateral shear faults whereas extensional fractures are perpendicular to the minimum principal stress and compressional reverse faults are perpendicular to the maximum principal stress. The present-day stress field in north central Sumatra is still under debate. Whereas GPS data indicate a plate motion in NNE-SSW with oblique collision along the Sumatra arc (Cattin et al. 2009), the maximum principal stress direction is variable along the Sumatra fault (Cattin et al., 2009).

The regional deformation pattern as well as fault plane solutions from seismic data indicate a right-lateral strike-slip stress regime with the maximum principal stress axis in N-S (McCaffrey et al., 2000; Cattin et al., 2009). In such a stress regime one would expect a conjugate set of NW-SE and NE-SW striking strike-slip fracture, N-S striking extensional fractures, right-lateral Riedel shears in NNW-SSE direction and left-lateral Riedel shears in NNE-SSE direction, respectively, and E-W oriented reverse faults or compressional fractures. In contrast, Cattin et al. (2009) pointed out that in the region of the Tarutung Basin the maximum principal stress direction is in NE-SW within a strike-slip stress regime. Under this condition, the NW-SE striking faults would be compressional whereas NNE-SSW and ENE-WSW striking faults would act as strike-slip faults, and NE-SW fault would be extensional fractures (Fig. 15). From this perspective it is now worth to look at the structural pattern of fractures and faults and their strain type derived from field observations in the Tarutung basin.

The main fault types are (Fig. 15):

- Sinistral ENE-WSW fault striking 88° dipping NNW (*SLK*)
- Normal faults in WNW-ESE to NW-SE direction striking between 95 and 135° (*RK* & *STP*)
- Reverse or compressional faults in WNW-ESE direction (*STK & Ugan*)
- N-S oriented extensional fractures with aperture up to 70 cm (*Pianor-nor*)

- N-S, NW-SE and NNE-SSW striking travertine dykes indication dilative fractures allowing massive fluid flow and precipitation of calcium carbonate (blue symbols in Fig.5.5.

This fracture and fault pattern reflects a typical strike-slip related fracture pattern associated with compression at a high angle to the principal deformation zone (PDZ) (Storti et al., 2001) (Fig. 15b). After this concept the WNW-ESE striking normal faults would be related to negative flower structures whereas N-S trending normal faults would be generated under compression at a high angle to the principal deformation zone.

The normal faults striking parallel to dextral strike-slip fault of SFS as outcropping in *Panabungan* might reflect the compression which is parallel with *PDZ* (Fig. 15&17). Similarly, reverse faults in WNW orientation can be also generated in such a strain regime with compression at a high angle to the principal deformation zone (PDZ; Fig. 15). Conjugate synthetic and antithetic Riedel shears in NNW-SSE to NE-SW direction complete the secondary fracture pattern of a right-lateral shear zone under compression at a high angle to the principal shear zone. The ENE – WSW striking left-lateral fault could be rotated in a clockwise sense or it reflects local rotation of the stress field or it is generated under an older paleostress field (Fig.15).

Geothermal manifestations as travertine and hot springs (temperature of 38-66°C; Table 2) are predominately exposed at the eastern side of the Tarutung Basin and not at the western side where older volcanoes could serve as heat source with their subsurface remnants of magma chambers. One reason for the concentration of geothermal manifestations at the eastern side of the SFS could be a high amount of dilation caused by rotation due to right-lateral simple shear. Clockwise block rotation between right-lateral NW-SE striking fault segments could have generated dilations jogs and fractures where preferentially fluids discharge. This hypothesis is supported by the ENE-WSW striking left-lateral fault (Fault STK in Fig. 15) which could have been previously NE-SW oriented in a strain regime with

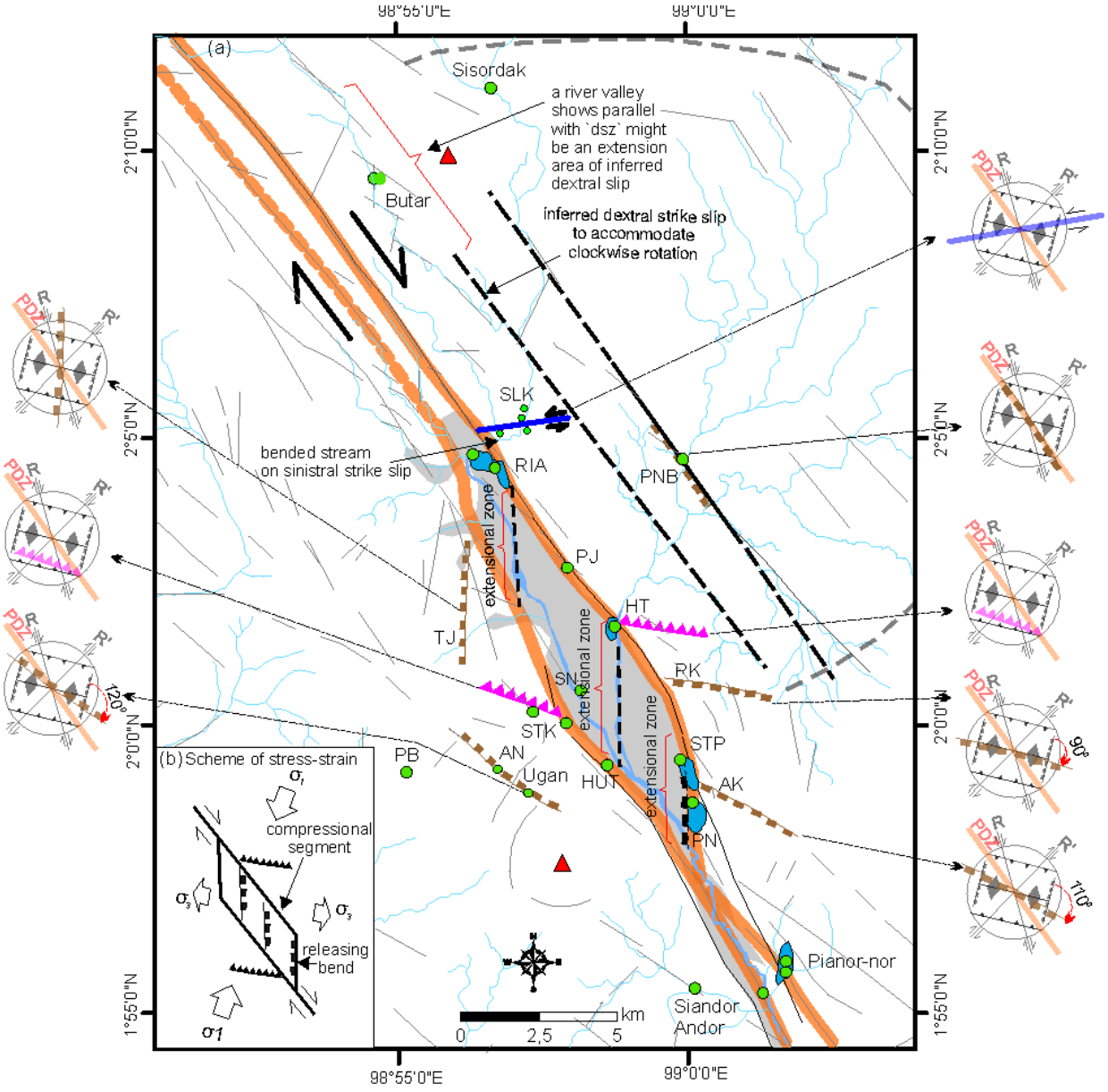

Figure 15. (a) Summary of the structural characteristic of the Tarutung Basin. The measured structures are compared with the theoretical fracture pattern forming NNE-SSW compressional strike –slip faulting. The orientation of measured structures at individual sites with respect to the theoretical fracture orientation is shown alongside the map. At location RK, AK, and AN clockwise rotation might have occurred due to dextral simple shear along the PDZ. PDZ = Principal Deformation Zone, R= Riedel shear, R'= anthithetic Riedel shear. Abbreviation of location as in Figure 13.(b) Scheme of tress-strain for the fault pattern in the Tarutung Basin. The presence of an E-W striking thrust fault with respect to the NNE-SSW current maximum stress direction might indicate compressional structures acting as sealing faults for fluid flow.

compression at a high angle to the SFS. The SFS fault is however hard to identify in the field because the extensive Toba Tuff formation covers possible fault exposures. In the satellite image this major dextral fault is identifiable extending to northwest as indicated by NW-SE oriented lineaments and river channels (Fig. 15).

It is noteworthy that regional clockwise rotation of Sumatra occured by an amount of 20° over the last two million years (Ninkovich, 1976; Nishimura, 1986) which also supports the thesis of local rotation at the Tarutung Basin. The south-eastern basin margin is occupied by travertine exposures striking N-S and 3-4 km long. This margin might represent a releasing bend of the Tarutung Basin (Fig.15b). Releasing bends in a pull-apart basin are highly extensional (Dhont et al., 1998) and are preferential locations for fracturing and fluid flow (Cunningham & Mann, 2007). In the Tarutung Basin, this extensional strain zone might have caused an increased process of the travertine precipitation from bicarbonate rich waters. However, the travertine is only exposed at the south-eastern releasing bends. Travertine might originate from limestone of the Alas Formation locally distributed beneath the basin, probably only distributed below the eastern and south-eastern basin margin. The interpretation stratigraphic position of this Alas Formation is shown in Regional Stratigraphic Scheme in Figure 5. Sealing fault or fault gauge in the SFS might prevent migration of the carbonate fluids to the north-western margin.

Whereas dilational fractures represent preferential fluid pathways as indicated by hot springs and travertine dykes, compressional fractures seem to act as barrier. The chemical analysis of fluids and gas sampled at the hot springs shows that the northern part of the Tarutung Basin is geochemically different from the southern part (Chapter 7). Whereas in the northern part acidic cold fluids discharge, in the southern part at Ria-Ria and south of it alkaline hot springs discharge. The bound between these domains is sharp along an ENE-WSW striking left-lateral fault. Under the current strain regime with a high angle compressional to the SFS this ENE-WSW striking fault would be compressive and presumably locked for fluid flow.

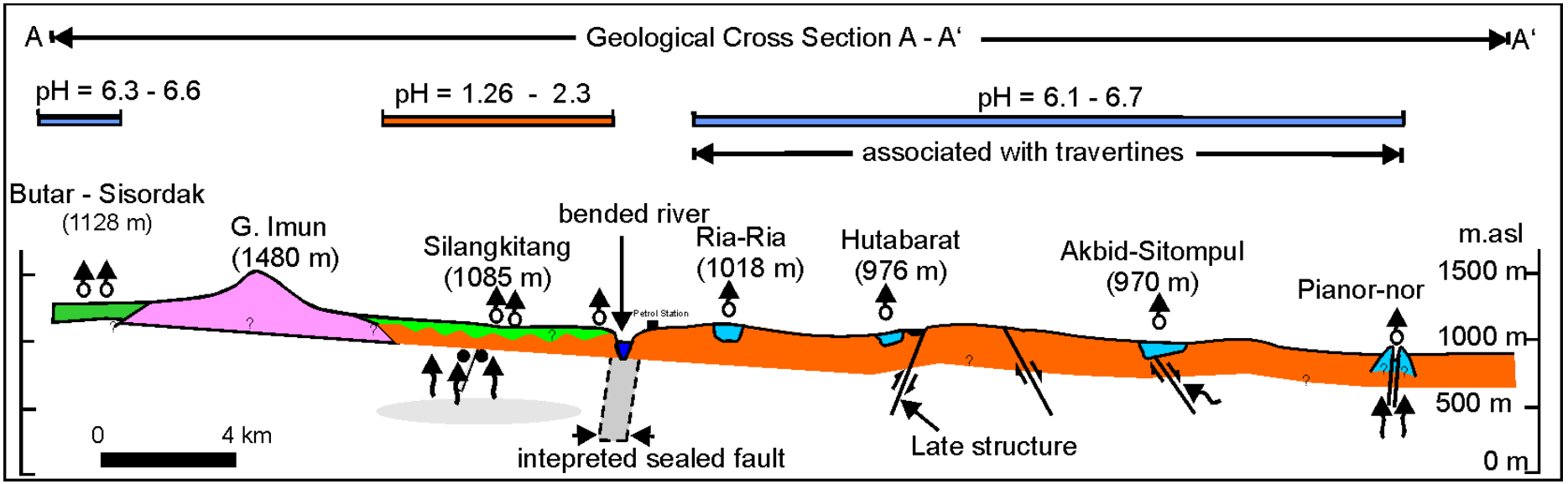

Figure 16. Geological cross section in N-S direction referring to the geological map in Figure 13 overprinted with thermal manifestation locations and their pH value.

5.4 Conclusions

Hot springs with high flow rates and travertine dykes occur only at the eastern and south-eastern side of the Tarutung Basin whereas volcanoes are located at the western side of the basin. The present-day inactive volcanoes might not relate to the hot springs at the eastern side. The temperature of the hot springs decreases from east to west where the volcanoes are located. This is a further indication that the volcanoes or their old magma chamber might not contribute to the geothermal activity in the Tarutung Basin. Chemical analysis of the hot springs from the eastern side and from warm to cold springs from the western side will deliver further indication how the hot springs are related to each other and from what source or reservoir they might discharge (see Chapter 7). Structural geological field work indicates that the geothermal activity is controlled by the extension along the eastern side of the Tarutung Basin possibly caused by clockwise block rotation and accompanied opening fractures along the right-lateral SFS. At the north-eastern side a circular morphology might represent a caldera underneath presumable a heat source might feed the hot springs.

Comparing the location of hot springs and travertine ridges with their internal fracture pattern, NW-SE and NNW-SSE to N-S and NNE-SSW trending fractures host most of the geothermal manifestations. The NW-SE trending faults represent right-lateral strike-slip faults, NNW-SSE and NNE-SSW trending fractures represent Riedel shears and N-S trending fractures represent extensional fractures within the current stress field, characterized by compression at a high angle to the principal deformation zone, the dextral Sumatra Fault System. This result is consistent with presumed present-day maximum stress direction in NNE-SSW direction although some faults as WNW-ESE normal faults can also be generated in a negative flower structure setting under a maximum principal stress direction in N-S. Fault plane solutions of earthquakes confirm this variability of the maximum principal stress direction between N-S to NE-SW (Cattin et al., 2009) probably as a result of the oblique subduction along the Sumatra arc.

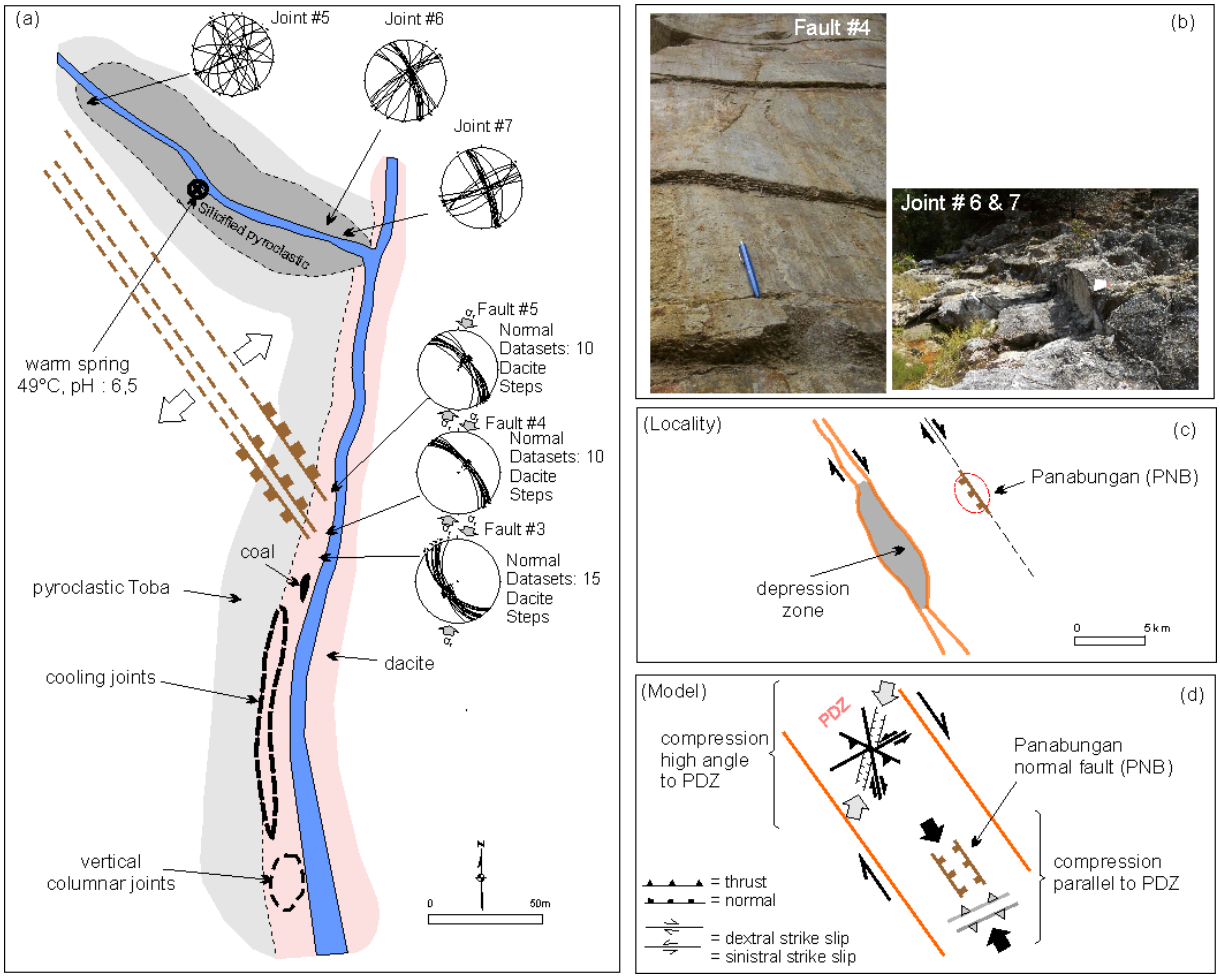

Figure 17. (a). A detailed geological map of the Panabungan area, which is located 5 km east of Tarutung Basin (right red box in Fig. 13). (b) Steps on a large fault in Pleistocene dacite unit indicating a dip slip normal fault at location #4. At location ‘6 and ‘7 contain a vast number of NW-SE trending fractures parallel to the SFS as well as NE-SW striking fracture patterm possibly forming anthithetic Riedel shears assuming the secondary fracture pattern scheme of Storti et al., 2001 as illustrated in (d). (c) Location of Panabungan with respect to the Tarutung Basin. The presence of the large dip slip normal fault might indicate the dimension of area influenced by the deformation zone of the Sumatra Fault System. (d) Stress-strain model for compressional strike slip faults after Storti et al. (2001) comprises two types; (1) compression at a high angle to PDZ and (II) compression parallel to PDZ. Panabungan normal faults may represent compression parallel to the PDZ.

A complex fault pattern of extensional and compressional faults controls the Tarutung Basin. The non-optimal orientation of nearly E-W oriented left-lateral strike slip faults which cannot be generated in the present-day stress field, are presumable rotated faults, now being under compression. Compressional nearly E-W striking faults might act as barriers in the Tarutung Basin, indicated by acidic and alkaline springs separated by an E-W striking fault. A detailed analysis of the fluid chemistry of the hot springs will clarify the compartmentalization of the subsurface reservoir and the source of the fluids with implications on the impact of faults and fractures acting as conduits or barriers.

Favourable settings for geothermal utilization are at the east side of the Tarutung Basin whereas the inactive volcanic region on the western side seems not be a favourable location for geothermal utilization. Deviated wells with an inclination in N-S direction might be most preferable because a maximum of shear fractures representing preferential fluid pathways would be crossed by such a well geometry.

Our results demonstrate that field structural geology contributes significantly to the understanding of geothermal fields and can guide further exploration campaigns even in tropical environments with limited numbers of outcrops. Subsurface data from magnetotelluric and possibly seismic surveys might help to define heat source and geometry of the geothermal field. However, fault controlled geothermal systems as the Tarutung Basin do not exhibit a typical steam-brine interface with accompanied alteration clays so that conventional geothermal exploration methods as applied in volcanic fields might not be appropriate exploration methods. Greenfield exploration in Indonesia should incorporate field structural geological surveys to delineate preferential fluid pathways from a complex fracture pattern in the current stress field to ultimately contribute to successful development of geothermal fields.

Chapter 6

Travertine in Tarutung basin as indicator of the present-day extensional stress regime

This is an extended version from a sub-chapter of my published work on Journal of Asian Earth Sciences, 2013, vol. 74, p. 86-96

6.1 Introduction

The dynamics of neotectonic activities could be represented on the travertine exposures, which is known as travitonic (Altunel & Hancock, 1993; Hancock et al., 1999; Brogi, 2013; and references therein). A combination of both continuous fractures opening and calcium-bicarbonate rich water inflow on available opened fractures provide hints on deposited travertine for the current dynamics of tectonic activities (Nishikawa 2012) and is currently used as a strategy for geothermal and ore-deposit exploration (Brogi et al, 2012) to delineate a permeable zone on a hydrothermal system.

One of the early regional geological mapping works at Tarutung by Aldiss et al., (1983) and Apsden (1982) shows travertine exposure sites only on Ria-Ria and Hutabarat. Travertine exposure at Sitompul area was additionally described by Hasan et al (unpublished report, 2005). Newly travertine exposures at Akbid, Pansur Napitu and Pianor-nor areas are currently mapped by Nukman & Moeck (2013).

The occurrences of travertine in Ria-Ria were interpreted as part of an outflow zone from an unidentified high temperature system in the eastern area (Hochstein & Sudarman, 1993). However, my findings show that this travertine is an indication of a dissolution process at crustal depth, indicating an upflow zone rather than an outflow zone of the geothermal system (see Chapter 7). The deep crustal fluid is transferred to a shallower depth along SFS as shown from recent hydrochemical studies (Chapter 7). The vertical structures of the SFS serving as a fluid pathway is confirmed by an earthquake epicenters cluster as shown on passive seismic (Muksin et al., 2013a).

In this dissertation, the morphology of travertines and their fractures are analyzed to determine the type of fracture and their possible control on the present-day permeability structure in the geothermal system of the Tarutung Basin.

6.2 Methods

The structural data were measured majorly in the form of joints and open-fissures (Fig. 18 & 19). Striations are hardly observed on the travertine in this area. Hence, the kinematics sense of the fault is determined from the orientations of Riedel shears with respect to the interpreted major fault plane (Fig.19a). The trends of fracture and travertine ridge are compiled into a lower hemisphere projection. Stress analysis is performed by comparing the compiled fracture and ridges trend with known maximum principal stress direction (e.g. N-S to NNE-SSW).

6.3 Data Field Description

The travertine exposures in the Tarutung Basin are only distributed at the eastern and southeastern margin of the basin and form morphological ridges or dykes aligned along a NW-SE oriented lineament. NW-SE striking faults are not widely outcropping along the basin margin, but the NW-SE trend of major fracture planes are observed in Ria-Ria area (Figure 21a) and on DEM image. Travertine dykes are well exposed because the hard travertines are more resistant to weathering than the surrounding softer fluvial deposits.

There are three clusters of travertine exposures which are exposed on the eastern margin of Tarutung Basin, and 1 cluster is located off the basin in the southeastern area (Figure 20). They are located in the normal faults dipping to the west toward the depression zone. Spacing among each site on the three clusters is 4-5 km (Figure 20). All the travertine is deposited on the hanging wall of the normal fault blocks. In the following sections, the geographic sites of travertine exposures are described.

6.3.1 North of Tarutung Basin (*Ria-Ria*)

Ria-Ria travertine is characterized by its massive structures. The total dimension is 1.6 x 0.7 km, extending in NW-SE direction (Figure 19). Vertical veins striking 135 ° with various thicknesses up to 75 cm are filled with calcites and only minor aragonites. Hot water rich in calcium-bicarbonate-sulfate with a maximum temperature of 65.5°C is discharging through the fracture plane (Figure 19a). Sulphur deposits are also observed along the fault plane (Fig. 19b). Some filled calcite veins form a low angle to the NW-SE trending fracture planes (Figure 19a), indicating synthethic Riedel shears. The position of the Riedel shears with respect to the major fracture plane indicate a dextral movement along the NW-SE fault plane with is parallel to the SFS (Fig. 20).

6.3.2 Eastern margin of Tarutung Basin (*Hutabarat; HT*)

Hutabarat travertines are located in southeastern Ria-Ria (~ 5.3 km). The ridge cluster is parallel with the river bend in N-S. Fractures are hard to be observed, except a lineation of bubble gas within the spring pond striking NNE-SSW (N 18°) (Nukman & Moeck, 2013). The spring has a temperature of 44°C. The trend of the Hutabarat ridges in N-S is parallel

to maximum horizontal stress of the regional stress tensor in NNE-SSW are indicating subsequently of major extensional fractures and its Riedel shear fractures.

6.3.3 Southeastern margin of Tarutung Basin (*Sitompul-Akbid-Pansur Napitu*)

This area is the SE margin of the pull-apart basin of Tarutung which may act as the releasing bend segment of the basin. A laminated weak brittle travertine is the characteristic for the travertine cluster in the area of Sitompul-Akbid-Pansur Napitu. The travertine outcrop shows a NE-SW trend which is parallel with the lineaments on the southeastern margin of the basin as delineated from DEM map. The recent hot springs discharge through fractures on travertine in N-S to NNE-SSW direction.

6.3.4 Far South of Tarutung Basin (*Pianor-nor; PIA*)

Exposure travertine Pianor-nor has massive layers characteristic, forms an elongated ridge striking in N 18°. Open fractures up to 100 cm in width are observed at the centers of ridges. Seasonal thermal springs with significant sulfate content discharge from these open fractures. Maximum temperature of springs in this area could reach 42.5°C.

6.4 Discussion

The major trend of travertine fractures in Tarutung is mostly striking in NNE-SSW; while travertine ridges trends majorly in N-S and NW-SE. The fractures with N-S trend might be generated by current maximum principal stress in N-S direction which forms tension gashes in the direction. However, two travertine ridges orientations at Ria-Ria and Pansur Napitu areas are striking in NW-SE direction. The NW-SE trend of travertine ridge might suggest a transtensional regime (i.e strike slip fault with extensional component) rather than a pure strike slip on the dextral Sumatra Fault System (Nukman & Moeck, 2013).

A dynamic discharge rate of calcium-bicarbonate rich water and opening fractures are clearly shown in Pianor-nor travertine (Fig.18). The fractures without filled by calcite precipitation suggest two causing effects:

1) the rate of extension is faster than the fluid discharge rate,

2) a periodic (seasonal) fluid discharge controls the availability of thermal fluid at shallower depth.

The open fractures are in E-W direction perpendicular to the dominant travertine ridge trend in N-S along the current maximum principal stress σ_1 (Fig. 20 b & c) which presently could represent new fractures trending as formed by current stress. Precipitation of calcite from calcium-bicarbonate rich water takes place in fractures that open in σ_3 direction and strike along σ_1 (Fig. 20 b & c).

In contrast to open fractures in Pianor-nor's travertine (Fig. 18), fractures sealed with calcite and aragonite occur predominantly at the other three sites (Ria, HT, ST, PN). These travertines are deposited on the flank of the basin margin which is controlled by steeply dipping normal faults. Extensional viens would be oriented parallel to these normal faults. Precipitation of calcite from calcium-bicarbonate rich water will occur due to a pressure drop when entering the open fracture. This extensional tectonic related mechanism occurs at most travertines in other field in the worlds, e.g. Turkey and western Italy (Altunel & Hancock, 1993; Brogi 2010).

The localization of travertine on the eastern margin of Tarutung Basin might also suggest that the source of bicarbonate-rich geothermal fluid is from underneath the basin, with a preferential fluid flow to the eastern direction where the high extensional strain zones are dominant. A vertical structure of low resistivity value is also shown underneath the eastern margin of the Tarutung Basin, from magnetotelluric survey result of Sintia et al. (2013) which confirms the geological interpretation.

The fractures along the Tarutung Basin margin are induced by the tectonically active of SFS associated to the convergent plate margin (McCaffrey, 2009). Recent passive seismic investigation of Muksin et al (2013a) shows that an enormous amount of current local earthquakes occur along Tarutung Basin and Sarulla field (2856 events within 10 months recording period). This earthquake swarm could reactivate older fractures, maintaining the

existing permeability zone or creating a new fluid pathway which plays a role in hydrothermal fluid upwelling (Sibson, 1997).

6.5 Conclusions

The travertine studies in Tarutung Basin could characterize the present-day permeability structure in the area, i.e. 1) open fractures (also called extensional fractures) are striking N-S to NNE-SSW which occur at the eastern and southeastern margin of Tarutung Basin; 2) the open fractures in the northwestern margin of the basin and at the south of the basin are striking NW-SE; 3) extensional fractures are dipping vertical; 4) Those extensional fractures are formed likely on the oblique strike slip faulting rather than a pure strike slip system.

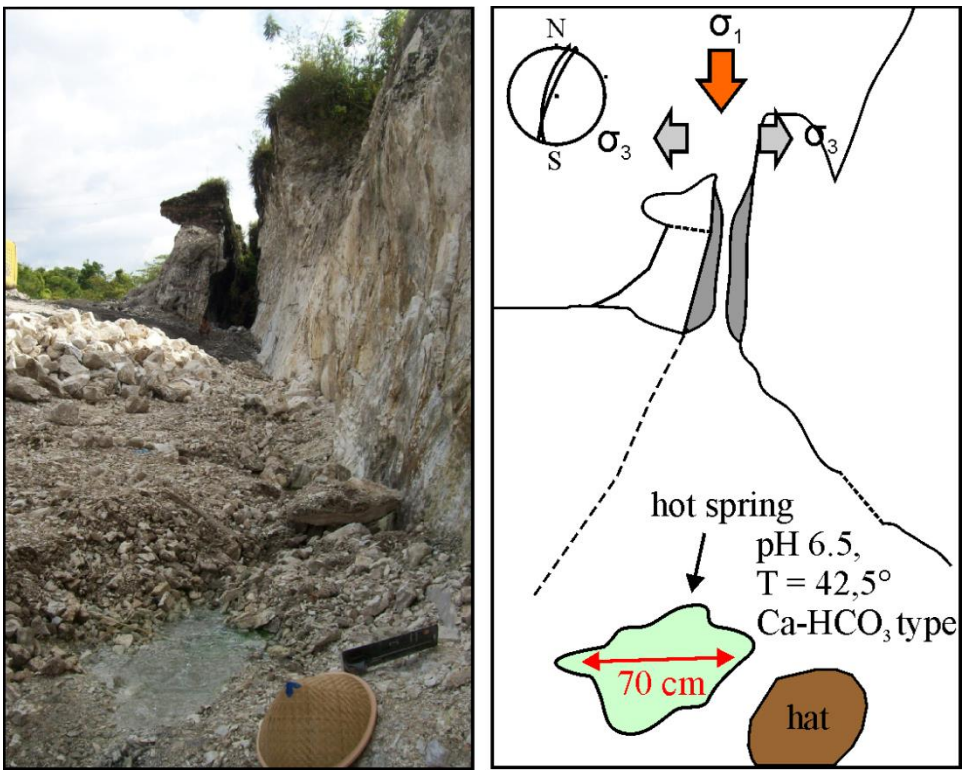

Figure 18. Open fractures on the massive travertine is exposed in Pianor-nor area striking in NNE-SSW. Warm springs with a low discharge rate (< 1 l/s) are discharging from the centers along the open fractures. Locality this exposures is shown in Figure 7.3.

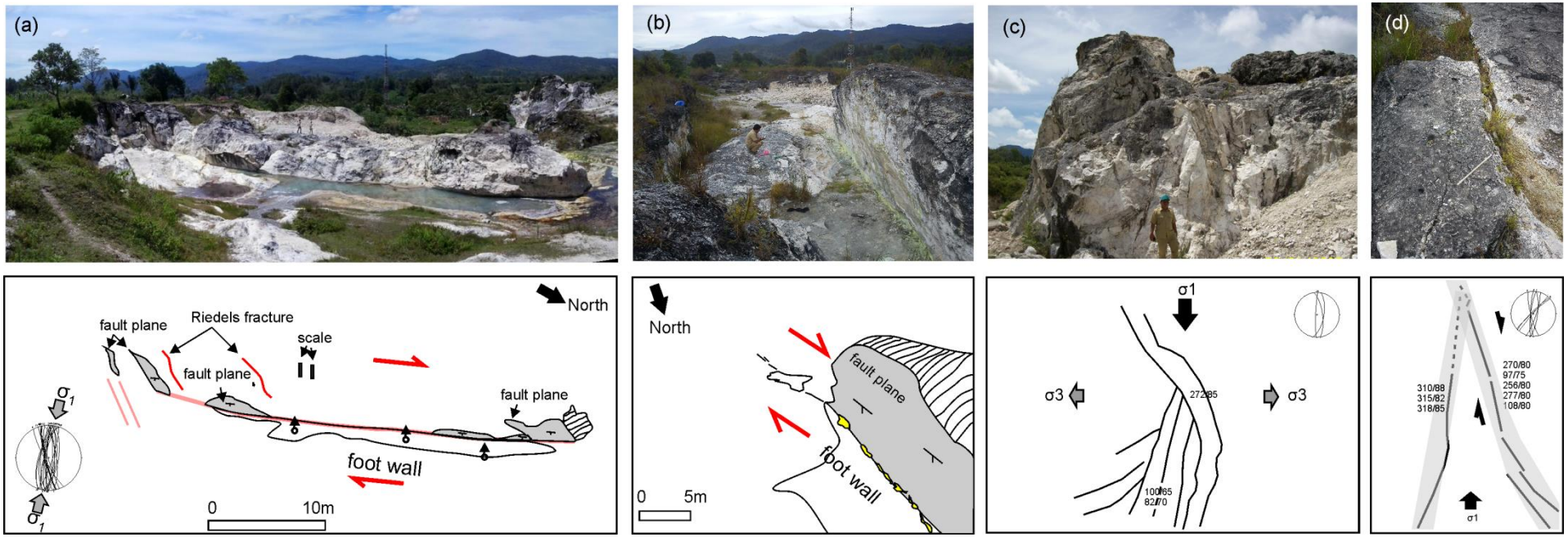

Figure 19. Exposure of travertine with active spring discharge at Ria-Ria area. The ridges of travertine are in elongated shape trending NW-SE. The orientation of Riedel shear fractures with respect to major fracture (a) is used to determine the kinematic of fault in this area (i.e. dextral strike slip).b) Dry sulphur deposit is observed at the margin of fault plane where the spring has been discharged.c) Exposure of travertine showing vertical layers as exposed at Ria-Ria area; A) The minimum stress is in horizontal direction (i.e. E-W) suggesting an extensional regime control. d) The Riedel shear fractures among the major fractures show an indication of a dextral sense movement.

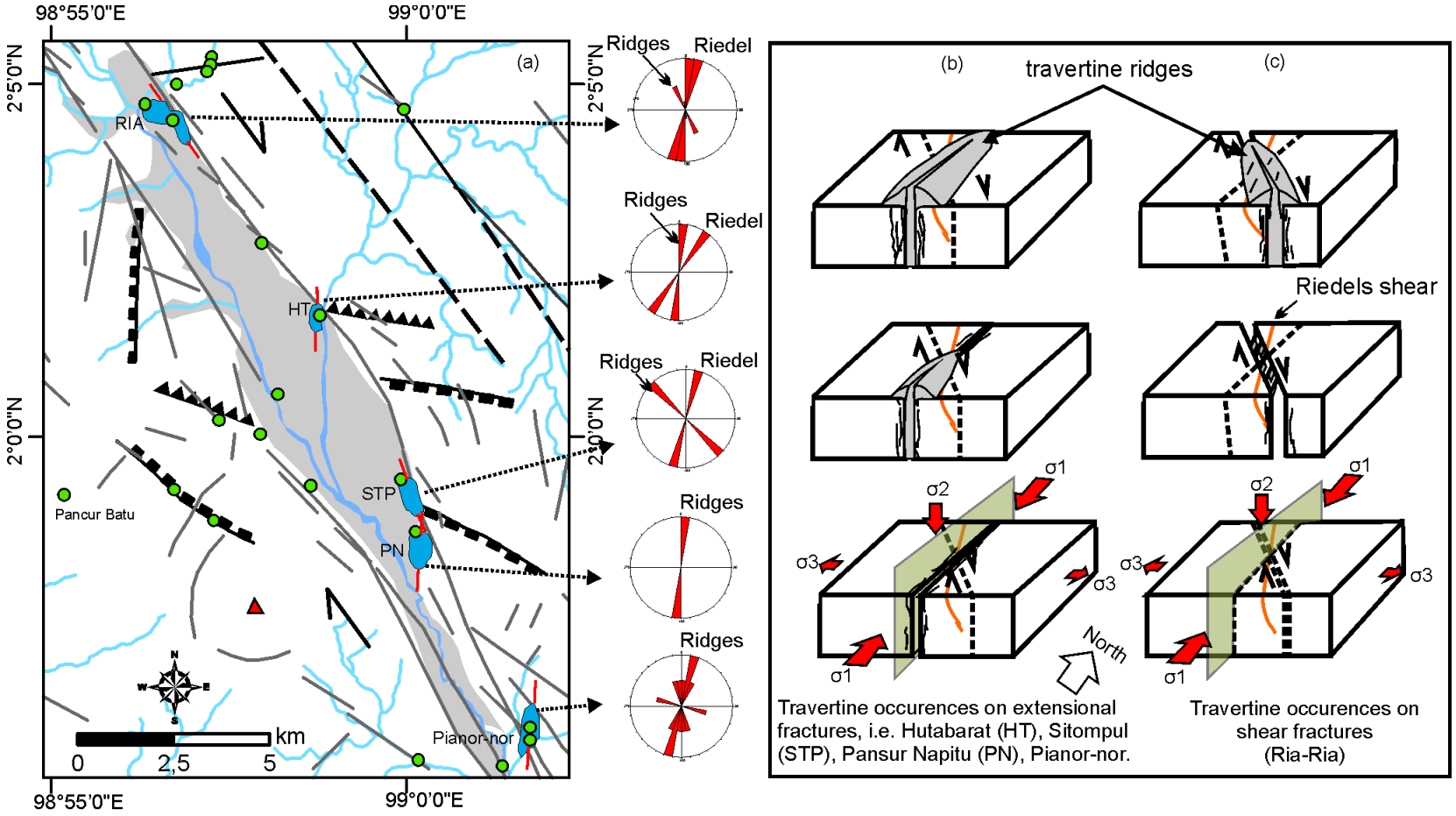

Figure 20. (a) Joints and travertine ridges orientations illustrated in directional rose diagrams. The red lines at travertine in the map represent the trend of travertine ridges. Schemes in (b & c) illustrated two types of travertine formation. Evolution goes from lower to upper images. (b) Dilational travertine type forming along extensional fractures (modified from Hancock et al., 1999; Mesci, 2004: Gursoy et al., 2007) parallel to the present-day maximum principal stress (σ_1) associated with NW-SE dextral shear fractures. The Riedel shears form in a NNE-SSW and NE.SW strike direction of the Tarutung tectonic setting. (c) Shear travertine type forming along shear fractures parallel to the main fault zone, the SFS.

Chapter 7

Hydrochemistry

Most of the content in this chapter is a part of submitted paper in Geofluid (2013)

Thermal springs and their hydrochemistry are described referring to geographic sites from the north, east, west, and south of Tarutung Basin. The comparison with the nearby geothermal field (~ 30 km) which has several exploratory wells, namely Sarulla field, is also shortly described.

7.1 Northern Area

Thermal manifestation at the northernmost area consists of hot springs at Sisordak and Butar discharging through weathered tuff and volcanic breccia as a member of Toba volcanic complex. The Sisordak springs have temperatures of 40-48°C and intermittently discharge in moderately steep topography. The major lithology of the area is altered volcanic breccia, a member of the Toba Volcanic Complex (TVC) with oxidized quartz veins exposed. The pH of the water is 6.5. Gas bubbles very likely consist of CO_2. The

fluid type of this spring is Na-Ca-HCO_3. The discharge rate of thermal fluid is approximately 1 l/s, estimated by measuring the time needed to fill a 1 liter bucket.

The Butar thermal area is located off the Tarutung Basin and recognized from shallow wells (approximately 30 m deep). The temperature is 48°C with a pH of 6,5. The fluid type is bicarbonate water (Fig.22). There are about 8-10 wells with 30-70 m depth which are exploited for bathing. The total discharge rate from the wells is approximately 5 l/s.

7.2 Eastern Area

Hot springs with temperatures of 35 – 65.5°C are associated with travertine deposits, namely Ria-Ria, Partali Julu (PJ), Hutabarat (Htb), Sitompul (Stp), Akbd (Ak) and Pansur Napitu (PN) (described in Chapter 6). The first five of those springs are located at a moderately steep cliff caused by normal faults at the eastern margin of the pull-apart basin, striking NW-SE and dipping to the west. This fluid is of Ca^{+2}-HCO_3^--SO_4^{+2} type with a pH range of 6.5-7. The total estimated discharge rate at those springs is 70 l/s, mostly from Ria-Ria (50 l/s; Hochstein & Sudarman, 1993).

CO_2 measurements from shallow holes in the soil, as reported by the Centre for Geological Agency Bandung-Indonesia (2005), show an enrichment of CO_2 at Ria-Ria, and is also recognized by Hochstein (pers.comm., 2013; Hochstein & Sudarman, 1993) as a cold CO_2 discharge area.

The Panabungan warm spring is situated 6 km to the northeast of the basin and has a temperature of 49,3°C, and pH of 6.5. Outcrops of silicified pyroclastic rocks are associated with the HCO_3^- rich water extending parallel with a steeply dipping normal fault zone striking NW-SE (Nukman & Moeck, 2012). The discharged fluid rate is approximately 50 l/s.

7.3 Western Area

Warm springs with temperatures of 31-38°C and pH values of 6-6.5 discharge in an area of lower elevation on the western margin of the Tarutung Basin (e.g. Air Soda, Hutapea, and Sait Huta) (Fig.21). The warm water can be accessed by groundwater wells (6-8 m depth). The estimated discharge rate of thermal fluid from these springs is about 5 l/s.

Further warm springs discharge at the western basin margin, (e.g. Ugan, Aek Nasia, and Pancurbatu). The Ugan warm spring discharges adjacent to a cold spring area separated by an oblique normal fault striking NW-SE (Nukman & Moeck, 2013). The major ions are Ca-SO_4-HCO_3 (Table 3 & Fig. 22a). The total discharge rate of Ugan warm spring is approximately 3 l/s.

7.4 Southern Area

The Pianor-nor spring has a temperature of 44°C and a pH of 6.5. This spring is associated with large terraces of travertine. Major ions are Ca^{+2}-SO_4^{-2}-HCO_3^{-} (Table 3 & Fig.22). This area is located outside of the basin but still within the SFS. On the western side of Pianor-nor (western strand of the SFS) a warm spring (31,8°C) with a pH of 5.9 discharges close to the margin of a river (e.g. Siandor-andor). The estimated discharge rate of Pianor-nor springs is 2 l/s.

7.5 Sarulla Field

Description of geothermal manifestation in Sarulla in this section refers to the work of Gunderson et al. (1995). The detail of hydrochemical data is presented in Appendix 5 and the locality of springs are presented in Figure 21. The characteristics of geothermal manifestations in Sarulla field in comparison with Tarutung are the presence hot springs and fumaroles with temperatures reaching boiling point. Manifestations in northern Sarulla (namley Namora-I-Langit group) are in the form of fumaroles, acid sulfate springs, and

intense acid sulfate alteration. The spring compositions are acid sulfate and neutral $Cl^{-}SO_4^{-2}$-HCO_3^{-} water type with a maximum temperature 119°C. To the south west direction of Namora-I-Langit, geothermal manifestation are in the form of fumaroles and boiling springs (in range of 95-96°C) with majorly Cl^{-} in composition. In the centre of Sarulla area, boiling springs (82 – 101°C) are discharging from the margin of a graben. Gas seeps and fumaroles are also extensively present. Geothermal manifestation located at the southern area of Sarulla (namely Sibual-buali) is dominated by extensive fumaroles (up to 100.000 m^2) by temperature 92-132°C. Jet-like blasting of steam is also observed. Most of the fumaroles in this area are situated at the proximity of SFS and Sibualbuali Volcano. The spring composition of Sibual-buali is a low to moderate bicarbonate.

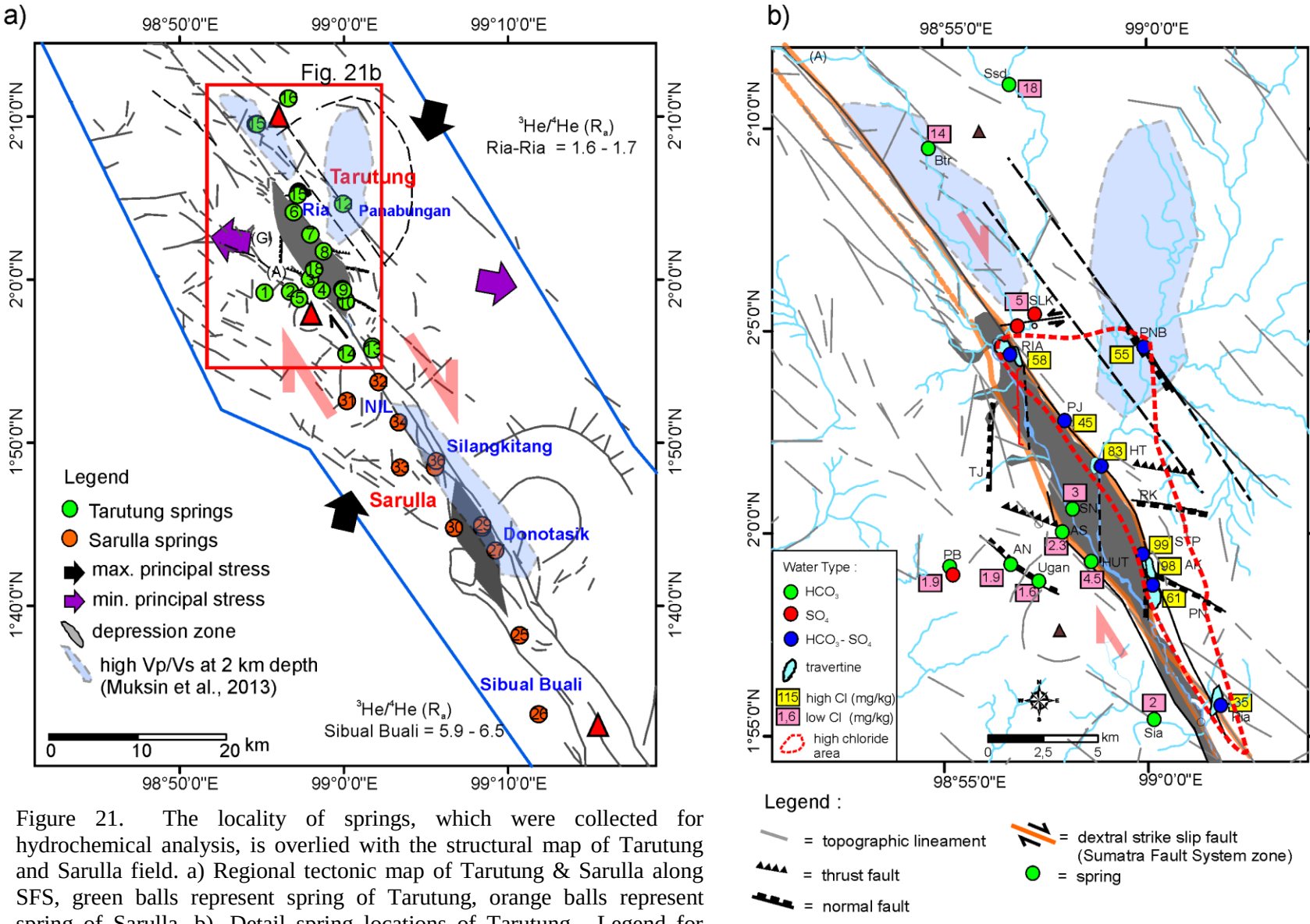

Figure 21. The locality of springs, which were collected for hydrochemical analysis, is overlied with the structural map of Tarutung and Sarulla field. a) Regional tectonic map of Tarutung & Sarulla along SFS, green balls represent spring of Tarutung, orange balls represent spring of Sarulla. b). Detail spring locations of Tarutung. Legend for spring numbers are referring to Table 3.

Table 3. The result of cations, anions, isotopes oxygen and isotope deuterium analysis from the Tarutung Basin

				Concentration in mg/kg											IB	in ^{o}/oo	
Springs	**Nr: Elev.**	**pH**	**T**	**Li**	**Na**	**K**	**Rb**	**Ca**	**Mg**	**SiO2**	**B**	**Cl**	**SO4**	**HCO3**	***)**	**$\delta^{18}O$**	**δD**
Western Area																	
Pancur Batu (1)	PB ; 1140	6	36,6	0,016	16,5	6,5	0,039	48,4	18,6	154,1	0,03	1,9	6,2	427,0	1	-9,55	-65
Aek Nasia (2)	AN ; 1104	6,5	34,6	0,024	21,5	6,6	0,035	84,5	32,3	141,0	0,03	1,9	5,8	610,0	5	-9,4	-63
Air Soda (3)	AS ; 954	6	31,1	0,024	17,7	6,4	0,041	29,2	11,1	132,9	0,04	2,3	4,9	427,0	-9	-9,02	-63,3
Hutapea (4)	Hut ; 953	6,5	37,9	0,166	60,2	9,5	0,050	38,7	18,8	135,8	0,17	4,5	4,0	549,0	1	-9,26	-62,6
UG (5)	Ug ; 977	7,7	32,6	0,002	10,33	5,95	0,012	14,77	6,99	140,6	0,03	1,62	11,72	244	-11	NA	NA
Eastern Area																	
Ria-Ria (6)	Ria ; 1018	6,5	63	0,648	102,0	26,0	0,386	384,0	90,8	102,6	2,25	57,8	459,0	1403,0	0	-9,46	-67,7
Partali Jalu (7)	PJ ;	6,5	35,4	0,422	55,9	13,6	0,195	394,0	95,7	106,7	1,16	45,6	523,2	1037,0	1	9,24	-64,2
Hutabarat (8)	Htb ; 977	7	44	0,744	89,9	20,5	0,321	623,0	168,0	67,2	2,06	89,3	987,8	1708,0	-2	-9,35	-71,1
Sitompul (9)	Stp ;	6,5	44,5	0,734	70,5	13,8	0,256	733,0	161,0	89,6	2,14	98,9	966,1	1830,0	0	-9,45	-68
Pansur Napitu (10)	PN ; 998	6,5	35,2	0,466	46,8	9,2	0,135	498,0	101,0	60,6	1,24	61,4	664,4	1128,5	0	-9,43	-71,7
Akbid (11)	Ak ;	7	43	0,674	70,1	14,0	0,225	723,0	159,0	98,5	2,03	97,7	959,8	1891,0	-1	-9,41	-73
PNB hot (12)	PNB; 1078	6,5	49,3	0,515	84,1	25,1	0,379	270,0	63,7	177,7	1,88	55,1	73,3	1403,0	5	-9,52	-70,7

*) IB = Ionic Balance

Table 3*...continued...*

Springs	Nr: Elev.	pH	T	Concentration in mg/kg Li	Na	K	Rb	Ca	Mg	SiO2	B	Cl	SO4	HCO3	IB *)	in °/oo $\delta^{18}O$	δD
Southern Area																	
Pianor (13)	Prj ; 886	6,5	44	0,465	31,0	8,7	0,135	653,0	162,0	72,4	0,73	35,4	783,0	1708,0	2	-9,86	-71,5
Siandor-andor (14)	Sia ; 900	5,9	31,8	0,056	42,18	11,08	0,049	15,45	4,50	160,0	0,11	2,63	0	335,5	-2	NA	NA
Northern Area																	
Butar (15)	Btr ; 1193	6,5	40,5	0,438	61,3	5,4	0,055	56,0	10,6	179,0	0,90	14,4	13,0	671,0	-5	-9,35	-66,7
Sisordak (16)	Ssd ; 1115	6,5	48,2	0,492	82,2	16,0	0,170	67,5	24,2	191,9	1,00	18,0	6,0	762,5	2	-9,28	-65,5
Silangkitang (17)	PS ;	3	22,5	0,010	2,3	1,2	0,013	1,8	0,6	76,3	0,03	4,9	341,3	0,0	-48	NA	NA
Centre Area																	
Sait (18)	St ; 957	6,5	40,2	0,135	62,79	16,35	0,087	42,77	17,24	174,2	0,14	3,69	9,23	854	-8	NA	NA

*) IB = Ionic Balance

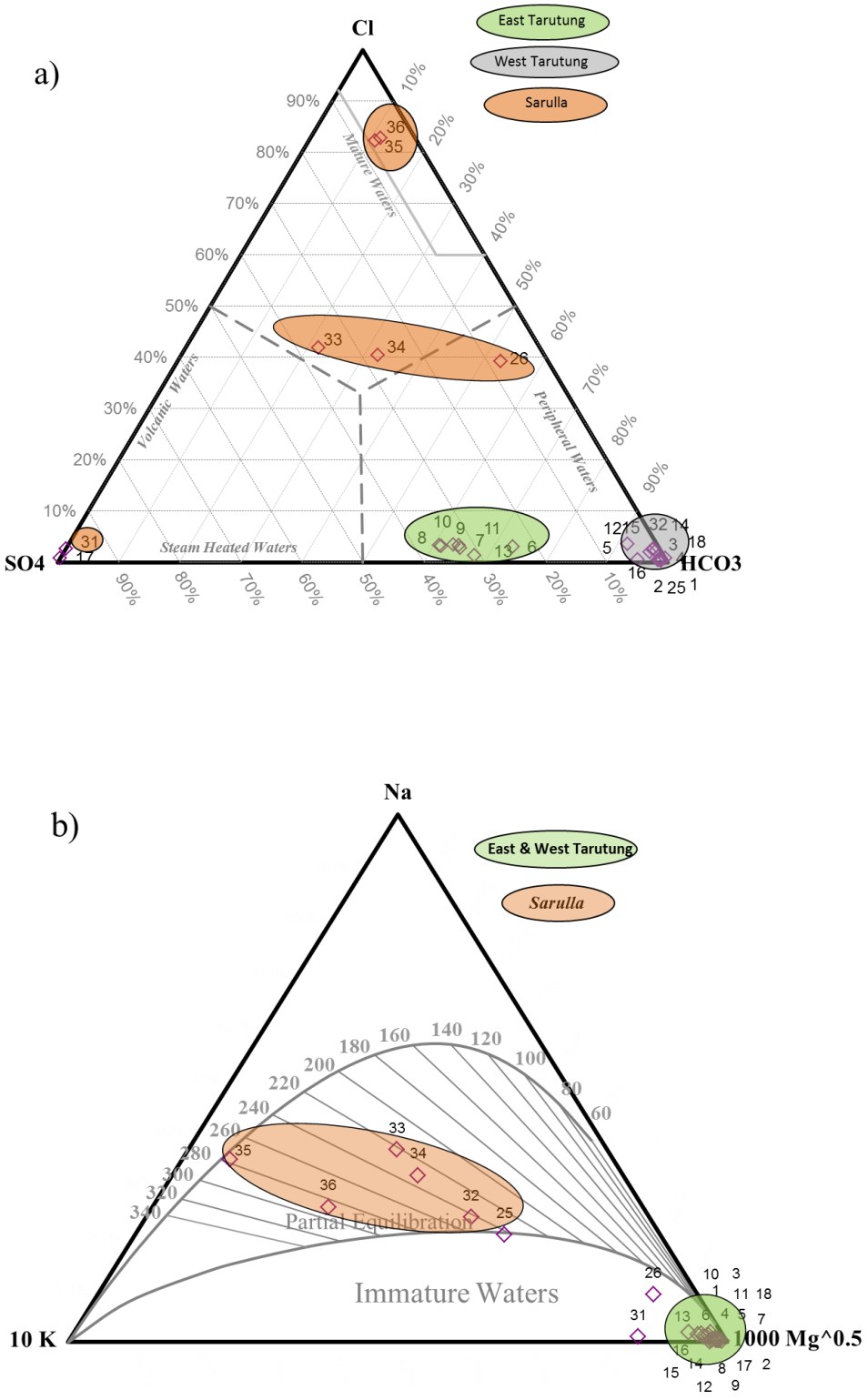

Figure 22. a) Relative concentrations of major anions (Cl^-, SO_4^{-2}, HCO_3) of Tarutung and Sarulla springs in Giggenbach (1998) Ternary Diagram. b). Relative concentrations of Na, K, Mg from Tartutung springs as shown in Giggenbach (1988) Ternary Diagram. Most of the waters are classified as 'immature' water.

7.6 Relative contents of Cl^-, SO_4^{-2}, HCO_3 and Na^+, K^+, Mg^{+2}

The relative contents of Cl^-, SO_4^{-2}, and HCO_3^-(Fig. 22) is commonly used to classify the water types and their position within a geothermal system (Ellis & Mahon, 1977; Giggenbach, 1988). The composition of the Sipoholon waters cluster in the bicarbonate-sulfate and bicarbonate corner on the Giggenbach ternary diagram (Giggenbach, 1988; Fig. 22a). The bicarbonate-sulfate springs have a higher temperature range (38 – 65.5°C) than the bicarbonate springs (22 – 38°C). One spring cluster has an acid water type at Silangkitang (SLK in Fig. 21) with a pH value of 1.6 – 3 and a maximum temperature of 22°C, which is in the range of the average temperature of local surface water (21-23°C).

The bicarbonate-sulfate springs with high temperature (38 – 65.5°C) have relatively high calcium content (Table 3). Therefore, this water is classified as a calcium-bicarbonate-sulfate (Ca^{+2}-HCO_3^--SO_4^{-2}) type. The origin of calcium is discussed in Section 7.10. Mg composition is more dominant than Na-K (Fig. 22b), indicating that a shallow dissolution is occurring (Reyes et al., 2010) (known as 'immature' waters of Giggenbach, 1988). This could imply that cations concentrations are not derived from a deep source. Ultimately, the cation geothermometer of Na-K would not represent deep temperature estimation.

Sarulla springs, however, are composed of Cl^- and Cl^- - HCO_3 geothermal water and reaching equilibration state (Fig. 22b), also known as 'mature' waters of Giggenbach (1988).

7.7 Relationship of conservative elements (B^{+3}, Cl^-)

The concentration of B^{+3} versus Cl^- clearly shows a positive correlation (R^2= 0,84; Fig. 23a). Springs with high B^{+3} concentrations (1.9 – 2.3 mg/kg) and Cl^- (54-115 mg/kg) are correlated with high temperature springs (35 – 63°C) (Fig. 23a) which is located at the eastern margin of the Tarutung Basin (Fig. 21). The low B^{+3} concentration (0.012 - 0.158 mg/kg) and low Cl^- concentration (1.5 – 5.26 mg/kg) occur in colder springs located at the western basin margin. In earlier studies, a positive correlation of high B^{+3} with high

temperature of springs also occur in Krafla (Iceland), which is probably caused by degassing magma (Arnorsson & Andresdottir, 1995). Variation of B^{+3} and Cl^{-} in Krafla is associated with the type of host rock in which alkaline basalt provides a large source of both elements.

The major volcanic host rock in Tarutung is andesitic which covers the whole area of the basin (see Stratigraphic Scheme in Figure 5); whereas granite is only localized in the western area. Andesitic host rocks containing significant B^{+3} concentration in average 15.3 mg/kg control the concentration of B^{+3} in spring waters located at the proximity of Kueishantao geothermal field (Taiwan) (Zeng et al., 2013). On the other hand, granite provides low B^{+3} source (Arnorsson & Andresdottir, 1995). Ultimately, in the case of Tarutung, andesite of Toru Formation might be a source of B^{+3}. The relatively high concentration of B^{+3} in the eastern area could be due to the existence of geothermal fluid with a high temperature, which could dissolve B^{+3} from such andesite.

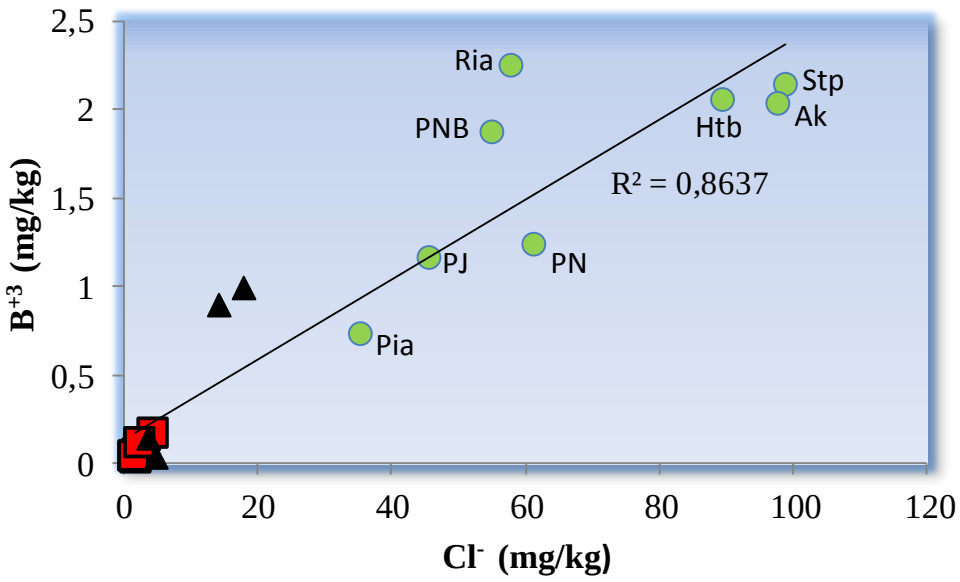

Figure 23. The correlation of conservative elements B^{+3} versus Cl^{-} indicates a positive correlation with temperature of springs. The green balls represent eastern springs with T = 38-65.5°C; red squares represent western springs with T =31-39°C, and black triangles represent northern springs with T = 23-48°C.

7.8 Geothermometry

The temperature of a geothermal reservoir can be estimated by the relative concentrations of cations (e.g., Na-K, K-Mg, Na-K-Ca) and the total dissolved silica (e.g. amorphous silica, chalcedony, or quartz) from a spring water sample (Ellis & Mahon, 1979; Fournier, 1981). The cation geothermometers are based on the assumption that the last equilibrium state between the fluid and minerals of the host rock is attained (Fournier, 1981, 1991; Giggenbach, 1988, 1991) (see section 4.4.2).

To investigate the equilibrium state of geothermal fluid and host rock, a comparison of major chemical composition within the geothermal fluid and the host rock could be used. The major cations of geothermal fluids and rocks are Na, K, Mg, Ca (Giggenbach, 1988). The equilibrium reaction between geothermal fluids and the prevailing rocks could or could not be attained (*the definition is described in Section 4.1.5*), which depend on the degree of kinetic mineral dissolution and deposition reactions, vapor loss, dilution and fluid mixing from different sources (Giggenbach, 1988). The formulation of an equilibrium state indicator based on the major cations analysis is introduced by Giggenbach (1988) by means of a four cations (Na-K-Mg-Ca) diagram. The Na-K-Mg-Ca diagram consists of $10c_K/(10c_K+c_{Na})$ as a horizontal axis and $10c_{Mg}/(10c_{Mg}+c_{Ca})$ as a vertical axis (Fig. 24). An equilibrium state of geothermal fluid with the crustal rock is shown on an equilibrium line as a function of temperature (Fig. 24).

One example of an equilibrium state of fluid-rock based on the Na-K-Mg-Ca diagram is well shown on the Sarulla field case. The four springs from Sarulla field (chemical data from Gunderson et al., 1995) are situated on the center of the diagram (shown as a red triangle in Fig. 24) at the proximity of local volcanic rock (shown as diamond symbols in Fig. 24). The trend of equilibration from Sarulla springs is shown on a red curve connecting springs #30, #SN, #27, and #29 and pointing to the equilibrium line at temperature 280°C. Interestingly, the measured temperature from the exploratory wells located at the proximity of those springs show a maximum temperature of 310°C, confirming a presence of a high temperature system underneath Sarulla field, probably controlled by young volcanism (Gunderson et al., 1995).

In the case of Tarutung, most of the cations in the Na-K-Mg-Ca diagram (Fig. 24) deviate from the equilibrium line indicating a non-equilibrium state of fluid and rock due to a dissolution process rather than equilibration. Therefore, a cation geothermometer such as Na-K could not be applied (Giggenbach, 1988; Reyes et al, 2010; Hochstein et al., 2013). However, some cations among those four (Na-K-Mg-Ca) might still reach an equilibrium, i.e. K-Mg, which requires a shorter time to reach equilibrium than Na-K (Fournier, 1989). Giggenbach & Gougel (1992) introduce the coupling of K-Mg geothermometer with the Silica geothermometer which can be used to estimate temperature at shallow level.

The diagram of log K^2/Mg against log SiO_2 consists of full equilibrium lines based on dissolved silica and K^2/Mg concentrations (Fig. 25) Giggenbach & Gougel, 1988; Reyes et al., 2010; Hochstein et al., 2013). The dissolved silica in a solution might consist of amorphous, chalcedony, and quartz (Fournier, 1981). Most of the Tarutung spring waters are plotted in between chalcedony and amorphous silica solubility lines. The springs located at the eastern area, which have a high temperature (35-63°C), are clustered close to the chalcedony solubility line, whereas the western springs (temp. <38 °C) are clustered between the chalcedony and amorphous silica solubility lines. Chalcedony is soluble in fluid solution at temperatures not higher than 180°C, whereas quartz is more soluble in high temperature (> 180) (Fournier 1981). Therefore, the presence of chalcedony within Tarutung springs is used as the basis for geothermometry calculation. In this case, chalcedony geothermometer equation of Fournier (1981) is applied, e.g.

$$T°C = (1302 / (4.69 – \log c.SiO_2)) – 273.15.$$

The result of geothermometer calculation from eastern springs of Tarutung is 82 – 115 °C of temperature (Table 4).

In comparison with Sarulla field, the geothermometry calculations (Na-K) result in 214 – 287°C, indicating a higher temperature system than Tarutung. The subsurface temperatures as measured from the deep wells in Sarulla are in the range of 218- 310°C (Gunderson et al., 2000) (Table 4) which confirms the estimated temperatures from the geothermometry calculation with 6% of deviation.

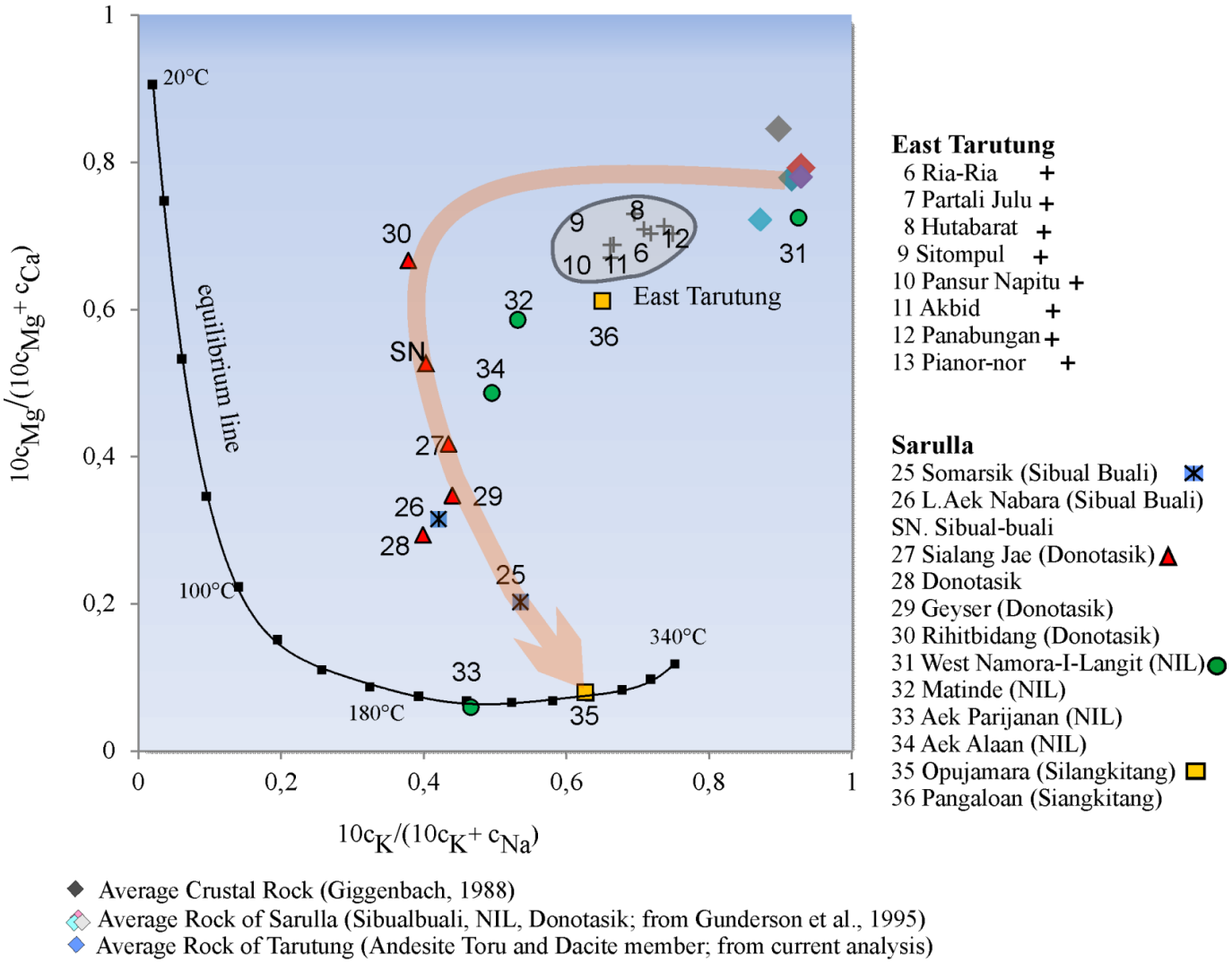

Figure 24. The 10c.K/(10c.K +c.Na) and 10 c.Mg/(10 c.Mg + c.Ca) diagram (Giggenbach, 1988) from the spring of Tarutung. The spring of Sarulla are also included based on hydrochemistry analysis from Gunderson et al. (1995) (Appendix 4).

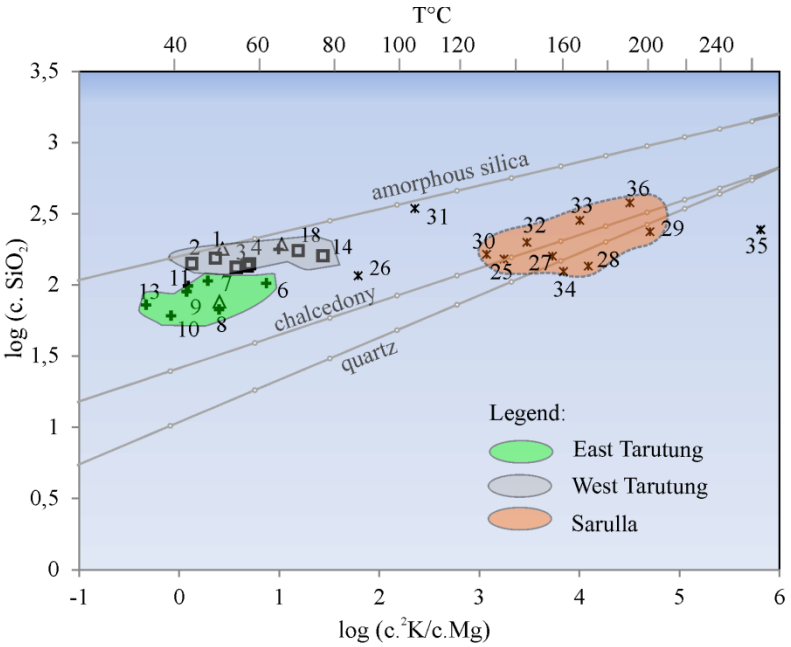

Figure 25.
Cros plot log (c.SIO_2) versus log (c.^{2}K/c.Mg) adapted from Giggenbach & Glover (1992) for Tarutung and Sarulla springs. The solubility lines of amorphous is based on equation log(c.SiO_2)=4.52-(731/(t°C+273.15));
chalcedony, log(c.SiO_2)=4.69-(1032/(t°C+273.15));
quartz, log(c.SiO_2)=5.19-(1309/(t°C+273.15)) of Fournier 1981).
Log (c.^{2}K/c.Mg) = 14-(4410/(t°C+273.15)) of Giggenbach (1991).

Table 4. Results of geothermometry calculation for Tarutung and Sarulla springs. Results of Sarulla springs are based on hydrochemical data of Gunderson et al. (1995). The measured temperatures fromwells in Sarulla are based on works of Gunderson et al. (2000). The geothermometer equations are described in the caption of Figure 25.

Site	T. Springs (°C)	Chalcedony (°C)	Amorphous Silica (°C)	Na-K (°C)	Measured from Wells (°C)*
Ria (#6)	65.5	112	18	320	-
PJ (#7)	39.8	115	20	315	-
Htb (#8)	53	87	-2	308	-
Stp (#9)	44	104	12	292	-
PN (#10)	38	82	-6	292	-
Ak (#11)	44	110	16	294	-
Pia (#19)	42.5	91	2	331	-
Srl-25	68	138	39	244	218-248
Srl-26	72	120	25	208	
Srl-27	82	142	42	212	-
Srl-28	101	130	33	202	-
Srl-29	92	172	67	214	-
Srl-30	101	144	44	196	-
Srl-31	97	206	96	566	260
Srl-32	75	158	56	243	
Srl-33	80	188	80	222	
Srl-34	96	124	28	231	
Srl-35	96	175	70	277	277-287
Srl-36	95	215	103	287	

7.9 Acid Springs

Sulfate acidic springs (pH 1.26 – 2.2) with low temperatures (22-24°C,), e.g Silangkitang (SLK) (Fig.21) occur close to spring with neutral pH (e.g Butar-Sisodrak (North) and Ria-Hutabarat-Sitompul-Akbd-Pansur Napitu (South). Sulfate-rich waters usually form in geothermal systems due to the interactions of degassed H_2S with waters in a shallow aquifer (Ellis & Mahon, 1977; Henley et al, 1984). However, acid water in Silangkitang might not be controlled by the oxidation of H_2S derived from magma. The temperature and pH of Silangkitang springs is also too low for a magmatic water type. One plausible reason to define the origin of H_2SO_4 is the existence of sulphur source at shallow depth, i.e. coals which contain pyrite. One of the results from the structural mapping in this research is also an observation of coal seams interbedded with unconsolidated clay that underlied Toba Volcanic Complex. This coal seems exposed at the northern and eastern areas of Tarutung (sites SLK & PNB in Fig. 21). The stratigraphic position of this coal unit is in between andesite Toru Fm (in the lower part) and dacite rock unit (in the upper part) as shown on stratigraphic logs in Appendix 2. The pyrite within the coal may form acid sulfate through oxidation process by waters.

7.10 Oxygen and deuterium stable isotopes

The origin of thermal water can be determined from the ratio of oxygen stable isotope ($^{18}O/^{16}O$) and hydrogen stable isotope ($^{2}H/^{1}H$) with respect to the isotopic composition of the meteoric water line (MWL) (Craig, 1963; Truesdell & Hulston, 1980). A large oxygen shift line from MWL to the magmatic water 'box' indicates that the water has been enriched with $\delta^{18}O$ due to isotope oxygen exchanges during fluid-rock interaction which commonly occur in a high temperature state.

The isotopic composition of the Tarutung springs is for $\delta^{18}O$ = - 9, 86 to - 9,02 $^{o}/_{oo}$ and for δD = -62,6 to -71,7 $^{o}/_{oo}$, respectively (Fig. 26). The ^{18}O trend is slightly shifted from the MWL suggesting water rock interactions. The magmatic water component in the Tarutung springs is in the range of 5-10 %, indicating a less magmatic than meteoric in origin. A large variation of deuterium isotopes indicates an evaporation effect, as occurs mostly on cold springs.

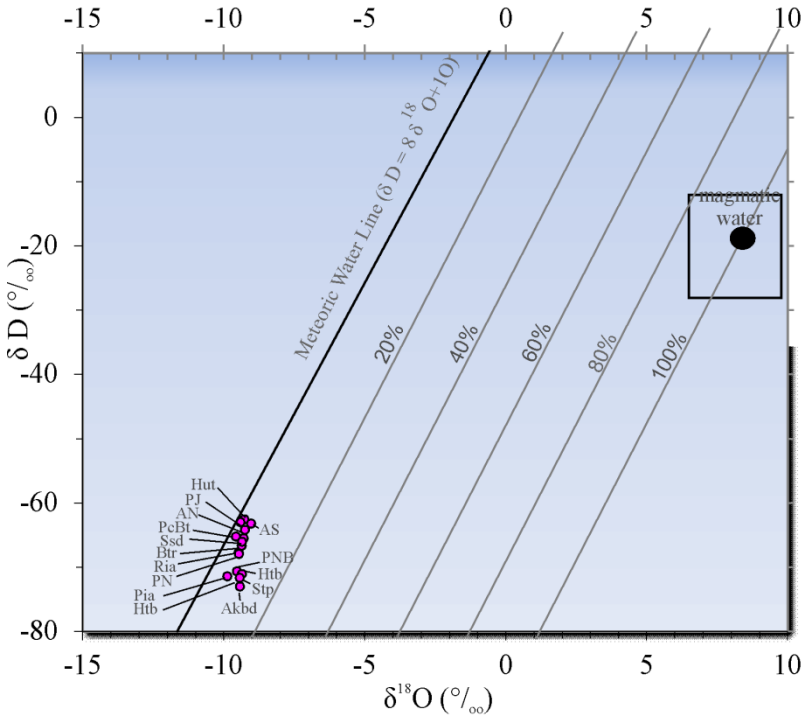

Figure 26. Cross plot of oxygen versus deuterium isotopes of Tarutung springs with respect to Standard Ocean Water (SMOW) line. The Tarutung springs lies close to the SMOW suggesting mostly meteoric water origin (~90%) and are up to only 10% of deep water origin.

7.11 Discussion

Based on spring water analyses, the water discharging in the Tarutung Basin can be classified into three spring clusters:

- **eastern margin**: calcium-bicarbonate-sulfate springs with high temperature (35–65.6°C) associated with massive travertines, and high chloride contents (54 – 116 mg/kg).
- **western margin & far-northern area**: bicarbonate waters with lower temperatures (31-36 °C) and low chloride content (1.6 – 14.4 mg/kg).
- **northern area** : sulfate cold spring (22.5°C), low chloride content (4.9 mg/kg).

There are obvious significant differences in the geochemical characteristics of the thermal springs discharging on the eastern, northern, and western margins of the Tarutung Basin.

Extensive travertine deposits exposed at the eastern side of the basin require a large volume of fluid saturated with bicarbonate water and calcium. However, there are no carbonates exposed but limestone of the Alas Formation occurs 25 km north of Tarutung (Fig. 13). Both dissolution of calcium from the limestone by shallow meteoric water and a topographic driven flow might subsequently control the calcium-carbonate rich water formation and its flowing to the Tarutung Basin. Another interpretation is that the limestone of Alas Fm may extend to the southeastern area in the subsurface and over the Late Carboniferous rocks (Bohorok Fm) in the eastern area of Tarutung Basin. The latter interpretation is proposed in this research and shown on the regional stereographical scheme of Tarutung Basin in Figure 5.

A drastic change of spring type at opposing valley sides from sulfate cold spring to hot spring with calcium-bicarbonate-sulfate in composition occurs at the vicinity of the northern basin (i.e. Silangkitang & Ria-Ria). The characteristic of permeability structures at both areas could explain this phenomenon. The result from structural mapping shows an observable fault zone striking ENE-WSW filled by fine grained unconsolidated sediments (as discussed in Chapter 5). This fault gouge might act as a permeability barrier which inhibits fluid flow from southern area (i.e Ria-Ria) to northern area (i.e. Silangkitang).

Deep fluid contributions

Because the concentration of Cl^- is not controlled by mineral solubility (Arnorsson, 2000; Browne & Rodger, 2006), its presence in spring waters represents the contribution from a deep fluid source (Ellis & Mahon, 1977; Fournier, 1979; Henley et al, 1984; Reyes et al., 2010). The high chloride concentration in spring waters is at the east-southeastern Tarutung Basin, which is identified to be located at the extensional-transtensional zone (as described in Chapter 5). Deep fluid source might ascend to shallower depth through the vertical and permeable faults system. Seismic tomography studies in Tarutung area shows high anomalies value of ratio P-Wave to S-Wave velocity (i.e. Vp/Vs), and low P-Wave (Vp) velocity at 2-4 km depth located at the northeastern area (Hutabarat – Panabungan) (Muksin et al., 2013a) (Fig.21). The high Vp/Vs might correspond to fluid bearing

fractures (Muksin et al., 2013), which is confirmed by the presence of springs with high discharge rate. The high Vp/Vs, shown as light blue areas in Figure 21, is situated at the area where the high Cl^- concentration are discharged, relatively high boron (B^{+3}) content (Fig.23) and also with high temperature (38 – 65.5°C). High seismic attenuation as revealed at the northeast of Tarutung Basin might correspond to a relatively high temperature zone (Muksin et al., 2013b) of geothermal reservoir.

In brief, a bundle of anomalies is located at the eastern side of the Tarutung Basin, e.g. 1) large amount of extensional faults (as discussed in Chapter 5 & 6); 2) spring waters with significant Cl^- content, elevated temperatures and extensive exposures of recent travertine deposits (Sec. 6.1), 3) high ratio of P-wave velocity and S-wave velocity (Vp/Vs), and 4) low resistivity structures. In contrast, the low Cl^- concentrations in the western spring waters (1,6 – 3 mg/kg; Table 3) suggests that there is no deeper fluid circulating to the western area. Although both areas are controlled by a releasing bend along the same fault zone of SFS, the permeability structures at depth might be different assuming that the geothermal upflow is centralized underneath the Tarutung Basin.

To define the origin of the heat source and heat transfer mechanism, helium isotopes data are used in the analysis. Two samples for isotope Helium from Ria-Ria springs (eastern Tarutung) results in 1.62 and 1.71 of Ra (= $^3He/^4He$) (Halldorsson et al., 2013); whereas the Helium isotope ratio measured in the Sibualbuali volcanic centre of Sarulla shows higher values in range of 5.9 - 6.58 R_a (= $^3He/^4He$) (Halldorsson et al., 2013). Locality of helium measurement is shown in Figure 21a.

The low value of R_a indicates more helium derived from crustal level (i.e. ^4He) than helium derived from the mantle (i.e ^3He) (Mamyrin & Tolstikhin, 1984; Griesshaber et al., 1992; Newell et al., 2005) which might occur in Tarutung Basin. In contrast, a high Ra in Sarulla indicates that the helium derived from the mantle (i.e. ^3He) is more dominant within the geothermal system than the helium derived from the crust (i.e. ^4He).

The comparison of helium isotope analysis from Tarutung Basin and Sarulla field indicates that different flows of crustal and mantle fluids occur, although relatively not at a large distance (~ 30 - 40 km) (Fig. 21). However, those two geothermal fields have different volcanic settings although they are situated along the similar fault zone of deep crustal reaching fault of Sumatra (SFS). One of the differences is that active volcanic activities occur more in Sarulla field than in the Tarutung Basin (Gunderson et al., 1995; Hickman et al., 2004). The presence of magma chamber and its degassing process, somehow, could contribute to the total helium budget (Oxburg et al.,1987; Ballentine & Burnard, 2002) which might occur in Sarulla field. In other words, a lesser contribution of helium derived from the mantle, as shown from Tarutung samples (Halldorsson et al., 2013), could be due to the absence of large magma chambers at crustal depths or less permeable lower crust structures cap such chamber.

7.12 Conclusions

The fluid characteristic of Tarutung springs indicate an up-flow from a low temperature geothermal system (<120°C) with a minor contribution of magmatic water. The heat source origin is indicated from a deep crustal level with heat disturbances from the mantle. However, the non-equilibration of fluid-rock is occurring, although there is an indication of deep derived fluid within the geothermal system. This typical field might not be commonly found in active plate margin settings. The absence of a large or active magma chamber underneath Tarutung Basin might differ from the nearest geothermal field of Sarulla where active rhyolitic-andesite volcanism is currently occurring. Heat transfer controlling the geothermal system of both fields is transferred from depth to a shallower level through a similar deep crustal reach fault, i.e. Sumatra Fault System.

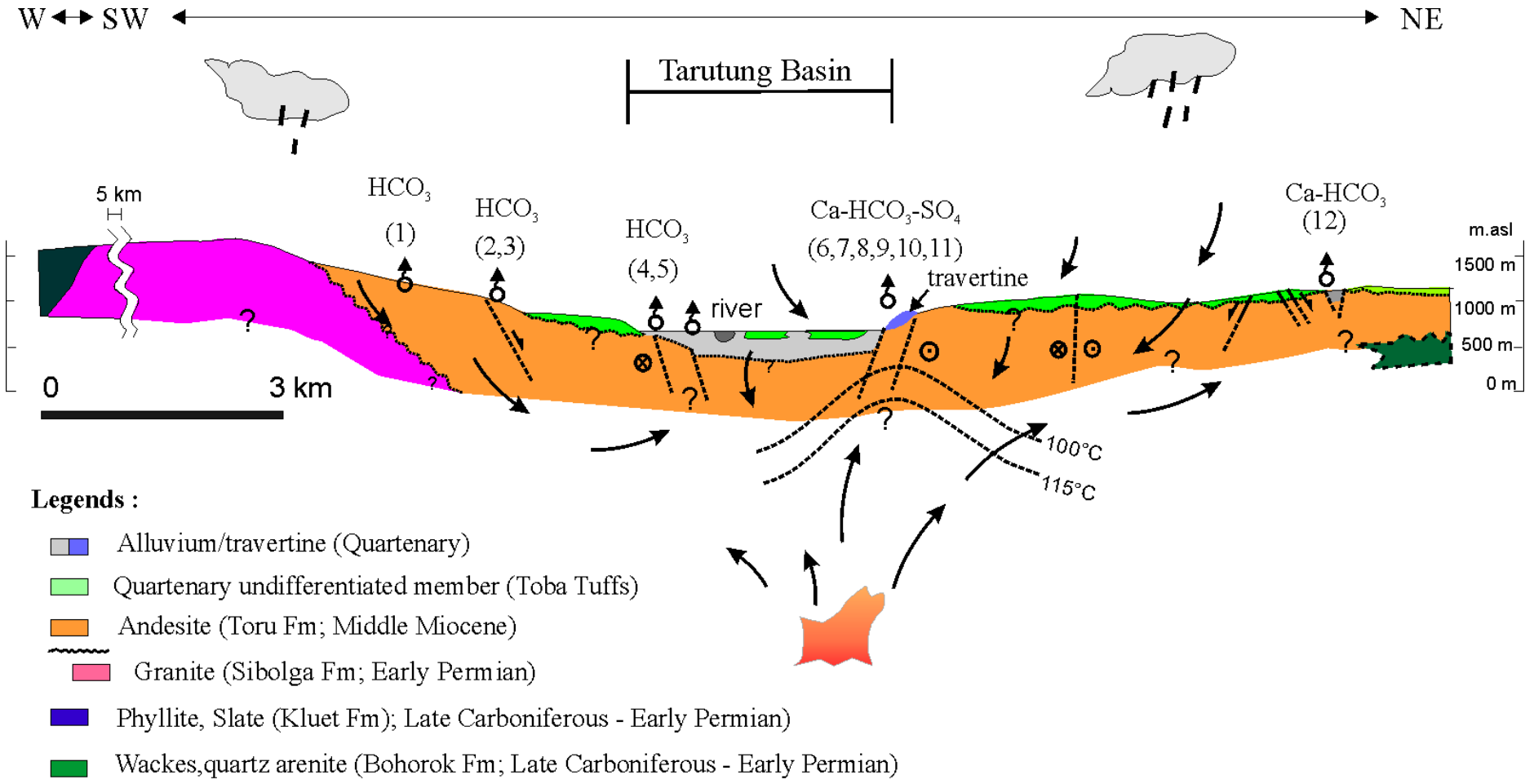

Figure 27. Conceptual model of the geothermal system in Tarutung Basin is shown on a geological cross section in E-W direction. (see also Fig. 13 for references of geological symbols, and Fig. 16 for another cross section in N-S direction.

Chapter 8

Conclusions

The important findings of this research are:

1. The effect of clockwise rotation as induced by dextral strike slip is generating a dilation zone which controls a new permeable zone in the Tarutung geothermal system.
2. The existing fracture is rotated and stands at a high angle to the current compressive stress direction. The compressional state is now generating reverse faulting, and enhances the formation of fault gouges which probably causes low permeability.
3. A non-equilibrium state of fluid-rock interactions of thermal waters of the Tarutung springs indicates that crustal derived fluids contribute to the system rather than mantle derived fluids.
4. A minor contribution of deeper magmatic fluids and an extensive meteoric water infiltration occurs through the interpreted permeable zone, i.e. along the eastern margin of the Tarutung Basin.

The contribution of current research results.

1) More detailed data of springs are obtained and a structural geological map is constructed. There are now 18 warm and hot springs that were mapped and sampled for hydrochemistry analysis. One fourth of the springs had not been mapped by previous workers. The analysis from these updated data could provide a more comprehensive understanding of the geothermal system in the Tarutung Basin

2) The upflow of the Tarutung geothermal system is related with the un-equilibrated and crustal derived fluid. Generally, the un-equilibrated geothermal fluid occurs in the outflow zone. The lesson from Tarutung might provide a new perspective to better understand fields in similar settings, i.e. a structural control on fluid flow and low temperature system.

3) An integrated method consisting of structural geology and hydrochemistry could provide a useful approach for geothermal exploration in active tectonic settings to identify the geothermal system including permeability structure, fluid origin, and estimated subsurface temperature (see Fig.28).

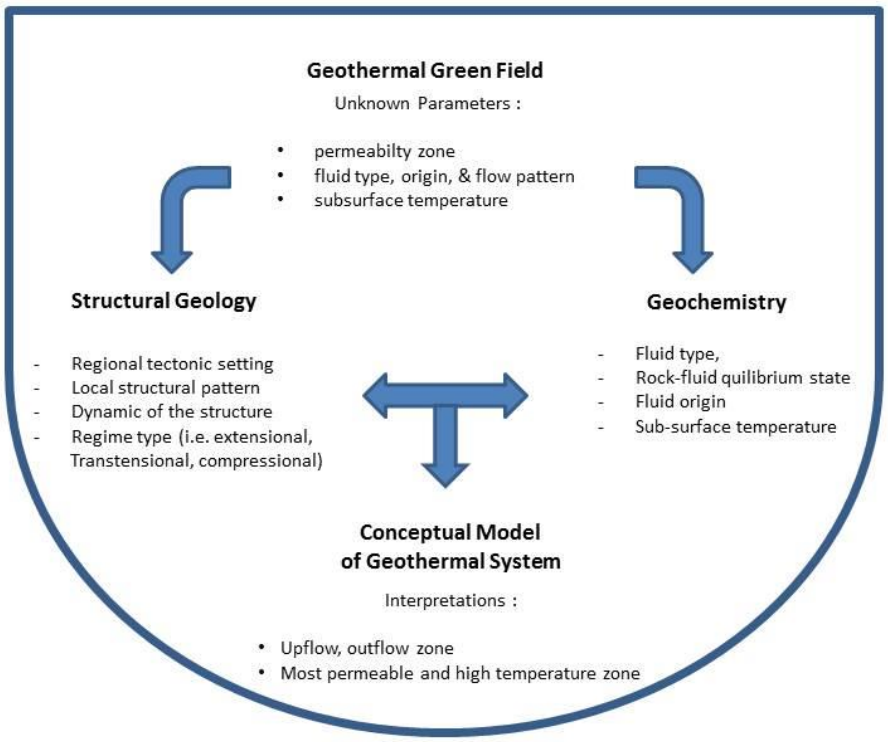

Figure 28. Result of research in a chart flow : a conceptual model of a geothermal system is outlined based on structural geology and geochemistry studies

References

_____,2013. Tapanuli Utara Dalam Angka. Badan Pusat Statistik (BPS), Board of Statistic Indonesia, Katalog:1102001.1205

_____,2012. Kondisi Kelistrikan Sumatra Utara. Report Dinas Energi & Pertambangan (Energy & Mining Board) Sumatra Utara .

Aldiss, D.T., Whandoyo, R., Sjaefudien, AG.,Kusjono., 1983. Geological Map of the Sidikalang, Sumatra. Quadrangle 0618. Scale 1:250.000, Geological Research and Development Centre, Bandung, Indonesia.

Altunel, E., Hancok, P.L., 1993. Morphology and structural setting of Quartenary travertines at Pamukkale, Turkey. Geological Journal, 28, 335-346.

Anderson, E.M., 1951. The dynamics of faulting and dyke formation with applications to Britain. Edinburg, London.

Angelier, J., 1994. Fault slip analysis and paleostress reconstruction. In: Hancock, P.L. (Ed.),Continental Deformation. Pergamon, Oxford, 53-100.

Ardiwinata, N., Setiawan, Asngari, Suparjo, E., Kurniawan, S., 2005. Penyelidikan geokimia panasbumi daerah Sipoholon Kabupaten Tapanuli Utara, Sumatra Utara. Report of Centre of Geology Research, Bandung.

Arnorsson, S., Stefansson, A., 2007. Fluid-fluid interactions in geothermal systems, Reviews in Mineralogy and Geochemistry. 65, 259-312.

Arnorsson, S., Andresdottir, A., 1995. Process controlling the distribution of boron and chlorine in natural waters in Iceland. Geochemica et Cosmochimica Acta, 59, 4125 - 4146.

Apsden, J.A, Kartawa, W., Aldiss, D.T., Djunuddin, A., Whandoyo, R., Diatma,D., Clarke,M.C.G,Harahap,H., 1982. The Geology of the Padangsidempuan and Sibolga, Quadrangle 0617-0717, Scale 1:250.000, Geological Research and Development Centre, Bandung, Indonesia.

Aydin, A., Nur, A., 1980. Evolution of pull-apart basins and their scale independence. Tectonics, 1, 91-105.

Ballentine, C. J., Burnard, P. G., 2002. Production, Release and Transport of Noble Gases in the Continental Crust In : Porcelli, D., Ballentine, C. J., Wieler, R., (Eds.), Reviews in Mineralogy & Geochemistry 47, Noble Gases in Geochemistry and Cosmochemistry, 481-529.

Ballentine, C. J., Burgess, R., Marty, B., 2002. Tracing Fluid Origin, Transport and Interaction in the Crust. In : Porcelli, D., Ballentine, C. J., Wieler, R., (Eds.), Reviews in Mineralogy & Geochemistry 47, Noble Gases in Geochemistry and Cosmochemistry, 539-614.

Barber, A.J., 2000. The origin of the Woyla Terranes in Sumatra and the Late Mesozoic evolution in the Sundaland margin. Journal of Asian Earth Sciences, 18, 713-738.

Barber, A.J., Crow, M.J., 2003. An evaluation of plate tectonic models for the development of Sumatra. Gondwana Research, 6, 1-28.

Barber, A.J., Crow, M.J., De Smet, M.E.M., 2005. Tectonic Evolution. In: Barber, A.J., Crow, M.J., Milsom, J.S. (Eds.), Sumatra; Geology, Resources and Tectonic Evolution. Geological Society, London, Memoirs, 31.

Barber, A.J., Crow, M.J., Milsom, J.S. (eds). 2005. Sumatra: Geology, Resources and Tectonic Evolution Geological Society, London, Memoirs, 31.

Bellier, O., Sebrier, M., 1995. Is the slip rate variation on the Great Sumatran Fault accommodated by fore-arc stretching? Geophysical Research Letter, 22, 1969-1972.

Bemmelen, R.W., 1949. The Geology of Indonesia, v. IA, Martinuj Nujhoff, The Hague.

Bernard, R,. Taran, Y., Pennisi, M., Tello, E., Ramirez, A., 2011. Chloride and Boron behavior in fluids of Los Humeros geothermal field (Mexico): A model based on the existence of deep acid brine. Applied Geochemistry, 26, 2064-2073.

Bibby, H.M., Risk, G.F., Caldwell, R.G., Heise, W., 2009. Investigations of deep resistivity structures at the Wairakei geothermal field. Geothermics, 38. 98-107.

Blattner, P., 1985. Isotope shift data and the natural evolution of geothermal systems. Chemical Geology, 49, 187-203.

Brogi,A., Capezzuoli, E., Aque, R., Branca, M., Voltaggio, M., 2010. Studying travertines for neotectonics investigations: Middle-Late Pleistocene syn-tectonic travertine deposition at Serre di Rapolano (Northern Apennines, Italy). International Journal Earth Sciences (Geologische Rundshau) 99, 1383-1398.

Brogi, A., Capezzuoli, E., Buracchi, E, Branca, M., 2012. Tectonic control on travertine and calcareous tufa deposition in a low-temperature geothermal system (Sarteano, Central Italy). Journal of the Geological Society, 169, 461-476.

Browne, P.R.L., 1978. Hydrothermal alteration in active geothermal fields. Annual Reviews Earth Planetary Sciences, 6, 229-250.

Browne, P.R.L., 1998. Hydrothermal alteration in New Zealand geothermal systems. In: Arehart & Hulston (Eds.), Water-Rock Interaction, Balkema, Rotterdam.

Browne, P.R.L., Rodgers, K.A.,2006. Occurrence and significance of anomalous chloride waters at the Orakeikorako geothermal field, Taupo Volcanic Zone, New Zealand. Geothermics, 35, 211-220.

Bruhn, R.L., Yonkee, W.E., Parry, W.T., Yonkee, W.A., Thomson, T., 1994. Fracturing and hydrothermal alteration in normal fault zones: PAGEOPH, 142, 609-404.

Caine, J.S., Evans, J.P., Forster, C.B., 1996. Fault zone architecture and permeability structure. Geology, 24, 1025 – 1028.

Cameron, N.R., Clarke, M.C.G., Aldiss, D.T., D.T., Apsden, J.A., Junuddin, A., 1980. The geological evolution of northern Sumatra. In: Indonesia Petroleum Association, Proceedings of the 9th Annual Convention, Jakarta, 9, 149-187.

Cattin, R., Chamot-Rooke, N., Pubellier, M., Rabaute, A., Delescluse M., Vigny, C., Fleitout, L., Dubernet, P., 2009. Stress change and effective friction coefficient along the Sumatra-Andaman-Sagaing fault system after 26 December 2004 (Mw=9.2) and the 28 March 2005 (M_w=8.7) earthquakes. Geochemistry, Geophysics, Geosystems, 10, Q03011, doi: 10.1029/2008GC002167.

Chang, C.L., 1984. Triangular diagrams for predication of aquifer chemistry, Geothermal Research Council Transactions, 8, 373-376.

Chester, F.M., Logan, J.M., 1986. Composite planar fabric of fault gouge from the Punchbowl fault, California. Journal of Structural Geology, 9, 621-634.

Chesner, C.A., 1998. Petrogenesis of the Toba Tuffs, Sumatra, Indonesia, Journal of Petrology, 39, 397-438.

Chesner, C.A., Rose, W.I., Deino, A., Drake, R., 1991. Eruptive history of Earth's largest Quartenary caldera (Toba, Indonesia) clarified. Geology, 19. 200-203.

Clark, I. D., Fritz, P., 1997. Environmental isotopes in Hydrogeology. New York: Lewis Publishers.

Clarke, M.C.G., Ghazali, S.A., H. Harahap, Kusyono, Stephenson, B., 1982. Geology Map of the Pematangsiantar, Sumatra. Quadrangle 0718, Scale 1 : 250.000, Geological Research and Development Centre, Bandung, Indonesia.

Craig, H., 1963. The isotopic geochemistry of water and carbon in geothermal areas; In Tongiorgi, E. (Ed.), Nuclear Geology in Geothermal areas: Pisa, Italy, Consiglio Nazionale delle Ricerche, Laboratorio de Geologica Nucleare, 17-53.

Craig, H, Lupton, J.E., 1976. Primordial neon, helium and hydrogen in oceanic basalts. Earth Planetary Science Letters, 31, 369-385.

Cunningham, W.D, Mann, P., 2007. Tectonic of strike-slip restraining and releasing bends. Geological Society, London. Special Publication 20, 1-12.

Curewitz, D., Karson, J.A., 1997. Structural settings of hydrothermal outflow: Fracture permeability maintained by faults propagation and interaction. Journal of Volcanology and Geothermal Research, 79, 149-168.

Daubre, M., 1879. Application de la method experimentale a l'etude des deformation et des cassures terrestres. Bull. Soc. Geol. Fr., 3, 241-141

Deming, D., 1994. Fluid flow and heat transport in the upper continental crust. Geological Society, London, Special Publications, 78, 27-42.

Dhont, D., Chorowicz, J., Yürür., T, Froger, J.L., Köse, O., Gündogdu, N., 1998. Emplacement of volcanic vents and geodynamics of Central Anatolia, Turkey. Journal of Volcanology and Geothermal Research 85, 33-54.

Ellis, A.J., 1970. Quantitative interpretation of chemical characteristics of hydrothermal systems. Geothermics Special Issues 2, 2 (Plate .1), 516-528.

Ellis, A.J. 1977. Chemical and Isotopic Techniques in Geothermal Investigations, Geothemics, 5, 3 – 12.

Ellis, A.J., Mahon, W.A.J., 1977. Chemistry and Geothermal Systems, Academic Press.

Ellis, A.J., Wilson, S.H. (1960). The geochemistry of alkali metals ions in the Wairakei hydrothermal system, N.Z.J. Geol. Geophys. 3, 593-617.

Erbas, K, Jaya, M.S, Moeck, I., Deon, F., Brehme, M., Regenspurg, S., Frick, S., Kranz, S, Bäßler, R, Heunges, E. 2011. Concepts for Sustainable Geothermal Energy Development in Remote Geothermal Areas of Indonesia, Transactions Geothermal Resources Council, 35.

Faulds, J., Moeck, I., Drakos, P., Zemach, E., 2010. Structural assessment and 3D geological modelling of the Brady's geothermal area, Churchill country (Nevada, USA): A preliminary report. Proceedings, Thirty-Fifth Workshop on Geothermal Reservoir Engineering, Stanford University, California. SGP-TR-188.

Faulds, J., Hinz, N., Kreemer, C., 2012. Structural and tectonic controls of geothermal activity in the Basin and Range province, Western USA. New Zealand Geothermal Workshops, Auckland, New Zealand.

Faure, G., 1991. Principles and Applications of Inorganic Geochemistry, United States of America: Macmillan Publishing Company.

Fauzi, McCaffrey, R., Wark, D., Sunaryo, Prih Haryadi, P.Y., 1996. Lateral variations in slab orientation beneath Toba caldera, northern Sumatra. Geophysical Research Research Letters, 23, 443-446.

Fontaine, H., Gapoer, S., eds). 1989. The Pre-Tertiary Fossils of Sumatra and their Environments. CCOP Technical Papers, 19, United Nations, Bangko.

Fossen, H., 2010. Structural Geology. Cambridge University Press.

Fournier, R. O., 1977. Chemical geothermometers and mixing models for geothermal systems, Geothermics, **5**, 41-40.

Fournier, R.O., 1979. Geochemical and hydrologic considerations and the use of entalphy-chloride diagrams in the prediction of underground conditions in hot springs systems, Journal of Volcanology and Geothermal Research, 5,1-16.

Fournier, R.O.,1979. Geochemistry and dynamics of the Yellowstone National Park hydrothermal system. Ann. Rev. Earth Planet. Sci. 17, 13-53.

Fournier, R.O., 1989. Lectures on geochemical interpretation of hydrothermal waters. The United Nations University, Geothermal Training Programme, Reykjavik, Iceland.

Fournier, R.O., 1981. Application of water geochemistry to geothermal exploration and reservoir engineering, In Geothermal System: Principles and Case History; Rybach, L., Muffler, L.J.P (Eds.), John Wiley & Sons.

Giggenbach, W.F., 1984.Mass transfer in hydrothermal alteration systems: Geochimica et Cosmochima Acta **48,** 2693-2711.

Giggenbach, W.F., Glover, R.B., 1992. Tectonic regime and major processes governing the chemistry of water and gas discharges from the Rotorua geothermal field, New Zealand, Geothermics, 21, 121-140.

Giggenbach, W.F., Minissale, A.A.,Scadriffio, G., 1988. Isotopic and chemical assessment of geothermal potential of the Coli Albani area, Latium region, Italy. Applied Geochemistry, 3, 475-486.

Giggenbach, W.F. 1992. Isotopic shifts in waters from geothermal and volcanic systems along convergent plate boundaries and their origin. Earth and Planetary Sceince Letters, 113, 495 – 510.

Giggenbach, W,F., 1997. The origin and evolution of fluids in magmatic-hydrothermal systems. In: Barnes,H. (Ed), Geochemistry of Hydrothermal Ore Deposits 3rd Ed., John Wiley & Sons Inc., New York, 737-796.

Giggenbach, 1988. Geothermal solute equilibria: Derivation of Na-K-Mg-Ca geoindicators. Geochimica et Cosmochimica Acta, 52, 2749-2765.

Griesshaber, E., O'Nions, R.K., Oxburgh, E.R., 1992. Helium and carbon isotope systematics in crustal fluids from the Eifel, the Rhine Graben and Black Forest, F.R.G. Chemical Geology, 99, 213-235.

Grindley, G.W., 1970. Subsurface structures and relation to steam production in the Broadlands Geothermal Field, New Zealand. Geothermics, Special Issue 2.

Gunderson, R.P.,Dobson,P.F.,Sharp,W.D.,Pudjianto,R., Hasibuan, A., 1995. Geology and thermal features of the Sarulla Contract Block, North Sumatra, Indonesia. In: Proceedings World Geothermal Congress, 2,687-692.

Gunderson, R., Ganevianto,N., Riedel, K., Azwar, L.S.,Suleiman,S., 2000. Exploration results in the Sarulla Block, North Sumatra, Indonesia. In: Proceedings World Geothermal Congress, Kyushu-Tohoku, Japan.

Khodayar, M., Björnsson, S., Einarsson, P., Franzson, H., 2010. Effect of tectonics and earthquakes on geothermal activity near plate boundaries: A case study from South Iceland. Geothermics, 39, 207-219.

Halldorsson, S.A., Hilton, D.R., Troll, V.R., Fischer, T.P., 2013. Resolving volatile sources along the western Sunda arc, Indonesia. Chemical Geology, 339, 263-282.

Hamilton, W., 1979. Tectonics of the Indonesian Region. United States Geological Survey Professional Paper 1078.

Hancock, P.L., 1985. Brittle microtectonics: principles and practice. Journal of Structural Geology, 7, 437-457.

Hancock, P.L., Chalmers, R.M.L., Altunel, E., Cakir, Z., 1999. Travitonics : using travertines in active fault studies. Journal of Structural Geology 21, 903-916.

Hedenquist, J. W., 1990. The thermal and geochemical structure of the Broadlands-Ohaaki geothermal system, New Zealand: *Geothermics* **19**, 151-185.

Hedenquist, J. W., Stewart, M. K., 1985. Natural CO2-rich steam heated waters in Broadlands-Ohaaki geothermal system, New Zealand: theirchemistry,distribution and corrosive nature. Geotherm. Resour. Council Trans. 9(Part II), 245-250.

Henley, R.W., 1985. The geothermal framework for epithermal deposits. In : Berger, B.R., Bethke, P.M., (Eds), Geology and Geochemsitry of Epithermal Systems. Society of Economic Geologist. El-Paso, USA.

Henley, R.W., 1984. Chemical Structure of Geothermal Systems. In : Fluid-Mineral Equilibria in Hydrothermal Systems. Henley, R.W., Truesdell, A.H., Barton, P.B, (Eds). Society of Economic Geologist. El-Paso, USA.

Hilton, D. R., Fischer, T. P., Marty, B., 2002. Noble Gases and Volatile Recycling at Subduction Zones. In : Porcelli, D., Ballentine, C. J., Wieler, R., (Eds.), Reviews in Mineralogy & Geochemistry 47, Noble Gases in Geochemistry and Cosmochemistry, 319-362.

Hochstein, M. P., Browne. P.R.L, 2000. Surface manifestations of geothermal systems with volcanic heat sources. In : Encyclopedia of Volcanoes. Academic Press. 835-855.

Hochstein, M.P., Moore, J.N., 2008. Indonesia : Geothermal prospects and developments. Geothermics, 37, 217-219.

Hochstein, M.P., Sudarman, S., 1993. Geothermal resources of Sumatra. Geothermics, 22, 181-200.

Hochstein, M.P, Simanjuntak, J., Sudarman, S., 2010. Geothermal prospects of the eastern Banda Arc Islands (Indonesia). In: Proceedings World Geothermal Congress, Bali, Indonesia.

Hochstein, M.P., Sudarman, S., 2008. History of geothermal exploration in Indonesia from 1970 to 2000. Geothermics, 37, 220-266.

Hochstein, M.P., Soengkono, S., 1997. Magnetic anomalies associated with high temperature reservoirs in the Taupo Volcanic Zone (New Zealand). Geothermics, 26, 1-24.

Hochstein, M.P., Zheng, K., Pasvanoglu, S., Vivian-Neal, O., 2013. Advective (Heat Sweep) Geothermal Systems. In: Proceeding Thirty-Eight Workshop on Geothermal Reservoir Engineering, Stanford University.

Ibrahim, R.F., Fauzi, A., Suryadarma, 2005. The progress of geothermal energy resources activities in Indonesia. In: Proceedings of the WGC 2005, April, Antalya, Turkey, Paper No. 142.

Hickman, R.G, Dobson, P.F., van Gerven, M., Sagala, B.D., Gunderson, R.P., 2004. Tectonics and stratigraphic evolution of the Sarulla graben area, North Sumatra, Indonesia. Journal of Asian Earth Sciences, 23, 435-448.

Huchon, P., Le Pichon, X., 1984. Sunda Strait and central Sumatra fault. Geology 12, 668-672.

Hutchison, C.S., 1989. Geological evolution of South-East Asia. Oxford Monographs on Geology and Geophysics, 13.

Hutchison, C.S., 1993., Gondwana and Cathaysian block, Paleothethys sutures and Cenozoic tectonics in South-East Asia, Geologische Rundshau, 82, 388-405.

Kamah, M.Y., Silaban, M.S.P., Mulyadi, 2000. Cooling indications of the Ulubelu geothermal system, South Sumatra, Indoensia. In: Proceeding of the WGC 2000, May-June, Japan. P. 1319-1323.

Katili, J.A., 1971. A review of geotectonic theories and tectonic map of Indonesia. Earth Science Reviews 7, 143-163.

Knight, M.D., Walker, P.L., 1986. Stratigraphy, paleomagnetism, and magnetic fabric of the Toba tuffs: constraints on the sources and eruptive styles. Journal of Geophysical Research 91, 10355-10382.

Mahon, W.A.J., 1970. Chemistry in the exploration and exploitation of hydrothermal systems. Geothermics, Special Issue 2.

Mamyrin, B.A., Tolstikhin, I.N., 1984. Helium isotopes in nature. Elsevier, Amsterdam.

Marini, L., 2000. Geochemical techniques for the exploration and exploitation of geothermal energy. Dipartimento per lo Studio del Territoro e delle sue Risorse, Univesrita degle Studi di Genova, Italia.

McCaffrey, R., 2009. The tectonic framework of the Sumatran Subduction Zone. Annual Review of Earth and Planetary Sciences. 37, 345-366.

McCaffrey, R., Zwick, P.C., Bock, Y., Prawirodirdjo, L., Genrich, J.F., Stevens, C.W., Puntodewo, S.S.O., Subarya, C., 2000. Strain partitioning during oblique plate convergence in northern Sumatra: Geodetic and seismologic constraints and numerical modeling. Journal of Geophysical Research 105, 28363-28376.

Means, W.D. 1987. A newly recognized type of slickenside striation. Journal of Structural Geology 9, 585-590.

McCarthy, A.J., Elders, C.F., 1997. Cenozoic deformation in Sumatra: oblique subduction and the development of the Sumatran Fault System.

Meyer, H., Schönicke, Wand, U., Hubberten, H, W., Friedrichsen, 2000. Isotope studies of hydrogen and oxygen in ground ice-experiences with the equilibration technique. Isotopes Environmental Health Study, 36. 133-149.

MetCalfe, I., 1983. Conodont faunas age and correlation of the Alas Formation (Carboniferous), Sumatra. Geological Magazine 120, 579-586.

Moeck, I., 2005. Hydrotektonik von Grundwasseleitern: Rekonstruktion von Spannungsfeldern und 3D Modellierung einer geologischen Karte des Zentral-Algarve (Südportugal). PhD Dissertation, Technischen Universität Berlin.

Moeck, I., 2013. Catalog of geothermal play types based on geologic controls. Renewable & Sustainable Energy Reviews (submitted).

Moore, D.E., Hickman, S.,Lockner,D.A.,Dobson,P.F.,2001. Hydrothermal minerals and microstructures in the Silangkitang geothermal field along the Great Sumatra fault zone, Sumatra, Indonesia. GSA Bulletin, September 113, 9, 1179-1192.

Muksin, U., Bauer., K., Haberland, C., 2013a. Seismic Vp and Vp/Vs structures of the geothermal area around Tarutung (North Sumatra, Indonesia) derived from local earthquake tomography. Journal of Volcanology and Geothermal Research, 260, 27-43.

Muksin, U., Haberland, C., Bauer, K., Weber, M., 2013b. Three-dimensional upper crustal structure of the geothermal system in Tarutung (North Sumatra, Indonesia) revealed by seismic attenuation tomography. Geophysical Journal International, doi:10.1093/gji/ggt383.

Muraoka, H., Takashi, M., Sundhoro, H, Dwipa, S., Soeda, Y., Momita, M., Shimada, K., 2010. Geothermal systems constrained by the Sumatra Fault and its pull-apart basins in Sumatra, Western Indonesia. In: Proceedings World Geothermal Congress – Bali Indonesia, 1-9.

Newmann van Padang, M., 1951. Catalogue of the active volcanoes of Indonesia (Part 1). International Volcanological Association, Napoli, Italia.

Ninkovich, D., 1976. Late Cenozoic Clockwise Rotation of Sumatra, Earth and Planetary Science Letters 29, 260-275.

Nishimura, S., 1978. Volcanoes and volcanic rock in Indoneisa (2). Tsukumo Earth Sciences, Kyoto University, 13, 1-9.

Nishimura, S., Nishida, J., Yokoyama, T., Hehuwat, F., 1986. Neo-tectonics of the strait of Sunda, Indonesia. Journal of South East Asian Earth Sciences 1, 81-91.

Nukman, M. Moeck, I., 2013. Structural controls on a geothermal system in the Tarutung Basin, north central Sumatra. Journal of Asian Earth Sciences, 74, 86-96.

Ortner, H., Reiter, F., Acs, P., 2001. Easy handling of tectonic data: the programs TectonicsVB for Mac and TectonicsFP for windows. Computer & Geosciences 28, 1193-1200.

Oxburgh E. R., O'Nions, R. K., 1987. Helium loss, tectonics, and the terrestrial heat budget. Science, 237, 1583-1587.

Petit, J.P., 1987. Criteria for the sense of movement on fault surfaces in brittle rocks. Journal of Structural Geology, 9, 597-608.

Pollard, D.D., Aydin, A., 1988. Progress in understanding jpointing over the the past century. Geological Society of America Bulletin, 100, 1181-1204.

Polyak, B., Tosthikin, I. N., 1985. Isotopic composition of the Earth's helium and the problem of the motive forces of tectogenesis. Chemical Geology, 52, 9-33

Powell, T., Cumming, W., 2010. Spreadsheets for geothermal water and gas geochemistry. In: Proceedings 35th Workshop on Geothermal Reservoir Engineering, Stanford University, California.

Radja, V.T., 1985. The status of geothermal energy development in Indonesia up to the year 2000. Geothermal Research Council Transaction, 9. 487-497.

Ramsay, J.G., Lisle, R.J., 2000. The techniques of modern structural geology, Vol. 3: Applications of continuum mechanics in structural geology. Academic Press.

Reyes, A.G., 1990. Petrology of Philippine geothermal systems and the application of alteration mineralogy to their assessment. Journal of Volcanology and Geothermal Research, 43, 279-309.

Reyes, A.G., Christension, B.W., Faure, K., 2010. Sources of solutes and heat in low-entalphy mineral waters and their relation to tectonic setting, New Zealand. Journal of Volcanology and Geothermal Research, 192, 117-141

Rock, N.M.S., Syah, H.H., Davis, A.E.,Hutchisons, D., Styles, Lena, R., 1982. Permian to Recent Volcanism in Northern Sumatra, Indonesia: a Preliminary Study of its Distribution, Chemistry, and Peculiaritiesm, Bulletin Volcanology, 45-2.

Rybach, L., Muffler, L.J.P., 1981. Geothermal Systems, Conductive heat flow, Geothermal anomlies. In: Rybach, L., Muffler, L.J.P., (Eds.), Geothermal systems: Principles and case history, 3-31.

Rowland, J.V., Sibson, R.H., 2004. Structural controls on hydrothermal flow in segmented rift system, Taupo Vocanic Zone, New Zealand. Geofluids, 4, 259.283.

Schmidt, K., Koschinsky, A., Garbe.Schönberg, D., de Carvalho, L.M., Seifert, R., 2007. Geochemistry of hydrothermal fluids from the ultramafic-hosted Logatchev hydrothermal field, 15°N on the Mid-Atlantic Ridge: temporal and spatial investigation. Chemical Geology, 242, 1-21.

Scholz, C.H., Anders, M.H., 1994. The permeabilty of faults. In: The mechanical involvement of fluids in faulting. U:S: Geological Survey Open-File Reports 94-228, 247-253.

Segall, P., Pollard, D.D., 1980. Mechanics of discontinuous faults. Journal of Geophysical Research, 85, 4337-4350.

Sibson, R.H., 1977. Fault rocks and fault mechanisms. Journal of the Geological Society, 133, 191-213.

Sibson, R.H., 1997. Fault rocks and fault mechanisms. Geological Society of London Journal, 133, 191-231.

Sibson, R.H., 1996. Structural permeability of fluid-driven fault-fracture meshes. Journal of Structural Geology,18, 1031-1042.

Sieh, K., Natawidjadja, D., 2000. Neotectonics of the Sumatra Fault, Indonesia. Journal of Geophysical Research, 105, 28,295 – 28,326.

Sintia, W.N., Munoz, G., Kholid, M., Suhanto, E., Ritter, O., 2013. Subsurface conductivity image from MT data of the Sipoholon geothermal field, Indonesia. In: International Conference on Recent Developments and Concepts for the Sustainable Exploitation of the Geothermal Resources in Indonesia, ITB Bandung-Indonesia.

Soengkono, S., Hochstein, M.P., 1992. Magnetic anomalies over the Wairakei geothermal field, Central North Island, New Zealand. In: Proceeding of the 3rd NZ Geothermal Workshop, 195-202.

Scholz, C.H., Anders, M.H., 1994. The permeability of faults. In: The mechanical involvement of fluid in faulting. Geological Society of London Journal, 133, 191-231.

Storti, F., Rossetti, F., Salvini, F., 2001. Structural architecture and displacement accommodation mechanisms at the termination of the Priestley Fault, northern Victoria Land, Antarctica. Tectonophysics 341, 141-161.

Tchalenko, J.S., 1970. Similarities between shear zones of different magnitutes. Bulletin of the Geological Society of America.,81, 1625-1640.

Truesdell, A.H., 1991. Origin of acid fluids in geothermal reservoirs, Geothermal Resources Council Transactions, 15.

Truesdell, A.H., Hulston., J.R., 1980. Isotopic evidence on environments of geothermal systems, In : Handbook of Environmental Isotope Geochemistry, P. Fritz and J.C. Fontes (Eds.), 1, 179 – 226.

Wellhan, J.A., Poreda, R.J., Rison, W., Craig, H., 1988. Helium isotopes in geothermal and volcanic gases of the western United States, II. Long Valley Caldera. Journal of Volcanology and Geothermal Research, 34, p.201-209.

Whitford, D.J., 1975. Strontium isotopic studies pf the volcanic rocks of the Sunda arc, Indonesia and theor petrogenetic implications. Geochimica et Cosmochimica Acta, 39, 1287-1302.

Woodcock, N.H., Schibert, C., 1994. Continental strike-slip tectonics. In: Hancock, P.L., (Ed.), Continental Tectonics, Pergamon, Oxford, 251-263.

Yokoyama, T., Dharma, A., Hehanusa, P., 1989. Radiometric ages and paleomagnetism of the Sigura-Gura Formation, upper part of the 'Toba Tuffs' in Sumatra, Indonesia. Peleogeography, Paleoclimatology, Paleontology, 72, 161-175.

Zeng, Z., Wang, X., Chen, C., T., A., Yin., X.,Shen, S., Ma, Y., Xiao, Y., 2013. Boron isotope composition of fluids and plumes from the Keuishantao hydrothermal field off northeastern Taiwan: Implication for fluid origin and hydrothermal process. Marine Chemistry, 157, 59-66.

Zucca, J.J, Hutchings, L.J., Kasameyer,P,W., 1994. Seismicity velocity and attenuation structure of the Geysers Geothermal Field, California. Geothermics, 2, 111-126

APPENDIX 1. List of structural geological measurements on striated fault planes.

				Fault Plane		Striation		
Sites	**Longitude**	**Latitude**	**Elevation**	**Dip**	**Dip.Dir**	**Azimuth**	**Plunge**	**Kinematic**
Silangkitang	98°57'18"	2°05'21	1076	354	75	35	90	sinistral
(Fig.10,				350	76	36	88	
dacite,				355	70	32	90	
probably				352	75	34	86	
Late-Miocene.				352	72	52	88	
				352	78	38	90	
				352	75	34	86	
				355	70	32	90	
				350	76	36	88	
Hutabarat	98°58‘54‘‘	2°01‘43‘‘	976	6	64	348	62	Thrust
(Fig.10),				7	64	343	62	
andesite,				5	60	348	60	
Early- Miocene				2	62	344	60	
				6	62	346	60	
				6	65	344	58	
				5	63	342	58	
				5	60	345	58	
				7	60	345	60	
				2	60	346	58	
Akbid	98°59‘10‘‘	1°58‘11‘‘	1079	222	50	176	40	Normal
(Fig.10)				228	42	184	30	
andesite,				218	45	175	40	
Early-Miocene				218	45	161	31	
Rumah Kapal	98°59‘‘41“	2°01‘07‘‘	1074	191	65	179	62	Normal
(Fig.10)				190	65	179	70	
andesite,				178	70	168	68	
Late-Miocene.				190	65	170	70	
Ugan	98°57‘18‘‘	1°58‘49‘‘	1106	28	75	334	30	Normal
(Fig.10)				64	65	354	28	
Andesite,				46	66	332	78	
Late-Miocene.				44	72	353	42	
				54	76	344	42	
				46	70	328	42	
				54	76	342	30	
				48	60	310	42	
				38	78	325	48	
				20	72	334	40	
Panabungan	99°00‘02“	2°04‘30“	1101	234	60	232	65	Normal
(Fault#1,				240	70	218	65	
Fig.10)				220	62	242	70	
Dacite,				220	60	240	68	
probably				247	65	200	55	
Late-Piocene.				258	62	204	60	
Panabungan				222	58	220	55	Normal
(Fault#1,				234	56	220	58	
Fig.10)				248	58	226	58	
Dacite,				240	60	234	58	
probably				233	61	223	58	
Late-Piocene.				245	58	228	58	
				224	58	220	58	
				240	60	235	58	
				238	65	220	60	

				Fault Plane		Striation		
Sites	**Longitude**	**Latitude**	**Elevation**	**Dip**	**Dip.Dir**	**Azimuth**	**Plunge**	**Kinematic**
Panabungan	99°00‘02‘‘	2°04‘31‘‘	1122	50	60	44	60	Normal
(Fault#2,				62	60	52	60	
Fig.10)				47	60	52	60	
Dacite,				74	65	32	70	
Probably-				53	72	22	70	
Late-Pliocene.				44	78	28	82	
				56	70	22	70	
				42	62	23	62	
				40	62	35	62	
				50	60	36	60	
Panabungan	99°00‘01“	2°04‘32‘‘	1117	62	70	60	70	Normal
(Fault#3,				45	65	40	65	
Fig.10)				56	65	48	65	
Dacite,				48	70	48	65	
Probably-				53	65	38	65	
Late-Pliocene				51	66	45	65	
				41	65	35	65	
				44	62	35	65	
				45	62	35	65	
				45	70	32	70	
Sitaka	98°57‘39“	2°00‘40‘‘	1240	4	70	46	62	Thrust
(STK,				24	65	52	60	
Fig.10)				24	62	34	65	
Dacite member -				24	62	52	60	
of Toru Fm,				28	80	102	60	
Late-Miocene.				20	88	114	65	
				32	85	118	70	
				356	60	24	55	
				12	60	45	55	
				24	60	52	60	
Tunjul	98°56‘27‘‘	2°01‘43‘‘	984	274	40	-	-	Normal
(TJ,				249	46	-	-	
Fig.10)				250	46	-	-	
Andesite,				276	52	-	-	
quartz viens,				111	80	-	-	
Early-Miocene.				114	75	-	-	
				113	75	-	-	Normal
				111	75	-	-	
				263	52	-	-	
				238	42	-	-	
				243	42	-	-	
				298	82	-	-	
				303	82	-	-	

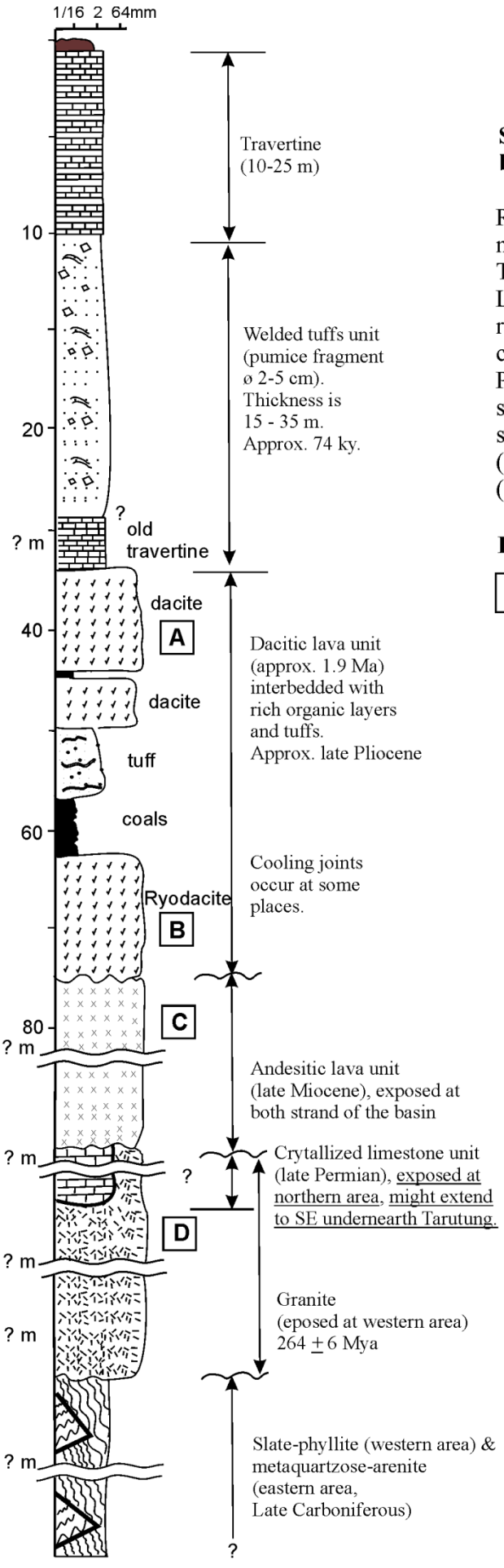

Appendix 2

Stratigraphic Log of Tarutung Basin, based on surface geological mapping.

Rock sequence of #**A** to #**C** is based on measured stratigraphic logs at north of Tarutung Basin Lattitude 98.95456°; Longitude 2.08960°, elv: 1052 m.asl. The rock sequence above #**A** is based on composite stratigraphic logs measured at Panabungan and Ria-Ria area. The rock sequence below #C is based on regional stratigraphic relationships by Aldiss et al. (1983), Clarke et al. (1982), and Apsden (1982).

Legend :

A - **D** = sample code, analysed using XRF (see Appendix 3)

APPENDIX 3.

Bulk oxide compositions of the rock formations in the Tarutung Basin and its vicinity based on XRF analysis.

		OXIDES in %											
SITES	**Coordinate**	**SiO_2**	**Al2O3**	**MnO**	**MgO**	**CaO**	**Na_2O**	**K_2O**	**TiO_2**	**P_2O_5**	**Fe_2O_3**	**LOI (%)**	**Sum (%)**
133 (Granite Sibolga)	(474067;231513)	65,79	15,29	0,10	1,46	2,83	2,74	5,00	0,82	0,30	5,21	0,89	100,43
Bohorok Fm	(520024;223568)	67,99	21,35	_	0,18	0,13	0,19	5,09	0,32	0,04	0,55	4,06	99,90
174 (Kluet Fm)	(465472;242699)	95,79	2,74	_	0,04	0,05	0,05	0,02	0,19	0,09	0,08	1,01	100,06
192012 (Alas Fm)	(487772;246683)	0,35	0,13	0,00	0,39	54,91	0,04	0,03	0,00	0,00	0,03	43,91	99,79
366 (Andesite Toru Fm)	(500109;218353)	63,20	16,70	0,12	1,91	5,77	2,91	2,57	0,56	0,11	5,96	1,18	100,99
Dacite Unit PNB (upper)	(500049;229342)	70,57	14,65	0,12	0,43	1,37	2,65	4,33	0,21	0,05	1,82	3,44	99,64
Dacite Unit PNB (lower)	(493403;224206)	70,79	13,43	0,04	0,38	1,69	3,08	4,46	0,21	0,06	1,55	2,33	98,02

Rock exposures in the eastern margin of Tarutung Basin : Bohorok Fm & Andesite Toru Fm. (see Chapter 7, Section 7.10)
Rock exposures in the western margin of Tarutung Basin : Kluet Fm, Granite Sibolga, & Andesite Toru Fm. (see Chapter 7, Section 7.10)

APPENDIX 4

Classification of major magmatic rocks from Tarutung based on alkalies and silica. The bulk compositions of the samples are listed in Appendix 3.

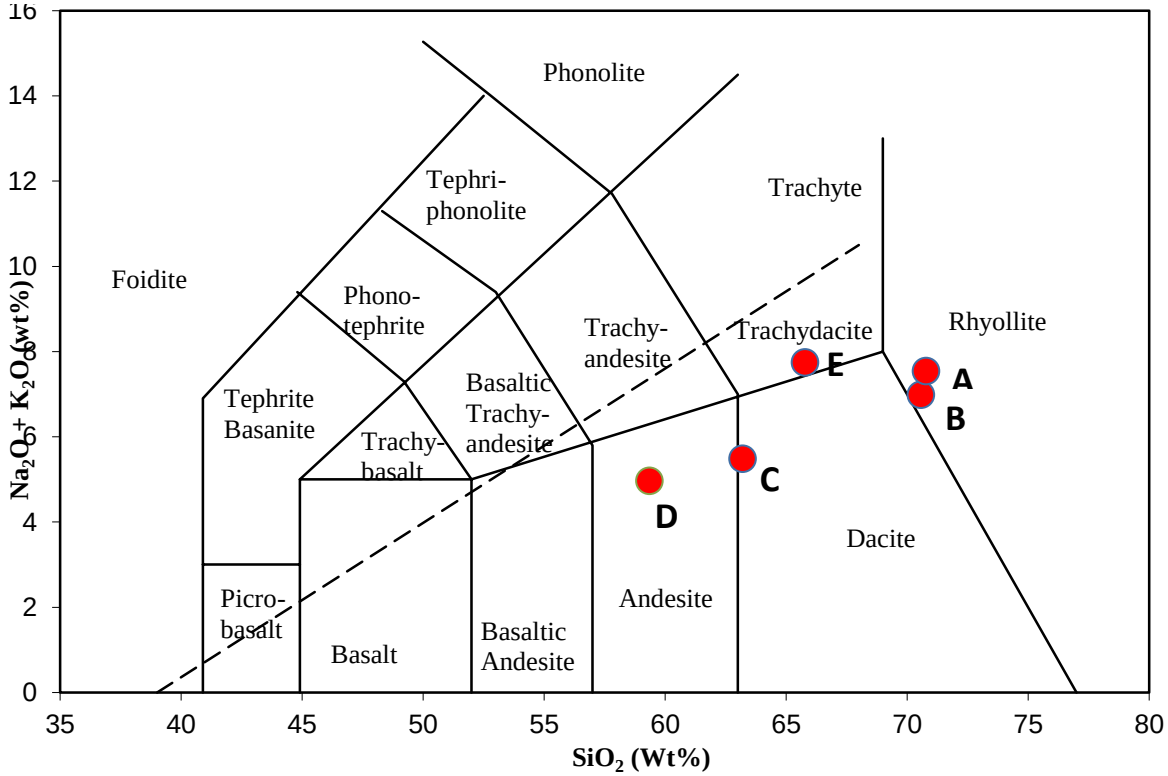

Legend : **A** = lower Dacite as exposed in Panabungan**; B** = upper Dacite as exposed in Panabungan**, C** = andesite of Toru Fm as exposed in Pansur Napitu**; D** = andesite of Toru (from Aldiss et al., 1983), **E** = granite of Sibolga.

APPENDIX 5

Hydrochemistry data from Sarulla springs (from Gunderson et al., 1995) and from South Germany cold spring (data from Griesshaber et al., 1992).

Springs	Code	pH	T(°C)	TDS	Li	Na	K	Rb	Ca	Mg	SiO_2	B	Cl	SO_4	HCO_3	Ionic Balance	R/Ra (*)
Sarulla																	
SibualBuali (Somarsik)	25	7,91	68	2230	0,59	450,7	51,99	NA	60,33	1,53	151,9	1,81	41	14	1456	9	5.9 – 6.5
L. Aek Nabara	26	7,5	72	1200	0,69	227	16,5	NA	96,3	4,43	116	2,99	288	57	390	2,6	NA
Sialang Jae	27	8,36	82	3025	6,51	890,1	68,45	NA	12,16	0,87	159,1	36,33	1084	125	638	0,5	NA
Donotasik	28	7,98	101	3647	6,7	1145	75,96	NA	11,31	0,47	135,6	46,72	1294	348	578	-0,3	NA
Donotasik Geyser	29	9,31	92	3667	7,41	1150	90,39	NA	3,01	0,16	236,5	47,26	1310	332	485	0,3	NA
Rihitbidang	30	8,5	101	1937	4,41	546,5	33,25	NA	4,65	0,93	163,8	21,59	560	142	457	0,4	NA
W-NIL Acid	31	3,09	97	697	0,05	27,96	34,72	NA	20,14	5,30	344,7	0,24	7,10	0,33	256	5,3	NA
Martinde (NIL)	32	8,05	75	2898	0,28	694,6	78,88	NA	14,7	2,08	198,7	6,74	48	0,7	24	45,3	NA
Aek Parijaman	33	7,79	80	2509	3,31	661,7	57,78	NA	52,13	0,33	283,1	18,66	599	1,13	519	9,9	NA
Aek Alaan	34	7,8	96	2356	4,12	694,9	68,25	NA	7,07	0,67	124,2	18,81	580	1,3	393	11,7	NA
Opujamara	35	8,65	96	2243	6,31	680,4	114,0	NA	2,30	0,02	244,4	35,88	947	7	79	4,7	NA
Pangalowan SW	36	8,66	95	2412	6,48	673,6	125,3	NA	3,11	0,49	376,8	35,54	980	6,1	68	4,1	NA

APPENDIX 6

Ratio helium isotope and ratio CO_2/ ^3H of Ria-Ria springs, Sibual-buali (from Halldorsson et al., 2013) and Eifel (Germany; from Griesshaber et al., 1992).Sample localities of Tarutung and Sarulla are shown in Appendix 5.

Isotopes	**Dry gas (%)**							
Springs (m.asl)	**Coordinate**	**Type**	**$^3He/^4He$ (ppm)**	**$CO_2/^3He$**	**He**	**N_2**	**Ar**	**CO_2**
Ria-Ria (Helatoba-Tarutung 1*)		Gas **	1.73	1107×10^9	0.37	0.74	0.0014	98.81
Ria-Ria (Helatoba-Tarutung2 *)		Gas **	1.64	1505×10^9				
Sibual-buali SUM10-24 (Sarulla)		Gas	6.18	16.3×10^9				
Sibual-buali SUM10-25 (Sarulla)		Gas	1.12	60×10^9				
Sibual-buali 615 (Sarulla)		Gas	6.65	25.8×10^9				
Sibual-buali 775 (Sarulla)		Gas	6.58	27.3×10^9				
Glees 1 (South Germany)		Gas	5.00	NA				
Glees 2 (South Germany)		Gas	4.76	NA				
Wehr (South Germany)		Gas	4.95	NA				

*) spring's name as used in Halldorsson et al. (2013)
**) sample container is Cu-Tube (Halldorsson et al., 2013)